MODELLING THE STRUCTURAL BEHAVIOUR OF THE FOLD-AWAY SHELTER

A thesis submitted for the degree of Master in Engineering (Research)
University of Technology, Sydney

Thomas Rolan E. Rondero
March 2006

CERTIFICATE OF AUTHORSHIP/ORIGINALITY

I certify that the work in this thesis has not previously been submitted for a degree nor has it been submitted as part of requirements for a degree except as fully acknowledged within the text.

I also certify that the thesis has been written by me. Any help that I have received in my research work and the preparation of the thesis itself has been acknowledged. In addition, I certify that all information sources and literature used are indicated in the thesis.

Signature of Candidate

Production Note:
Signature removed prior to publication.

ABSTRACT

The F-shelter underwent non-destructive monotonic load tests and destructive shake table test. The timber-framed shear walls with different sheathings; namely wood wool cement boards (wwcb) and F11 structural plywood were tested under uniaxial loading. Furthermore, finite element models (FEM) supplemented the experimental work. An FEM of the corner metal bracket and a 2-dimensional FEM for the timber-framed shear wall were generated and verified from the experimental work.

Behavioural responses from unidirectional lateral loading of the wall were obtained. For the dynamic test, the Kobe earthquake and Zone IV earthquake were simulated to determine the dynamic response of the F-shelter. Excitation was limited to 70% full scale displacement record of Kobe and 80% of Zone IV, due to the 100mm limitation in the allowable displacement on both sides of the shaker table. The shake table test showed that the F-shelter can withstand the simulated earthquakes.

FEMs were developed using ANSYS 7.2, a general finite element software. A requisite input data for the timber-framed shear wall FEM in lieu of a hinge connection corner joint for the timber-framed shear wall were generated through experimental work on the corner metal brackets and verified with the generated FEM. The results of the FEM of the *Dipterocarpus grandiflorus Blanco* (Apitong) timber-framed sheathed with wwcb were 5% to 9% higher than the average values for maximum deflections and maximum load capacity. The FEM results of the Radiata pine sheathed with F11 plywood, however, were 25% to 14% lower than the average values for maximum deflections and maximum load capacity.

This thesis has demonstrated the process of generating FEMs that can be used as a tool to improve and modify the F-shelter. The structural reliability of design and construction of the first F-shelter prototype was verified from the whole house test and structural modeling of the wall using FEM.

Table of Contents

List of Tables

List of Figures

List of Appendices
Located on compact disk

page 153

Appendix A F- shelter concept

1. Steps in erecting the Foldaway-shelter

Appendix B Philippine archipelago with its bounding trenches & subduction zones and active faults.

Appendix C Seismicity zone map of the Philippines

Appendix D Seismic zone map of the Philippines

Appendix E Distribution of earthquake generators in the Philippines

Appendix F Distribution of active and inactive volcanoes of the Philippines

Appendix G Wall corner joint test

1. Raw test results for Apitong and Radiata Pine frame in data file
2. Test results in Excel file
3. 82-degree Radiata Pine in tension
    a. Summary
    b. Average versus FEM

Appendix H Lateral nail resistance test

1. Plywood sheathing in Excel file
2. Wood wool cement board sheathing in Excel file

Appendix I Apitong wall frame test data

1. Test results in Excel file
2. Summary of the test results
    a. Average versus experiment test results
    b. Average versus FEM

Appendix J Radiata pine wall frame test data

1. Test results in Excel file
2. Summary of test results
    a. Load-deflection curves
    b. Average versus FEM

Appendix K Wall test with wwcb sheathing

1. Test results in Excel file
2. Summary of test results
    a. Wwcb and plywood load-deflection curves
    b. Average load-deflection curves for wwcb and plywood
    c. Load-deflection curves for wwcb 1–3
    d. Load-deflection curves for wwcb1, wwcb2 and average
    e. Wwcb versus FEM

Appendix L Wall test with plywood sheathing

1. Test results in Excel file
2. Summary of test results
    a. Wwcb and Plywood load-deflection curves
    b. P1 versus FEM

Appendix M F-shelter test

1. quasi-static test without metal plates
    a. 2, 3 , 4 and 5kN test results in Excel file
    b. Summary for 5kN with and without metal plates
2. quasi-static test with metal plates
    a. 1.5, 3 and 4kN test results in Excel file
    b. LC1-LVDT11
    c. LC2-LVDT3
    d. side with opening
    e. side without opening
3. dynamic test without metal plates
    a. 20, 50 70% of full excitation of Kobe earthquake
        I. Acceleration at top corner on loaded side; 50% Kobe (without reinforcements)
        II. Acceleration at top corner on opposite side; 50% Kobe (without reinforcements)
    b. 50% of full excitation of Zone IV
4. dynamic test with metal plates
    a. 5, 15, 30, 40 and 50% of full excitation of Kobe earthquake
        I. Acceleration at top corner on loaded side; 50% Kobe (with reinforcements)
        II. Acceleration at top corner on opposite side; 50% Kobe (with reinforcements)
    b. 50 and 80% of full excitation of Zone IV

Appendix N ANSYS files

1. Apitong wall frame
    a. Deformed shape at Pmax
    b. Nodal solutions
2. Radiata Pine wall frame
    a. Deformed shape at Pmax
    b. Nodal solutions
3. Wwcb sheathed wall
    a. Deformed shape at Pmax
    b. Nodal stresses at x and y directions
    c. Nodal solutions
4. Plywood sheathed wall
    a. Deformed shape at Pmax
    b. Nodal stresses at x and y directions
    c. Nodal solutions

1 Introduction

The project is a sequel of the fundamental research carried out by the Forest Products Research and Development Institute (FPRDI) on the conceptualization and prototyping of the Fold-Away Shelter (F-shelter). The prototype was shipped from the Philippines to Australia for structural testing was conducted. This project is focused on the development of finite element models (FEM) of the wall as well as to investigate the behaviour of the F-shelter when subjected to static and dynamic loads to improve the concept and verify its structural integrity.

1.1 Objective

The main objective of this study is to generate FEM as an analytical model of the F-shelter's timber-framed wall calibrated through structural tests on full-size specimens, as a tool to improve the existing F-shelter.

Specifically, this research aimed to

1) conduct preliminary tests on corner joints with metal brackets. The result of this test was used as an input data in generating the complete FEM for the two-dimensional wall. Compression and tension tests were conducted on wall frame corner joints in order to see the effect of the corner joint metal brackets.
2) conduct structural tests on full-size wall components and the whole F-shelter. Structural tests were specifically designed to calibrate the finite element model. The results from testing the full size wall component was used to verify predictions obtained from the finite element model analysis. Wall with and without sheathing was subjected to lateral loads. The F-shelter was tested using nondestructive monotonic and destructive dynamic loading.
3) consider an alternative timber framing, sheathing material (7mm thick plywood) and fastener and compare its performance with the existing Apitong wall frame sheathed with 8mm thick wood wool cement board (wwcb) sheathing and a galvanized steel nails of ø3.39mm by 25.46mm in length fastener.
4) generate a two-dimensional FEM that can predict the nonlinear behaviour of the timber-framed shear wall. It is well recognized that the behaviour of sheathing-to-frame connector is central to the lateral response of timber shear wall. Tests in accordance with AS 1649 (2001) were performed in order to model the sheathing-to-frame connector.
5) recommend modifications to structural components of the F-shelter in order to improve its performance against typhoon and earthquake forces. Experimental tests were undertaken on the shaker table to determine the weak points of the structure under earthquake excitation.

1.2 Scope of works

This study is Phase II of the development of the F-shelter technology (Figure 1.1). it took off from research and development work until prototyping of the new prefabricated sheleter concept. Testing and modelling were conducted in order.

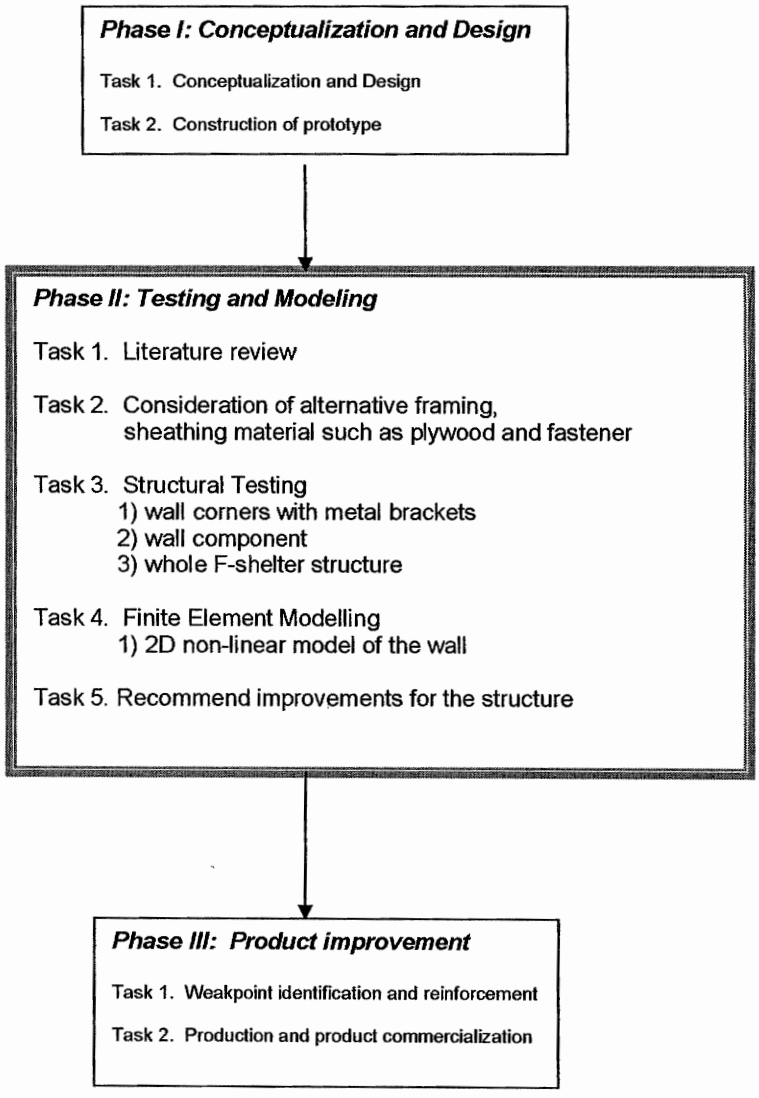

Figure 1.1 Workflow for the development of the F-shelter

2 Background

This section provides the rationale and short description of the foldaway technology.

2.1 Rationale

Throughout the Philippines' history, there has not been any attempt to provide an emergency shelter specifically for victims of calamities, whose houses are either partially or totally damaged. Instead, churches, gymnasia and public schools have served as temporary shelters. When these public shelters are not available, victims build makeshift shelters made of scraps (Figure 2.1).

An example of service rendered by the government to the displaced victims is shown in Table 2.1. The table shows a report by the Department of Social Welfare and Development on figures brought about by flood due to monsoon rains. Out of the 14 regions of the Philippines, 5 were severely affected, comprising 15 provinces with 26 cities. Shown in the table is the number of evacuation centres provided by the government and total number of persons served. Among the 473,377 persons served only 31,813 persons were staying in the indoor evacuation centres. The remaining 441,564 persons were served outdoor the evacuation centers staying on makeshift shelters. Victims that were not served flee to neighboring towns and to their closest relatives for recourse.

Table 2.1 Report on a flood calamity and figures on affected individuals

Calamity	Floods due to monsoon rains; 11 July 2002
Affected areas	5 Regions (NCR, CAR, I, II and IV)
Number of evacuation centres	184
Total number of affected families	1,644,199
Total number of persons served 1. Indoor evacuation centres 2. Outdoor evacuation centres	473,377 31,813 441,564

Source: www.reliefweb.int Philippines, DSWD Disaster Updates

Emergency shelters serve as immediate refuge for victims of natural- and man-made calamities. Some emergency shelters are temporary in nature, i.e., they are put up for the duration of the calamity and disassembled when victims are ready to return to their homes. Tents made from canvass or nylon on sturdy framework of either light metal, or hard plastic, or fiberglass is the best examples of temporary shelters. However, these are vulnerable to extreme weather conditions, aggravating the physical condition of traumatized occupants. Soriano *et al* (2000)

cited several disadvantages on the use of these shelters for prolonged periods during and after calamities. Aside from tents, displaced families of disaster-stricken communities are housed in schools, gymnasia, churches and other public buildings. Prolonged use of these facilities, however, leads to the disruption of daily community activities including those that were not directly affected by the disaster, adversely affecting the economic fabric of the community.

It is evident that the prevalence and magnitude of natural disasters have serious consequences on society and economy. The severities of natural disasters have notably increased in the Philippines. A review of statistics for the last hundred years (www.em-dat.net 2002), reveals that Asia is the most highly disaster afflicted region in the world, with about 90% of total affected people, over 50% of total deaths and total economic losses respectively

As the Philippines is located on the Pacific Rim of Fire, it is vulnerable to disasters of both hydro meteorological and geo-physical types (Rellin *et al* 2001). As in the previous years, the damage caused by hydro-meteorological disasters grew in 2002, with quite large populations being affected by floods and windstorms followed by population affected by earthquakes. Economic damage due to windstorms was also noticeable.

In addition to these unfortunate circumstances, lack of affordable houses is the third in line of the people's problems. Damage to houses caused by such disasters contribute to burden to the current national low-income housing backlog of 4.2 million units (www.adb.org 2002) and continues to increase yearly. The National Science Technology Plan for 2002-2020 (www.fnri.dost.gov.ph 2002), under section VIII.1.a.2 for Research and Development (R&D) programs for housing and shelter shall aim to contribute to the provision of housing needs and to augment the efforts of the government to cope with the growing housing backlog. Their R&D shall include the development and utilization of cost-efficient housing materials and components.

The Forest Products Research and Development Institute (FPRDI) has recently developed the "F shelter"- a fast-to-build, firm and foldaway emergency shelter made from either steel or wood structural frame locally manufactured medium and high-density wood wool cement boards for floors, walls and roof (Soriano *et al* 2000). This was in response to the growing need for emergency shelters as well as permanent houses.

In year 2000, the fast-to-build emergency shelter concept was subjected to three stages of engineering design processes, namely: (i) inception, (ii) concept design, and (iii) design production as elaborately described by Macleod and Hartvig (2001). This led to the foldaway shelter concept. During these stages, research engineers paid special attention to hard criteria such as the National Building Code (NBC) and the National Structural Code of the Philippines (NSCP), load criteria, specific client preferences and functional criteria. Improvements

addressing the soft criteria particularly cost, aesthetics, construction time, maintainability and durability are continuously being improved.

a b

Figure 2.1 Some makeshift shelters used in the aftermath of calamities. **a.** Structures made of bamboo poles and roofs with clothe as cover and **b.** Structure is supported by tree branches, bundled leaves as walls and corrugated galvanized iron sheets tied on top serving as roof.

2.2 General description of the F-shelter technology

The prototype F shelter is 4.8m (length) x 2.4m (width) x 3.0m (height) when folded and packed (Figure 2.2). The F-shelter is in its packed form when delivered and erected at the site.

Figures 2.3a-e shows the floor plan and four elevations of the F-Shelter. When it is unfolded and erected, it expands to a floor area of 4.8 x 4.8m and maximum headroom of 3.0m (Figure 2.5). With 4 unskilled workers, the structure can be erected and its components fixed in place in 15 minutes, and another 15 minutes is required of workers to attach architectural components and accessories such as windows and false posts. The floor is elevated on specially designed prefabricated footings with pedestals that can be adjusted when the terrain is uneven. Doors and windows are similar to those in conventional site-built shelters. Steps in the erection of the F-shelter are discussed in Appendix A.

The structure's timber frame is made entirely of *Dipterocarpus grandiflorus Blanco* which is locally called Apitong. The structure sheathing is made of wood wool cement board (wwcb) panels pre-cut to sizes and shapes. No special tools were used in the construction. This is to demonstrate that laymen could construct it with minimal supervision from a technical person. Frame to sheathing connectors are supplied by the wwcb suppliers as part of their product promotion. If the timber frame were wider, a longer flat head nails could have been used. Complete descriptions of the materials used in the construction is discussed in Chapter 4 of this thesis.

Figure 2.2. The emergency shelter is delivered to the site in a rigid case. The rigid case is mounted on adjustable prefabricated footings

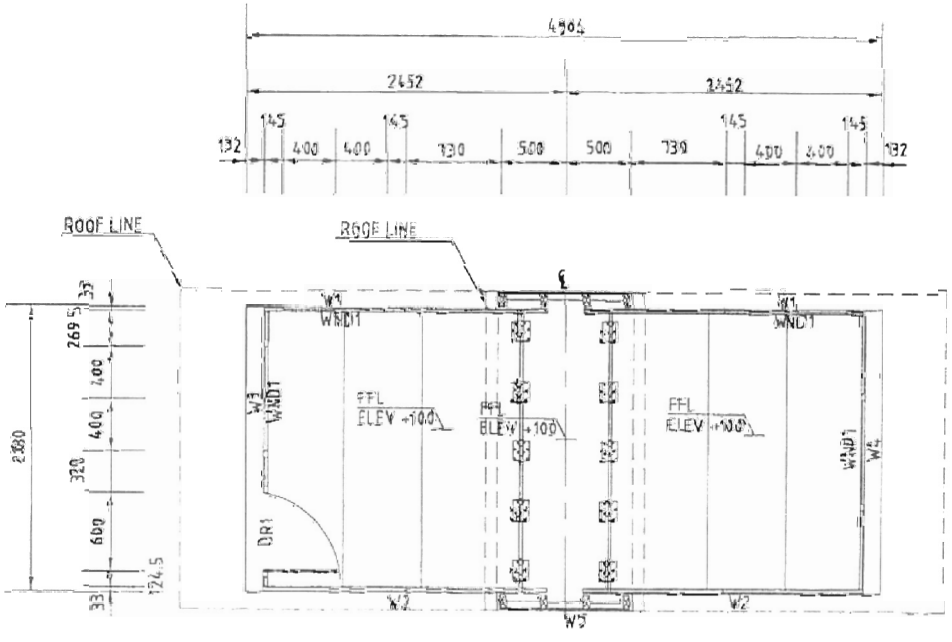

Figure 2.3a Floor plan of the F-shelter

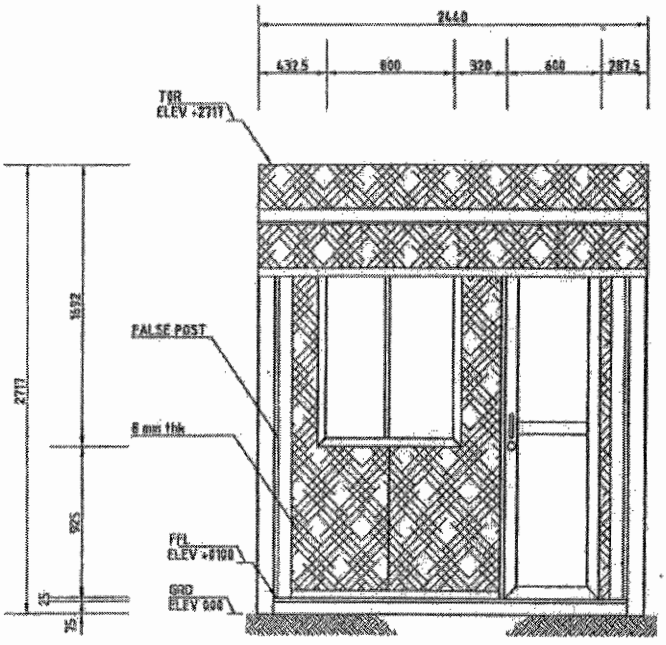

Figure 2.3b Front Elevation of the F-shelter

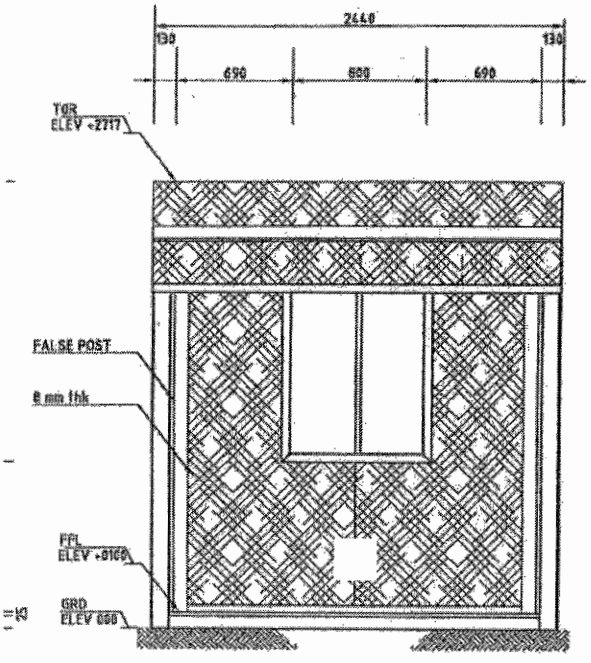

Figure 2.3c Rear Elevation of the F-shelter

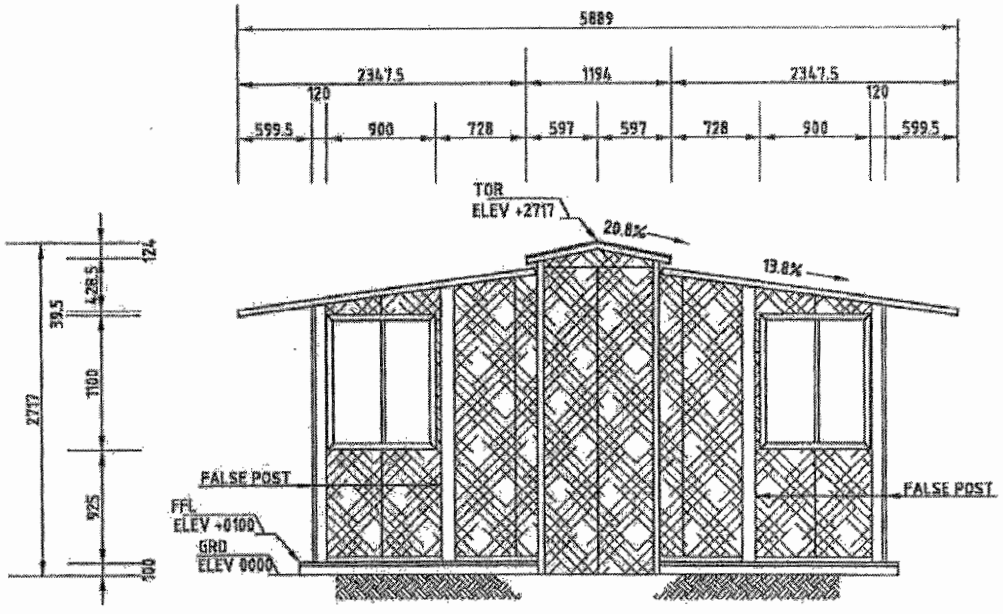

Figure 2.3d Left side elevation of the F-shelter

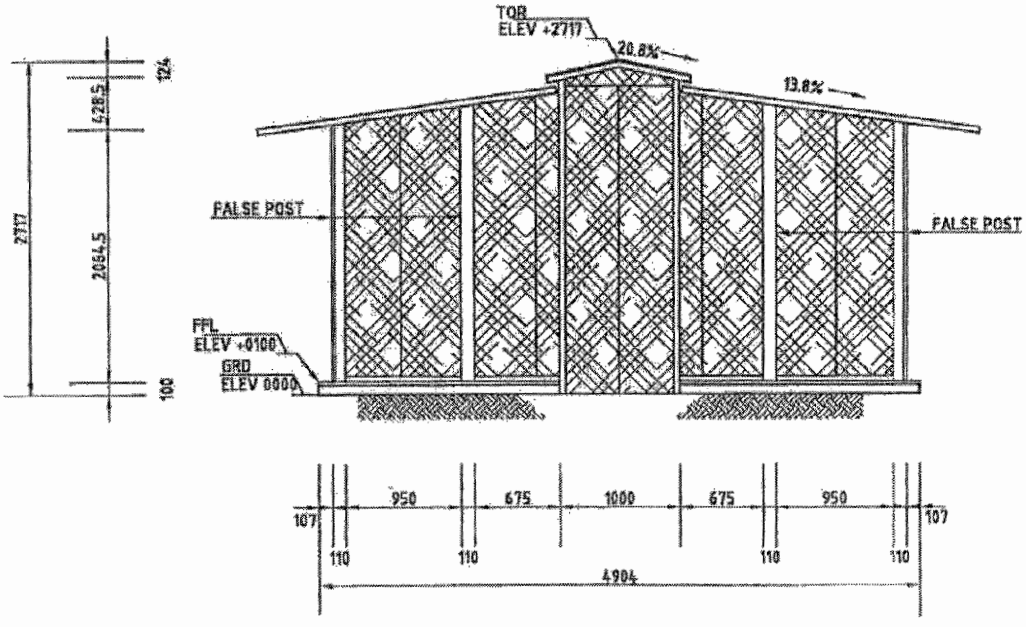

Figure 2.3e Right side elevation of the F-shelter

The shelter is basically a shell-type structure, as shown in Figure 2.4 (see also Figure 2.3a), i.e., without any internal partitions or divisions. The walls on the east side are without openings and the walls on the west side have openings (Figure 2.4). Wall 1 has a window opening and Wall 4 has a window and a door opening. The door opening is reinforced with a 5mm steel plate at the top and bottom. The dots represent hinges connecting adjacent components.

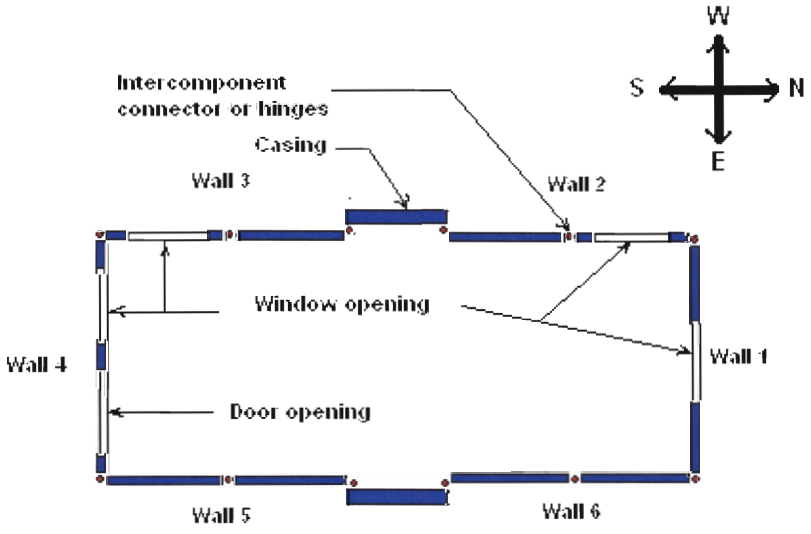

Figure 2.4 Floor plan; shown here are walls and interconnectors

Figure 2.5. The lumber-framed shop-fabricated emergency shelter, complete with false posts (used to cover of the wall to wall connection), stairs and tie-down straps anchored to ground, currently being service tested at the FPRDI.

2.3 Design criteria

The F-shelter was designed in accordance with NBC and NSCP 1992. Based on the simplified static procedure (Section 208.4.8.1 of NSCP 1991), the lateral forceis determined to be 500N for the earthquake load and 3,500kN wind loads derived from extreme loading situations we have. The governing design load consideration was wind. The walls were designed to withstand a 3,500N equivalent static force for wind load. With the occurrence of strong typhoons exceeding wind velocity of 200 kph as stated in NSCP 1992, a revision was made creating the NSCP 2001. This edition was released after the prototype F-shelter was constructed. The NSCP 2001 gave the equivalent static lateral force of 5,000N.

2.4 Importance in finite element modeling

The use of deterministic applied loads, structural dimensions and material properties generally dictate innovative shelter design. In reality, however, the structural behaviour of any shelter under applied loads such as gravity, wind and earthquake, is a random phenomena where the actual values are not known. Basically conventional permanent shelters are designed to withstand loads with the assumption that (i) connectors stay very rigid and (ii) structural elements remain undeformed after the loads are applied. In the case of the F shelter, these assumptions hold true when the shelter is erected and ready to be occupied. However, these do not hold true during transport and erection. The deformations and movements during these two stages have to be predicted so that improvements can be made. The transportability of the whole house and having its foldaway components are subjects to the integrity of the shelter to vibration and disturbance of connectors causing joint movements.

It is in this light that modeling the response of the F-shelter structure is necessary. Finite element software that could be programmed to simulate more realistic loads could give a better perspective on how the structure will respond to external loads. It is anticipated that the model generated in this study shall serve as future reference for the following.

(i) indices on structural soundness such as:
- earthquake resistance
- wind/typhoon resistance
- connector efficiency
- mass distribution

(ii) improvements for more economical design
- serviceability
- prolonged utility
- functionality with minimum maintenance
- safety of occupants

- reduced cost as a result of using fewer and smaller structural elements
- expand raw material sources such as alternative sheathing materials
- removal of redundant structural elements
- eliminates need for future full scale testing for the same structure

Thus, it is imperative that the overall stability, strength, geometric permanence, stiffness, and dynamic response of the structure at all load stages are understood. This will improve the F-shelter for the purpose that it was initially designed, i.e., as a fast-to-build structurally sound emergency shelter, and possibly lead to further uses such as mobile vacation shelters, field houses, and mass fabricated low-cost houses on permanent foundations, as has been suggested by interested local and overseas stakeholders during its initial introduction.

The F-shelter can potentially be converted to a permanent shelter even if initially intended as a temporary shelter. If the walls are structurally adequate and well connected, the shop-fabricated footings are the only components that are temporary. If the foundations are in-situ-built and embedded in the ground, then using the shelter for a prolonged period- perhaps as a permanent house – can be an alternative.

3 Literature review

3.1 Introduction

This chapter discusses major parts of the thesis regarding literature related to this project and is divided into three distinct topics, namely, a background on the condition of the Philippines regarding the occurrence of calamities, a review on the works conducted on component and whole-structure testing, and finite element modelling.

3.2 The Philippines, a calamity-prone area

The Pacific Rim is not only a community of the fastest-growing and most dynamic nations in the world. It is also an area exposed to a wide range of natural disasters. The Philippine archipelago, located near the western edge of the Pacific Ocean, is in the direct path of seasonal typhoons and monsoon rains that bring floods, storm surges, and their associated landslides and other forms of devastation. The Philippines also sits on the "Ring of Fire" where the continental plates collide and thus experience periodic earthquakes and volcanic eruptions. The exposure to natural disasters may be characterised as frequent, varied and severe; a combination which has made the country attentive to disaster mitigation.

According to a research group based in Brussels, the Philippines is the number 1 calamity country as surveyed between 1990 and 1999 (Balana, 1999). The geographical location of the country makes it susceptible to calamities. As a series of islands, the Philippines is always a pathway for tropical typhoons originating from nearby oceans/seas. Earthquakes in the Philippines are either tectonic or volcanic in origin. . The probability of future eruptions of the 22 active volcanoes is great, as stated in historical records (PHIVOLCS, 2000).

3.2.1 Earthquakes

3.2.1.1 Tectonic earthquakes

The Philippine archipelago lies between two of the world's major tectonic plates (Appendix B) (PHIVOLCS, 2000). The northwestward moving Pacific plate is presently pushing the Philippine Sea Plate beneath the eastern side of archipelago at the rate of about seven centimetres per year. The oceanic parts of the slower-moving Eurasian Plate are being subducted along the western side of Luzon and Mindoro at the rate of three centimetres per year. These plate interactions, displacements along the Philippine Fault Zone, which decouples the northwestward motion of the Pacific with the southeastward motion of the Eurasian Plate, and movements along other active faults are responsible for the present-day high seismicity of the Philippine archipelago (Appendix C). This is the same reason why the NSCP adopted two seismic zone

factors (Z) in designing structures. The seismic zone map (Appendix D) provided by NSCP shows two applicable seismic zone factors.

Numerous earthquake generators (Appendix E) and the recorded major earthquakes hitting the country reveal that the Philippines are indeed a seismically active earthquake country. It is a fact that, since earthquakes with magnitude 7 or more have affected the Philippines in the recent past, the likelihood of these destructive earthquakes occurring again in the future is indeed very high.

At least five earthquakes per day occur in the Philippines. Based on the distribution of earthquake epicentres, the most seismically active part of the Philippines is their eastern section, containing eastern Mindanao, Samar and Leyte with an average of 16 perceptible earthquakes per year. This is due to the active subduction process occurring along the Philippine trench.

3.2.1.2 Volcanic Earthquakes

The Philippine archipelago has more than 200 volcanoes distributed in five volcanic belts intimately related to subduction/convergent processes. Appendix F shows the distribution of the country's active and inactive volcanoes.

Considered most active are the volcanoes which have short periods of dormancy, namely: Mayon, Taal, Bulusan, Canlaon and Hibok-Hibok. Pinatubo Volcano was recently included among the most active in view of its ongoing activities. In June of 1991, the volcano exploded in one of the world's most violent and destructive eruptions of the 20th century.

A mitigation measure in avoiding the harmful effects of volcanic hazards is to delineate hazard zones for the most active volcanoes. PHIVOLCS has prohibited human settlement in the Permanent Danger Zones (PDZ) or the areas within a 4–6 km radius from the summits of the active volcanoes. PDZ increases depending on the nature of the eruption. Resettlement areas are assigned and people are housed in earthquake resistant structures in nearby areas.

3.2.2 Tropical typhoons

The Philippines is prone to tropical cyclones due to their geographical location, which generally produces heavy rains, and flooding of large areas and also strong winds which result in heavy casualties to human life, properties and destruction to agricultural products. An average of 19 typhoons visits the country per year, based on statistical data from 1948 to 2000, as shown in Table 3.1 (NCMC, 2001). In the Philippines, extreme wind is categorised, depending on the increasing magnitude of the wind speed, into moderately extreme (60 to 100km/hr), extreme

(101 to 184 km/hr) and severely extreme (185 km/hr or more) (NSCP, 1992). The NSCP (2001) has specified three wind zones (Figure 3.1) based on the geographic location. The three wind zones (I, II & III) having 125, 200 and 250 mph wind speeds, are commonly used values to design wind-resisting structures. This change in extreme wind velocities has also shifted wind design criteria from 200 to 250 km/hr. Phase I of the study has initially used a design wind criteria of a 200 km/hr wind velocity.

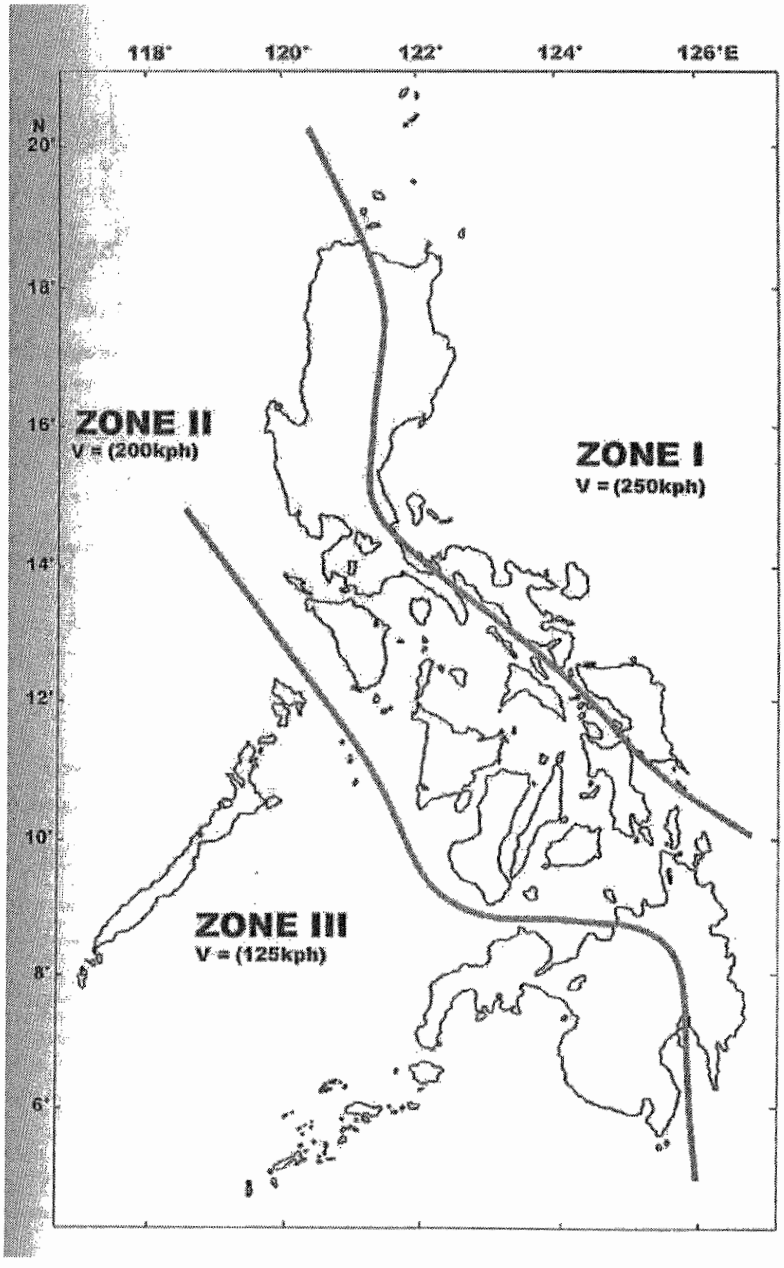

Figure 3.1 Three wind zones in the Philippines (NSCP, 2001).

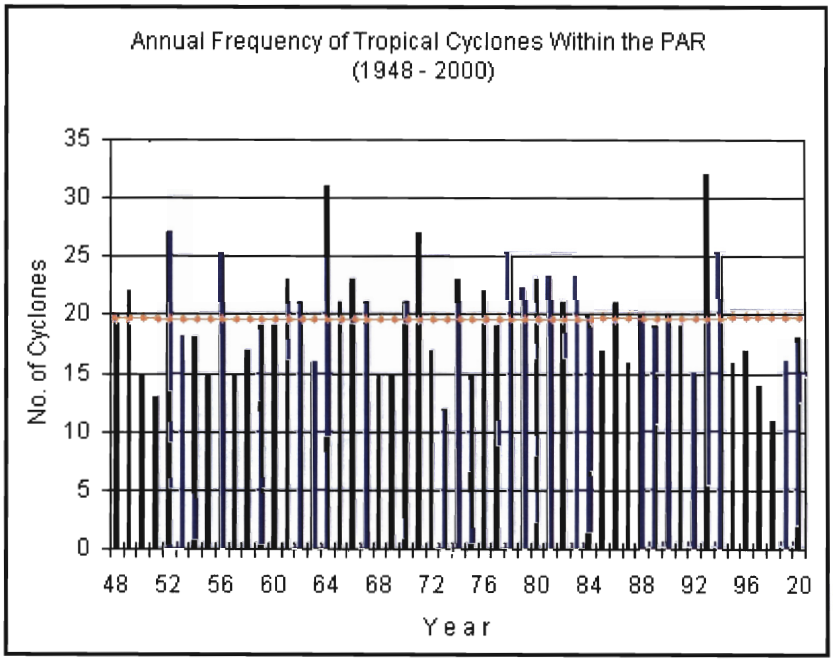

Table 3.1 Annual Frequency of Tropical Typhoons within the Philippine Area of Responsibility (PAR) for the years 1948–2000 (NCMC, 2001).

The study shows that typhoon extreme wind speed of 185 km/hr and above is experienced in several areas of the country during various months of the year (Rellin *et al.*, 1998). In the region of Luzon, the areas are namely, Itbayat, Basco, Vigan, Aparri, Tuguegarao, Dagupan, Muñoz, Casiguran, Port Area, Tayabas, Ninoy Aquino International Airport (NAIA), Ambulong, Infanta, Alabat, Daet and Legaspi. The affected areas in the Visayas region are Virac, Romblon and Masbate, Catrman, Tacloban, Guiuan and Mactan; while in the Mindanao region, extreme wind speeds are observed in the northernmost region, that is, in Surigao del Norte.

During 2001, a total of 17 tropical typhoons entered the Philippine Area of Responsibility (PAR). Reming (international name Xang Sane), with a peak wind speed of 300 km/hr and levelling down to 250 km/hr destroyed infrastructure worth US$ 19.3M (NCMC, 2001). The major reasons for this catastrophe is that Reming's wind speed exceeded the 200 km/hr maximum wind velocity, as indicated in NSCP (1998). Four other typhoons have recorded an average of 220 km/hr (NCMC, 2001), exceeding the value in NSCP (1992). The F-shelter design load criteria were based on the 1992 NSCP. The 2001 NSCP stated a maximum wind speed of 250 km/hr, so it is therefore imperative to know its actual capacity based on experiments.

Being an archipelagic country with 7,100 islands located in the so-called "typhoon alley of the world", the Philippines are exposed to very strong winds, especially during the passage of tropical cyclones. Figure 3.2 shows the frequency of the tropical typhoon passage around the

country for the period of 1948–2000. The northern part of the country is often the most devastated by typhoons. That is why residential houses are built in large scales in an effort to stand against typhoons. Furthermore, this area experiences the highest average wind speeds of 250 km/hr. The southern part of the country receives the least number of typhoons with an average wind speed of 125 km/hr. Hence, it is deemed necessary for the government to undertake measures that would help its 75 million Filipinos to undertake appropriate measures as well as structural and non-structural mitigation strategies to minimise the effects of extreme wind hazards.

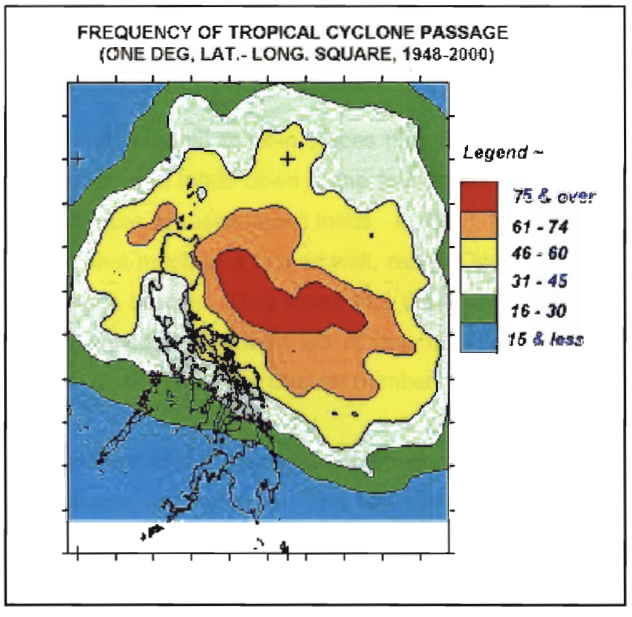

Figure 3.2 Frequency of Tropical Cyclone Passage (NCMC, 2001).

3.3 Experimental works

3.3.1 Introduction

Considerable research has been conducted to determine the behaviour of light-frame wood structures. This study contributes to the body of knowledge, using experimental work to determine particular details such as joint stiffness, lateral nail resistance, racking resistance of walls, entire F-shelter testing and a finite element model of the wall. Most of the available research does not aim to predict the total response of a structure, but instead provides behavioural characteristics of various components to achieve efficient and accurate solution techniques. In this section, some of the existing research is discussed with regard to the relevance of each project to this study.

This section discusses related literature that is relevant to this study and is divided into two parts. One relates to testing and the other focuses on the finite element modelling.

3.3.2 Metal brackets

Structural sheathing such as plywood, strandboard or particle board is essential for light-frame construction. Wall bracing is not usually required when these structural sheathings are used. In the absence of these structural sheathings, we see the skeletal form in the form of timber framing. However, if the sheathing is anticipated to lack in stiffness, reinforcements are needed to resist lateral loadings. In this project, we used metal stiffeners to reinforce the corners of the shear walls.

Structural sheathings and diagonal or let-in braces (Figure 3.3) installed in walls parallel to the wind flow, transmit lateral wind loads down to the foundation. There have been doubts about the efficiency of let-in braces to resist lateral loads. In 1977, Toumi and Gromala studied let-in bracing. They learned that much of a braced wall, racking strength is due to the interaction of board sheathing and let-in braces. They found that the 1" by 4" let-in braces used to support their unsheathed wall provided less than 2/3 of the 5200-lb value specified by the Federal Housing Administration (FHA) Technical Circular number 12.

Also, in 1983, Wolfe evaluated the structural contributions of 1" by 4" let-in bracing and metal strap bracing in light-frame wall systems. The test showed that each brace had an ultimate lateral resistance value of 600 lb. This means that it would take 9-1" by 4" let-in braces to provide the FHA minimum 5,200 lb lateral resistance in a wall. Furthermore, Dunagan from the Simpson Strong-Tie Company, Inc. (1999), showed that wood braces installed at 45 degrees failed at 1,125 lb, while braces installed at a 60-degree angle provided less resistance.

Tests conducted by Wolfe and Simpson Strong-Tie indicate that even metal bracing does not approach the FHA minimum standard of 5,200 lb. Wolfe's flat metal braces registered 1,500 lb of lateral resistance and Simpson Strong-Tie T-type braces resist a maximum value of 710 lb. Since their braces can only resist forces in tension, an X-configuration was proposed. Their tests' failure in metal braces generally occurred as a result of nail slippage or withdrawal. Therefore, size and the number of nails in braces add strength to the brace.

Clearly, metal let-in braces prevent walls from racking during construction and are not designed to replace shear wall load-carrying components. Use of these bracings may reduce stress concentrations on corners, especially on windows, or minimise cracks in plaster. Designers should carefully review designs on these let-in braces that exclude structural sheathings. Neither research nor mathematical predictions support the use of let-in wood or metal bracings in unsheathed walls (Fisette, 1997)

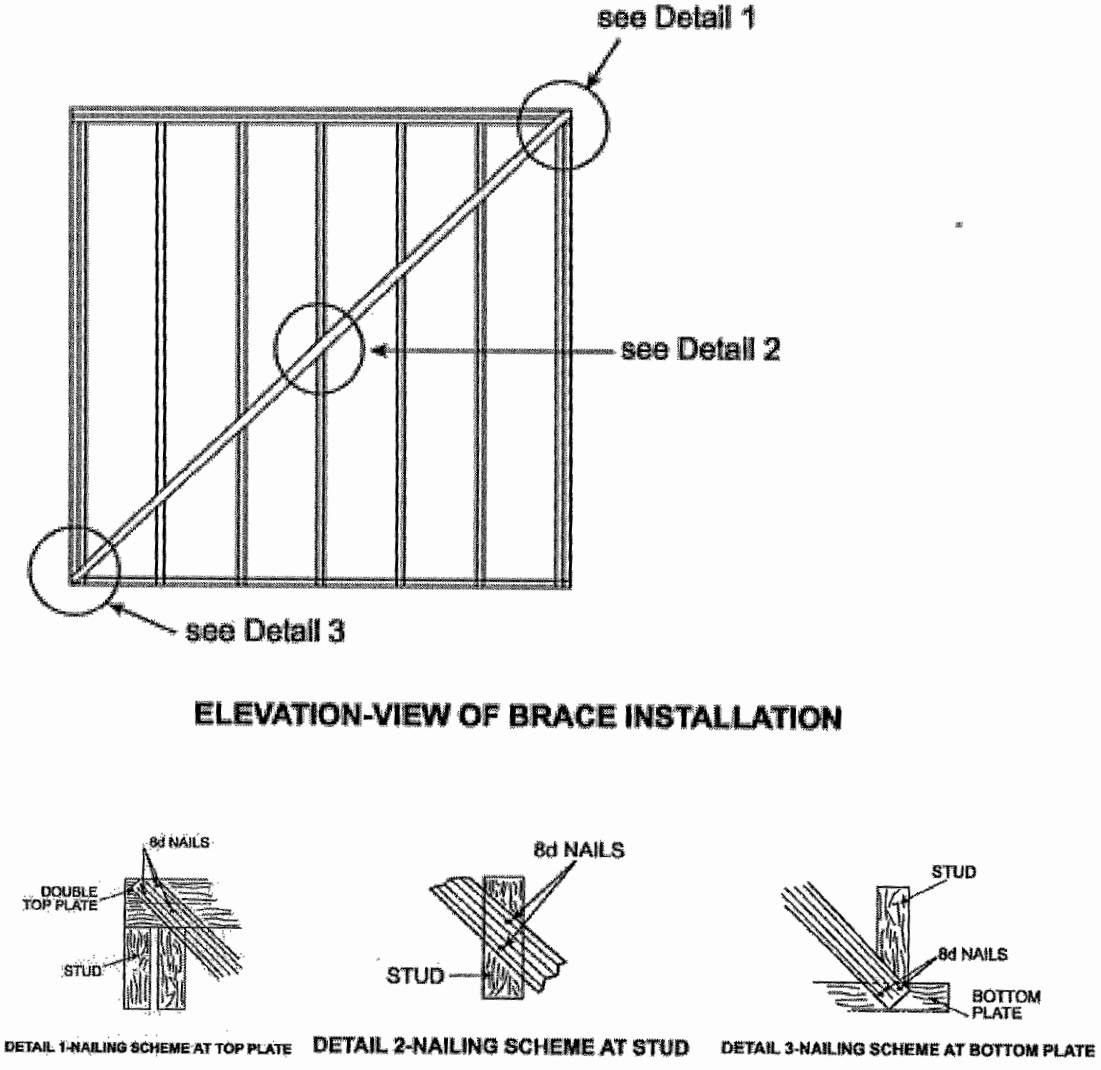

Figure 3.3 Elevation plan and joint details for a metal let-in bracket (www.icc-es.org 2006).

3.3.3 Shear wall testing

In this project, the performances of individual components such as shear walls and connections and their effect on the behaviour of the structure as a whole have been thoroughly examined. Component interactions play a major role in distributing loads to and from shear walls. The interactions depend upon component stiffness and connector efficiency.

In light wood construction the typical vertical elements in the seismic load path are shear walls. The shear walls are generally framed with vertical wood studs, and horizontal wood top and bottom plates. The wood framing is sheathed on one or both sides with several materials, such as plywood, oriented strand board, gypsum wall board or Portland cement plaster (stucco). The sheathing is nailed, stapled or screwed from the top to its base. The sheathing material is usually loaded in a state of "pure shear", which means sheathing can only resist racking. Other elements in the wall are designed to resist any vertical forces.

Wood-framed shear walls are primary lateral force-resisting elements in wood-framed structures. Traditional wall design requires fully sheathed wall sections restrained against overturning. Their behaviour is analogous to a deep cantilever beam with the end-framing members acting as flanges or chords to resist overturning forces, and the panels acting as a web to resist shear (Dolan and Johnson, 1997; Judd and Fonseca, 2002). This analogy is generally considered appropriate for wind and seismic design.

A remarkable body of literature exists concerning the lateral resistance of sheathed light-frame walls. As mentioned in the objectives (see Section 1.1 of Chapter 1) of the project, the project is to find out the ultimate load resistance (global stiffness) of the wall. There are three available methods to determine the lateral resistance of a wall; these are the quasi-static method, the pseudodynamic method and the shaking table method (Kausel, 1996). The method that was used in this project is the quasi-static test.

Most walls that were tested used the monotonic testing procedure recommended by ASTM, i.e., the load applied does not reverse and it is applied generally increasing fashion until failure occurs. ASTM E72 and ASTM E564 provide test procedures for shear walls but do not provide for the determination of allowable shears for design purposes. ASTM E72 is intended to provide comparative data for different construction elements or structural details and ASTM E564 provides methods for the determination of shear wall strength and stiffness.

Monotonic testing was the chosen method for testing shear walls because it provided a good indication of the performance under one-directional loading. Researchers like Toumi and Gromala (1977) evaluated the rate of loading, sheathing materials and let-in bracing, and

learned that racking strength is due to the interaction of board sheathing and let-in braces. Wolfe (1983) investigated the contribution of gypsum wallboard to the racking resistance of shear walls. He performed the test according to ASTM E564-95 (2000) to evaluate the influence of wall length, panel orientation and wallboard frame interaction. Wolfe found out that the racking resistance of walls with gypsum and structural wood panels was equal to the sum of the contributions of the elements independently.

It is noteworthy that researchers have attempted to compare different sheathing materials. Serrette *et al.* (1996)(from Jablin, 1995) compared plywood panels to 7/16" OSB panels subjected to static and cyclic loading. The test showed that the nominal capacity of plywood panels was approximately 17% greater than that of the OSB panels. Furthermore, plywood also exhibited a much greater deformation capacity at the maximum load.

Shear walls with openings are important to understand because most houses and buildings have openings in walls. In the F-house, ventilation is provided through the four windows and door opening. However, it was not in the scope of this study to evaluate the effects of openings in walls. Researchers like Fowler *et al.* (1982) (from Jablin, 1995) examined the effects of several parameters on the strength and stiffness of shear walls used in manufactured housing construction. The parameters studied included the size and configuration of the openings of the shear wall, and the size and location of the openings in the sidewall. They found that openings in the sidewalls had no effect on the distribution of the load and no significant increase in the strength for walls with panelling glued to both sides compared to walls with panelling glued to one side only. Nelson *et al.* (1985) continued Fowler's research. Johnson (1997) performed tests on shear walls with several aspect ratios, that is, walls with different opening orientations and the number of openings. From monotonic and cyclic tests, he concluded that the sheathing above and below openings could resist shear. Gypsum wallboard helps resist shear in the low to moderate loading but plywood resists most of the shear near capacity under monotonic loading. Sugiyama and Matsumuto's (1994) method to predict the behaviour of shear walls with openings was found to be conservative when compared to the full-scale tests, especially as the openings increased. Johnson's natural log prediction method proved to provide good predictions of the capacity and stiffness of the shear wall in both loading conditions. However, it should be noted that Johnson's results were based on limited data.

Other researchers have also investigated the overturning restraints on the performance of light-frame wood shear walls subjected to monotonic loading. Heine (1997) concluded that tie-down anchors enhance the overall performance of shear walls. Walls with no overturning restraints failed due to nail tear-through and stud separation along the bottom plate. These walls exhibited much lower stiffness and capacity than walls with overturning restraints. Rigid body rotation arising from uplift and separation along the bottom plate, occurred when tie-down anchors were used.

The current thinking is that the monotonic strength of shear wall system is sufficient, but that the sheathing and fastening systems capacities to resist earthquake or wind load are very critical and should be given greater attention. The shear wall should be able to resist cyclic loads and to dissipate energy (ductility). This is verified through a considerable amount of tests that were conducted by several researchers. By comparing the static and dynamic tests on standard 2.44 by 2.44 walls constructed of plywood or oriented strand board sheathing, Dinehart and Shenton (1998) found that the ultimate loads in the dynamic test are slightly less than those measured in the static test. However, the ductility of the wall, when measured dynamically, is between 34% and 42% less than the corresponding static ductility.

Some materials are more brittle (less ductile) than others and therefore will not perform well in an earthquake, even though their monotonic strength is adequate. The wwcb panels that were used as a major structural sheathing material for the F-shelter are suspected to be lacking in ductility. Their ability to resist shear and bending is a question under current investigation.

In recent years, there has been a move toward testing wood frame shear walls dynamically, using full reversed load cycles. This type of test is believed to be more representative of the load deformation history that the wall will experience during an earthquake, than the static or monotonic procedures outlined by ASTM E72 and ASTM E564.

3.3.4 House testing

The empirical work on full-scale testing is considered to be the most important component of this research. There are several studies that have conducted tests on an entire structure but none have covered experiments on foldaway shelters. Studies on whole-house tests of manufactured houses can be used as references. Some of these are as follows:

Stewart *et al.* (1989) tested a manufactured home, omitting all non-structural components. Prior to house testing, shear walls were tested according to ASTM E72-80 to determine individual stiffness to allow investigation on the load-sharing characteristics of the structure. The structure was then subjected to simulated lateral wind load. The displacements of the shear walls, the deformation of the structure as a whole and some failure modes of the structure were determined. The same parameters were obtained and the procedure was discussed in this study.

Another complete full-scale test was conducted by Philips (1990). He performed concentrated load testing on a small light-frame wood home. The purpose of his research was to evaluate the load-sharing characteristics of the structure. The structure was hand built and was representative of stick-built homes instead of manufactured homes. The house was tested in

various stages of its construction to determine the amount of load-sharing characteristics among various components. Philips found that only the roof system acted to distribute a concentrated load to different shear walls in the structure.

Another is the L-shaped house test conducted by CSIRO (Paevere *et al.,* 2000). The wood-framed house was subjected to static-cyclic loading. The purpose of the test was to measure the load distribution and deflected shape in detail in order to calibrate the finite element model. The global hysteresis response was characterised by ductile behaviour, pinching at the origin and degradation of strength and stiffness under cyclic loading. A limitation of the experiment is that all the observations are based on an unfinished house, which consists of the structural elements only.

3.4 Finite element models

3.4.1 Introduction

The finite element method is the implementation of a thoroughly formal mathematical theory for constructing approximate solutions to the partial differential equations occurring throughout engineering mechanics and physics. The implementation employs subdivision of the problem domain into a finite number of small regions called finite elements (Baker and Pepper, 1991; Schrobrich, 1990; ANSYS, 1998). The method was originally conceived by engineers in the 1950s to analyse aircraft structural systems using the scientific digital computer (Brauer, 1998). It has been applied to stress analysis and has been applied to other problems of continua such as thermal, electromagnetic, fluid and coupled fields (Cook, 1994).

The analysis begins by making a finite element model of the structure. The model is an assemblage of finite elements, with pieces of various sizes and shapes. The finite element model contains the following information about the structure to be analysed.

1. geometry, subdivided into finite elements
2. materials
3. excitations
4. constraints

3.4.2 Shear wall modelling

Several studies were conducted to create mathematical or finite element analysis (FEA) models for an entire building. Chehab (1982) developed a linear seismic analysis for a typical wood-frame house. Gupta and Kou (1987) developed a simple linear elastic building model containing seven "super elements" and nine global degrees of freedom to analyse the building tested by

Tuomi and McCutheon (1978). Currently, FEA modelling software was utilised to facilitate work as performed on manual numerical analysis. Kasal *et al.* (1994) used the ANSYS finite element software to analyse a one-storey light-frame house and was later verified by conducting tests of a full-scale house loaded cyclically. Goodman *et al.* (1996) developed a three-dimensional mathematical model for Crownpointe manufactured homes subjected to lateral loads and verified this by testing individual house components with the aid of modelling software. Jablin (1995) used interface elements to model manufactured homes using the POLO-FINITE software. Recently, He *et al.* (2001) developed a non-linear finite element model under static loading based on a mechanics representation of the load-deformation characteristics.

One study that also captured the attention of the author is that undertaken by Hite and Shenton (2002). They investigated the effect of vertical load on the static and cyclic lateral load. The shear wall is modelled using the ANSYS finite element program. The static non-linear behaviour of the wall, including the effect of the vertical load was modelled, and the result showed good correlation with the experimental results. Figure 3.4 shows the model of the wall. The main feature of the model was its modelling of sheathing to framing connections. They used two unidirectional springs to model the fasteners.

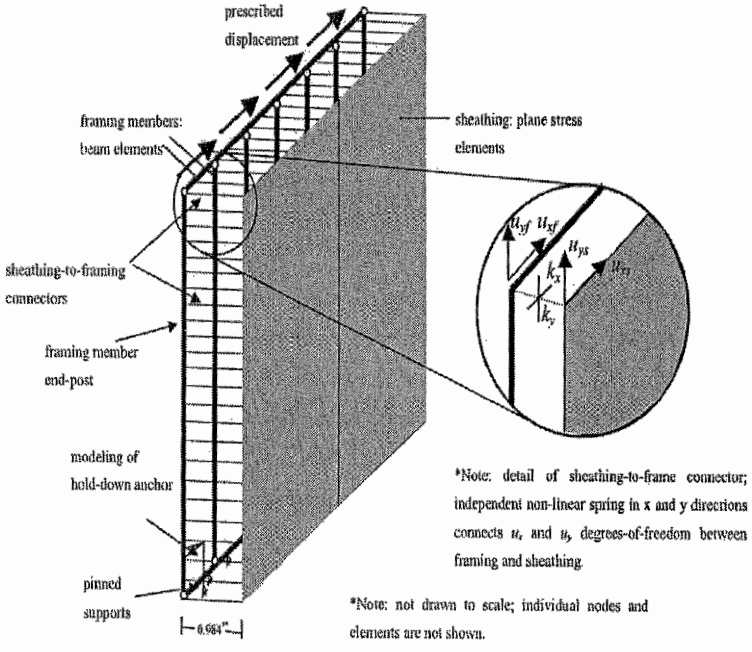

Figure 3.4 Finite element model of the wall (Hite and Shenton, 2002).

Kasal and Leichti (1992a) modelled and investigated the behaviour of an entire structure by modelling the roof/ceiling system as a semi-rigid beam supported by shear walls whose stiffnesses were approximated using American Plywood Association (APA) equations. When

compared to experimental results, the models produced reasonable results. They suggested that a more accurate method must be used to determine the stiffness of shear walls.

A numerical model developed by Folz and Filiatrault (2001) was incorporated into a computer program CASHEW (Cyclic Analysis of Shear Walls) and showed that it can accurately predict the load-displacement response and energy dissipation characteristic of wood shear walls. Their model is composed of three structural components: rigid framing members, linear elastic sheathing panels, and nonlinear sheathing-to-framing connectors.

In order to solve the problem of accurate shear wall stiffnesses, Kasal and Leichti (1992a) developed a procedure to transform a detailed finite element model of a wall into a less complex equivalent wall model. Figures 3.5 and 3.6 show a detailed model and an equivalent wall, as represented by Kasal and Leichti. By identifying the master degrees of freedom (DOF) that define the deformation of the wall, the equivalent wall was developed. Once these degrees of freedom were defined, the detailed wall was transformed to a set of four non-linear springs at each corner of the wall, with each spring representing one of the master DOF. The equivalent model produces results sufficiently close to the detailed model results. Although accurate, this procedure is not readily applicable to a general analysis and design program because the equivalent finite element models of the walls must be developed from the detailed finite element analysis. The modelling techniques presented can only be evaluated and quantified using a dependable full-scale test (Paultre and Proulx, 1997); that is why models are intertwined with experimental works for verification.

Following the research work of Kasal, and Kasal *et al* (1994) developed a model that combined all the previous work by Leichti, by using the ANSYS finite element software. The model of a full, single-storey structure uses super elements to approximate the roof and floor systems and quasi-super elements to approximate the shear walls and intercomponent connections. The results of analyses performed by this method agreed closely with the experimental results from full-scale tests on a one-storey 16' by 32' structure. Much like the Kasal and Leichti (1992b) work, this approach is not applicable to general finite element analysis, since quasi-super elements must be developed from detailed finite element models.

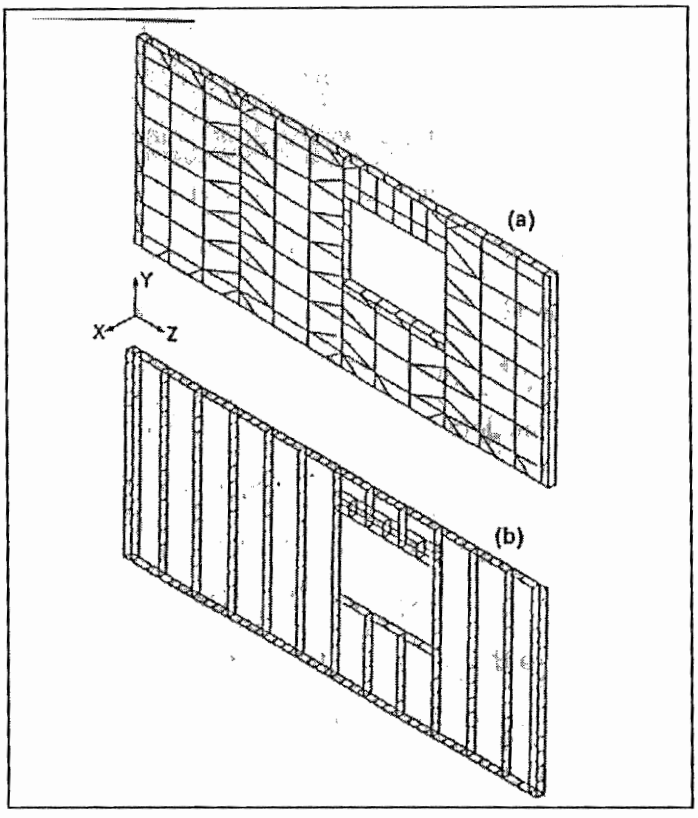

Figure 3.5 A detailed model of the wall; **a**. with sheathings and **b**. studs only (Kasal and Leichti, 1992a).

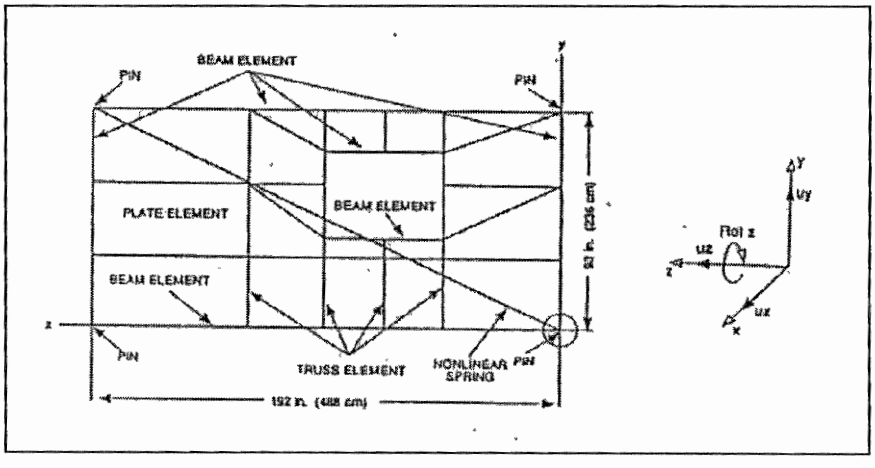

Figure 3.6 Equivalent wall (Kasal and Leichti, 1992a).

3.5 Summary

Relevant information on the Philippine condition of calamities has been presented. The fact is that the Philippines is a calamity-prone country in terms of earthquakes, typhoons, flash floods, and landslides.

Also presented is a review of the recent experimental works on metal let-in braces, timber-framed shear walls and whole-house testing. A considerable amount of work has been undertaken regarding tests on timber-framed walls, in contrast with tests done on whole-house testing. This is due to the costs involved in the specimen fabrication and instrumentations.

Furthermore, a review on the finite element modelling of timber-framed walls and whole-house modelling was undertaken. Two researchers works were found highly important and closely related to the study on hand. The first by Hite and Shenton (2002) on the modelling of the timber-framed wall, focusing on the non-linear behaviour of the sheathing-to-frame connector; and the second by Kasal and Leichti (1992b), wherein a complex model of the wall was simplified and behaviour of the complete house was modelled.

4 Materials and experimental procedures

4.1 Introduction

This chapter presents the materials used in this project, including properties that are essential in the development of the finite element models. Furthermore, detailed experimental procedures are presented in accordance with relevant standards.

The activities for the project are briefly summarised and presented schematically, as shown in Figure 4.1. The project involved experimental work and analytical modelling. Joint, wall component and whole-house tests were conducted. Negative and positive bending moments were performed on corner metal braces on the shear wall. The quasi-static method of loading was applied to the wall. The prototype F-shelter was tested using the quasi-static loading and shaking table.

Analytical modelling was performed in parallel with the experimental work. The finite element models were generated through the aid of the Swanson Analysis System (ANSYS), a general finite element analysis software. The predictive capabilities of the present numerical model are compared with the experimental results from the full-scale tests performed.

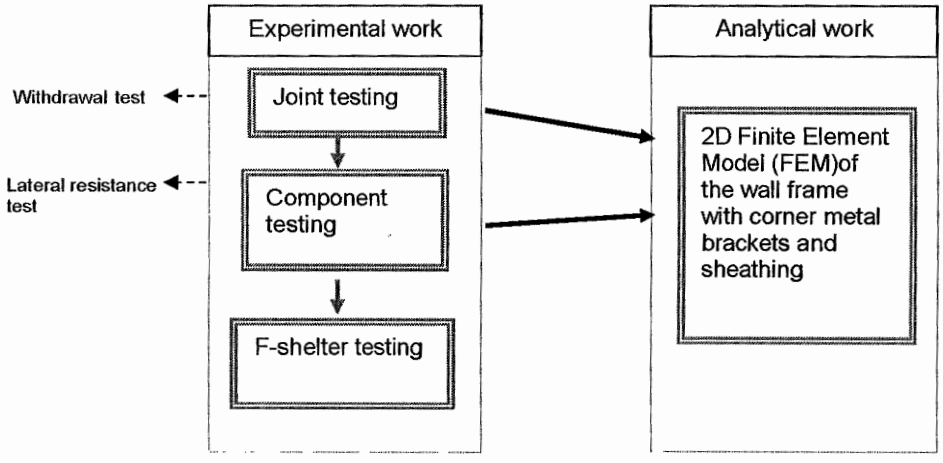

Figure 4.1 General flow of the project activites.

4.2 Materials

Table 4.1 presents a summary of the materials and related properties with the respective type of test performed. The accessories, instrumentation and equipment used are described in individual sections. Preliminary tests, namely, nail/screw withdrawal tests were performed to verify the results obtained from joint testing, and wall corner joints with metal brackets were tested to develop a model for this type of joint in the wall. Designed experimental works on timber-framed walls with uniaxial loading were implemented to calibrate the model.

Table 4.1 Summary of materials and properties.

	Materials	Type of test	Properties	
			MOE[a]	ν[b]
1	6G screw, 32 mm	Withdrawal test; ASTM 1761	200 GPa	0.3
	Ø3.39mm Galvanized nail, 25.46mm		200 GPa	0.3
	MGP 10 Radiata pine (45 x 90 x 150 mm)		10.5GPa	0.29
	Apitong (45 x 90 x 150 mm)		8.75 GPa	0.29
2	F11 softwood plywood (6 x 50 x 165mm)	Lateral nail resistance test; AS 1649-2001	10 MPa	0.29
	Medium density wood wool cement boards (8 x 50 x 165mm)		3 MPa	0.29
	Ø3.39 mm Galvanized nail, 25.46mm		200 GPa	0.3
	3.00mm Galvanized nail, 25mm		200 GPa	0.3
	MGP10 Radiata pine (23 x 50 x 165mm)		10.5 GPa	0.29
	Apitong (23 x 50 x 165mm)		8.75 GPa	0.29
3	Apitong timber frame	Uniaxial monotonic loading	8.75 GPa	0.29
	MGP10 Radiata pine timber frame		10.5 GPa	0.29
	Medium-density wood wool cement boards		3 MPa	0.29
	F11 softwood plywood		10 MPa	0.29
	Ø3.39 mm Galvanized nail, 25.46mm		200 GPa	0.30
4	F-shelter; Apitong framed and sheathed with wood wool cement boards.	Quasi-static test (non-destructive test) and shaker table test (destructive test)		

[a] Modulus of Elasticity

[b] Poisson's Ratio

4.3 Experimental procedures

4.3.1 Preliminary testing

The activities under the preliminary tests were conducted in order to supplement the data needed to develop the finite element model of the wall. In addition, they were aimed at verifying the results of the wall corner joint testing. The author found necessary to perform the withdrawal test due to the uncertainty of the result obtained from the wall corner joint testing.

The lateral nail resistance test was performed in order to obtain reliable data to be used in the development of the corner joint model.

The following sub-sections provide full details of the experimental procedures in accordance with recognised standards, as well as descriptions of the material properties and instrumentation.

4.3.1.1 Fastener withdrawal tests

Two fasteners were used in this type of test; the first is the 6G screw, 32mm in length and second is the ∅3.39mm, 25mm in length nail. The screw is fastened to an MGP10 Radiata pine wood prism and the nail is fastened to the Apitong wood prism. The test was performed in accordance with ASTM D 1761 (2000).

4.3.1.1.1 Screw withdrawal test specimen (Figure 4.2a and b)

The test provides the resistance of the wood specimen to the direct withdrawal of a single screw. The wood prism is fabricated from Radiata pine and the screw is 6G, 32 mm in length. Radiata pine and screw were used to find out if it could be an alternative frame and fastener for the shear wall.

Ten wood prisms were used, each having two screws driven in. A Radiata pine wood prism of 45mm by 90mm by 250mm and a bronze-coated screw of Gauge No .6 (2.8mm in diameter) 32 mm in length were used. The wood prism samples were taken randomly from five pieces of air-dried 45mm by 90mm by 3 m long Radiata pine. The lead holes were drilled in a bench drill to make sure that the holes would be made perpendicular to the surface of the wood. Two screws were threaded into lead holes approximately 10mm deep and 1.6 mm in diameter (Ø0.5). One screw was threaded into the tangential surface and the other to the radial surface. The average penetration of the screw was measured as 26 mm; this was based upon the measured average protruding length of 6 mm, inclusive of the screw head. The screws were threaded into the tangential surface at a distance of 82 mm from the end and 22.5 mm from the edge, and 82 mm

from the end and 45 mm from the edge in the radial surface. The screws were threaded manually using a No.2 Philips recess. Figure 4.2 shows the assembly and dimension of the specimen and screw positioning.

4.3.1.1.2 Nail withdrawal test specimen

Ten wood prisms were used, each having two nails driven in it. Apitong wood prisms of 23 mm by 68 mm by 250 mm and galvanised nails ∅3.39 mm by 25.46 mm in length were used. The wood prism samples were taken randomly from the actual wall frame. The rough edge of the prism was planed; that explains why the thickness is limited to just 23 mm. One nail was driven into the tangential surface and the other to the radial surface. The average penetration of the nail was measured at 20.46 mm; this was based upon the measured average protruding length of 5 mm, inclusive of the nail head. With respect to positioning, this is the same for the screws. The screws were threaded into the tangential surface at a distance of 82 mm from the end and 22.5 mm from the edge, and 82 mm from the end and 45 mm from the edge in the radial surface, as shown in Figure 4.2.

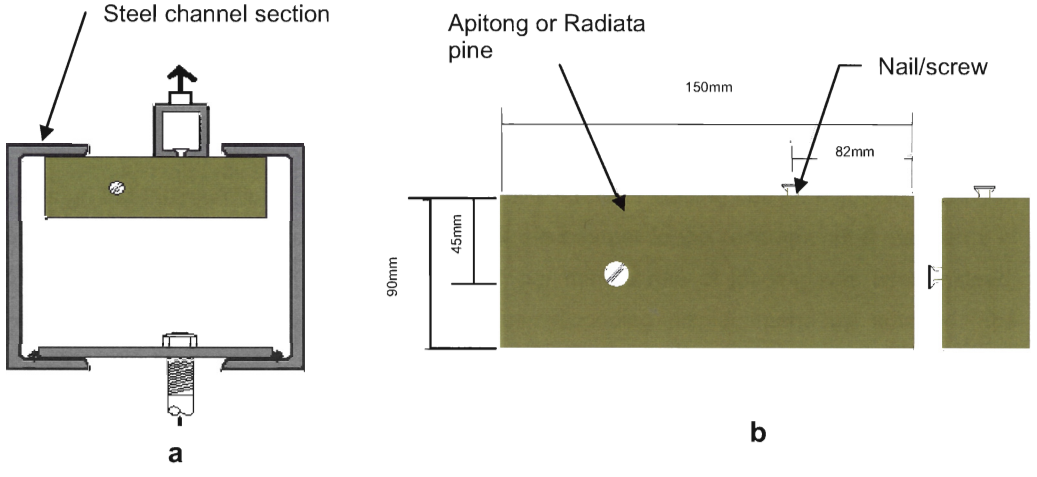

Figure 4.2 **a**. Assembly for screw withdrawal test and **b**. Dimension of the timber and location of the screw.

4.3.1.1.3 Procedure

The screw or nail was withdrawn by applying an axial tensile load at a uniform rate. Figure 4.2 presents the whole actual set-up of the screw withdrawal test. The specimen was firmly supported by two steel channels that were welded on the interior base side of the flange to form a U-shaped support. The support was constructed with a steel section so that there would be

no movements on the specimen. The line of loading and the threaded bolt connecting the support from the machine were aligned. This is to prevent accidental moment force induced from the withdrawal. A fabricated gripping device (Figure 4.3) made of four metal steel plates welded together was fitted to the base head of the screw. A groove and a countersunk 4 mm-diameter hole were located on the centre to fit the screw or nail to the device.

Figure 4.3 Fabricated gripping device with screw on centre

Although the Instron mini-Universal testing machine's rate of loading can be adjusted, it can not be set to lower than 5mm per minute, which is the nearest to the recommended standards of 2.52mm ± 25% per minute. Hence, the 5mm per minute rate of loading was used instead. Records for the maximum tension with the corresponding displacement are noted on the boards, while the load and displacement readings were recorded at a rate of 10 readings per second.

4.3.1.1.4 Instrumentation

The specimens were set up on the model 1026 Instron testing machine. The schematic diagram of the machine is presented in Figure 4.4. The machine consists of a fixed frame and a horizontal bar, called the crosshead, which can be either raised or lowered by turning the two threaded rods which support it. The test sample, which is attached to the fixed frame and the crosshead, experiences a deformation as a result of the crosshead motion.

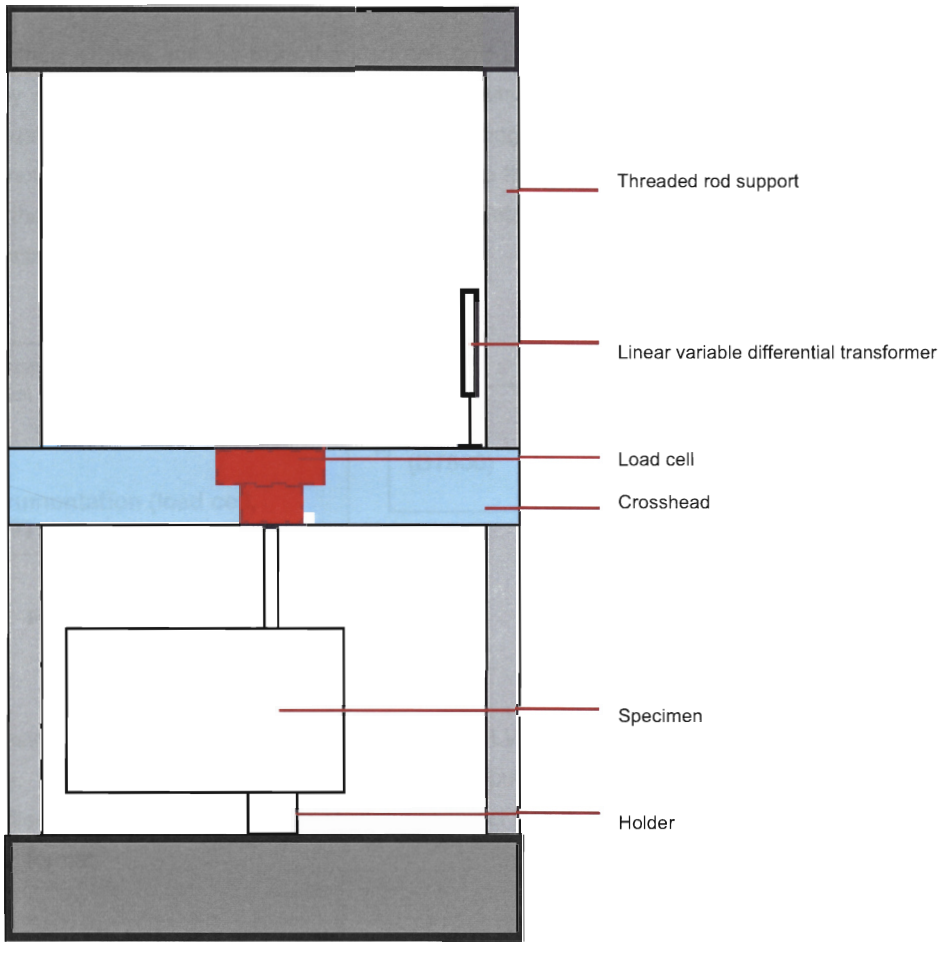

Figure 4.4 Schematic diagram of the Instron testing machine

The remaining parts of the testing machine consist largely of instrumentation for characterising the deformation of the test sample. A force sensor called the load cell measures the force exerted by the machine on the sample. The load cell, which is usually rated by the maximum load it can withstand, converts the sensed force into an electric signal.

A Linear Variable Differential Transformer (LVDT) of 300 mm travel range was used to measure the crosshead movement that also corresponds to the displacement measurement on the sample. The LVDT is an electromagnetic device that produces an electrical voltage proportional to the displacement of the movable magnetic core. As shown in Figure 4.4, the LVDT is installed just above the crosshead of the Instron testing machine. With this, a reference point was also installed.

The electrical signals coming from the load cell and LVDT are then transformed into digital output by a stand-alone data logger with analog inputs, digital I/O, voltage/current excitation, alarms, data storage, and time-stamping. The data logger can be left alone to collect data by itself remotely, or may be linked via RS-232/RS-485 to the computer. The digital output is read through the computer screen. Figure 4.5 shows the interconnectivities of the testing machine, instrumentations and computer.

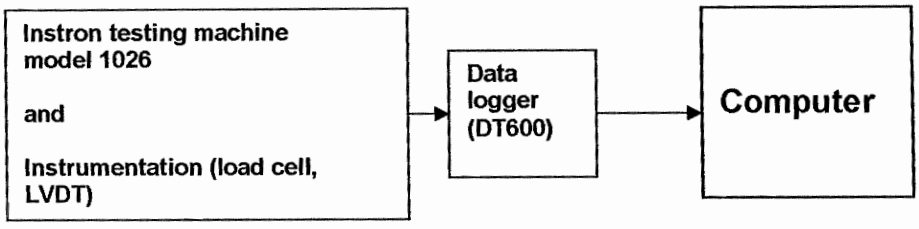

Figure 4.5 Schematic diagram of the test.

In the Instron testing machine, the load cell and the LVDT are connected to the DT600's two channels. An RS 232 connects the DT600 to the computer. Outputs in the computer are stored in data files. The data files are then changed to Excel files in order to transform the data to a graphical format.

4.3.1.2 Lateral nail and screw resistance test

The purpose of this test is to obtain reliable data to be used in modelling the sheathing-to-frame connection.

The test procedure determines the resistance to lateral movement offered by two nails in wood and sheathing material. The test is limited only to the materials and the size of nail used in the F-shelter. The sheathing materials are wood wool cement boards (wwcb) and F11-softwood plywood. The test procedure was performed in accordance with the Australian Standard 1649-2001; Timber – Methods of test for mechanical fasteners and connectors – Basic working loads and characteristic strengths.

4.3.1.2.1 Specimen

There were 10 samples for each type of sheathing having two nails driven on opposite sides, as depicted in Figure 4.6. The sheathing material was randomly obtained from 4–600 mm by 2400 mm wwcb and four 1200 mm by 2400 mm plywood panels. Others were obtained from the cut-

outs from the actual wall specimen. The finished sheathing dimension is 50 mm wide and 165 mm high. The wood prism, where the sheathing is fastened, is 23 mm by 50 mm by 165 mm. It is important to note that no lead holes were provided to drive the nails through the sheathing and the wood prism. This is to realistically simulate what happens in the field.

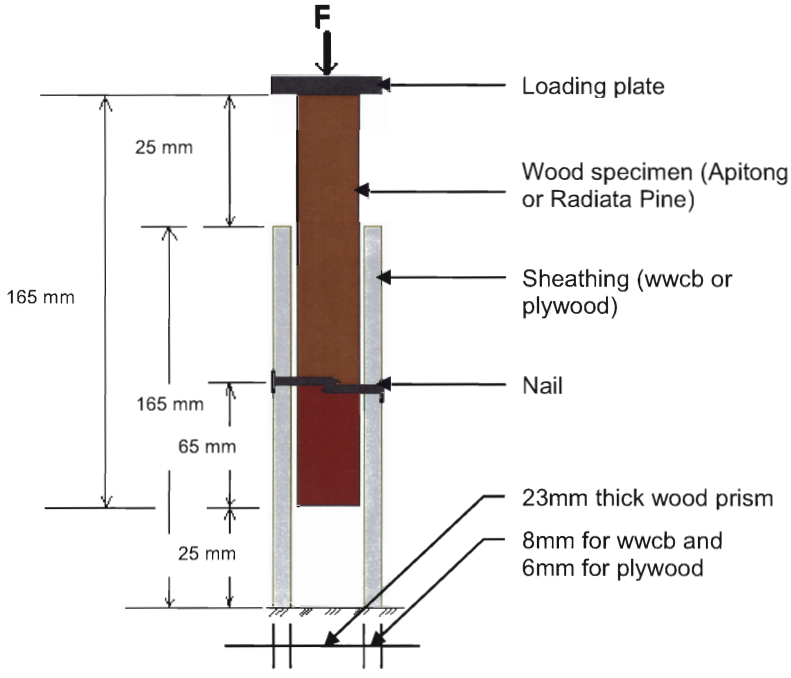

Figure 4.6 Schematic diagram for lateral resistance test

Each type of sheathing material has a corresponding nail type that was used. For the wwcb, galvanised iron-coated nails ∅3.39 mm by 25.46 mm in length and gauge no. 6 clout nails (25 mm by 3 mm) were used for the softwood plywood.

The assembly of the fastener (nail) in the specimen has a total overlap of 12 mm. Although this is not recommended by the AS 1649, such is the case in the actual construction of the F-shelter. Offsets in the nailing pattern in the actual wall were observed to a maximum of 10 mm. Furthermore, the minimum penetration of the nail which is 6 ∅ was not attained with wwcb sheathing and the suppliers recommended fastener; longer nails would have protruded on the opposite side that will cause splitting of the timber frame.

4.3.1.2.2 Procedure

The specimen was tested a day after it was assembled. Instead of applying tensile load as suggested by ASTM 1761, a compressive load was applied as suggested by AS 1649. A 50-tonne universal testing machine (UTM) was used to apply the compressive load at a rate of 2.54

mm per minute. The rate of loading was observed first before any test was conducted. Figures 4.7 and 4.8 depict the set-up for the wood wool cement board and plywood sheaths, respectively.

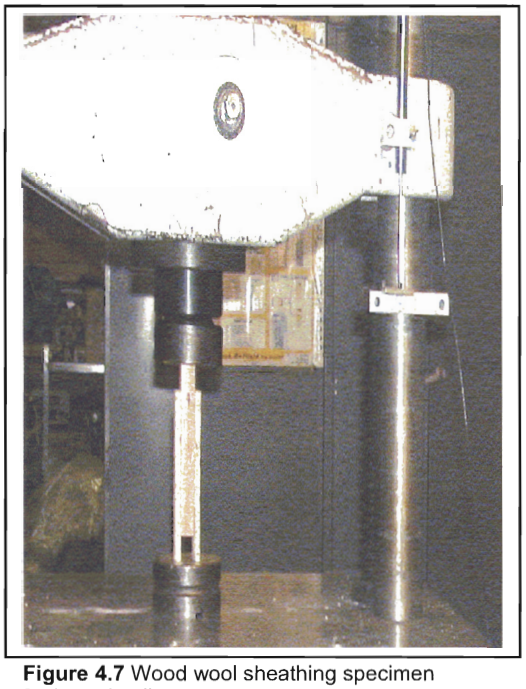

Figure 4.7 Wood wool sheathing specimen for lateral nail resistance test.

Figure 4.8 Plywood sheathing specimen for lateral nail resistance test.

Using a tri-square, it was ensured that specimens were at right angles when the load was applied. A spherical seat or head (Figure 4.9) was used to evenly distribute the load to the specimen just in case there was an uneven surface on the wood prism. No lateral support was provided to simulate the real wall-sheathing constraint condition when applied with an external load.

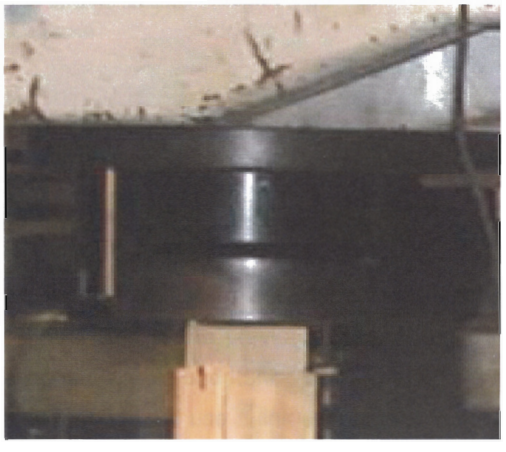

Figure 4.9 Spherical seat fitted in the UTM.

4.3.1.2.3 Apparatus

The test specimen is positioned in the 50-tonne Universal Testing Machine (UTM) which applies the compressive load. Deflections were measured using an LVDT. The data logger (Data Taker model DT600) recorded load and deflection reading outputs. The UTM and LVDT are linked to the data logger, using RS-232 ports.

The UTM load range was adjusted to the lowest load range of 20 kN to provide more sensitive readings. The machine consists of a fixed frame and crosshead that can either be raised or lowered. The specimen is fitted between the crosshead and the base of the UTM. At the crosshead, an LVDT was fitted to measure deflection of the specimen, as seen in Figure 4.10. An LVDT stopper was fitted to the vertical frame as a reference point in the deflection reading. A 10mm calibration block was chosen because the anticipated maximum deflection of the specimen would be less than 10 mm.

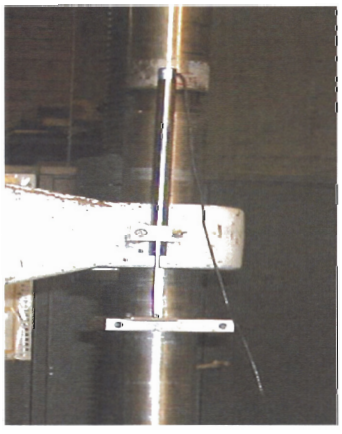

Figure 4.10 LVDT that is used to measure deflection.

4.3.2 Wall corner test with metal brackets

4.3.2.1 Test specimen

The primary reason for this test is to determine the stiffness of the corner frame through experimental work. As stated in the previous chapter, most shear walls are modelled using rigid-pin end connections (Tarabia and Itani, 1994; He *et al.*, 2001). The difference between this research and theirs is that this will use a link element on frame corners. This is the presumed effect of the metal braces at corners. Figure 4.11 shows the F-shelter's typical wall framing with the corner metal brackets.

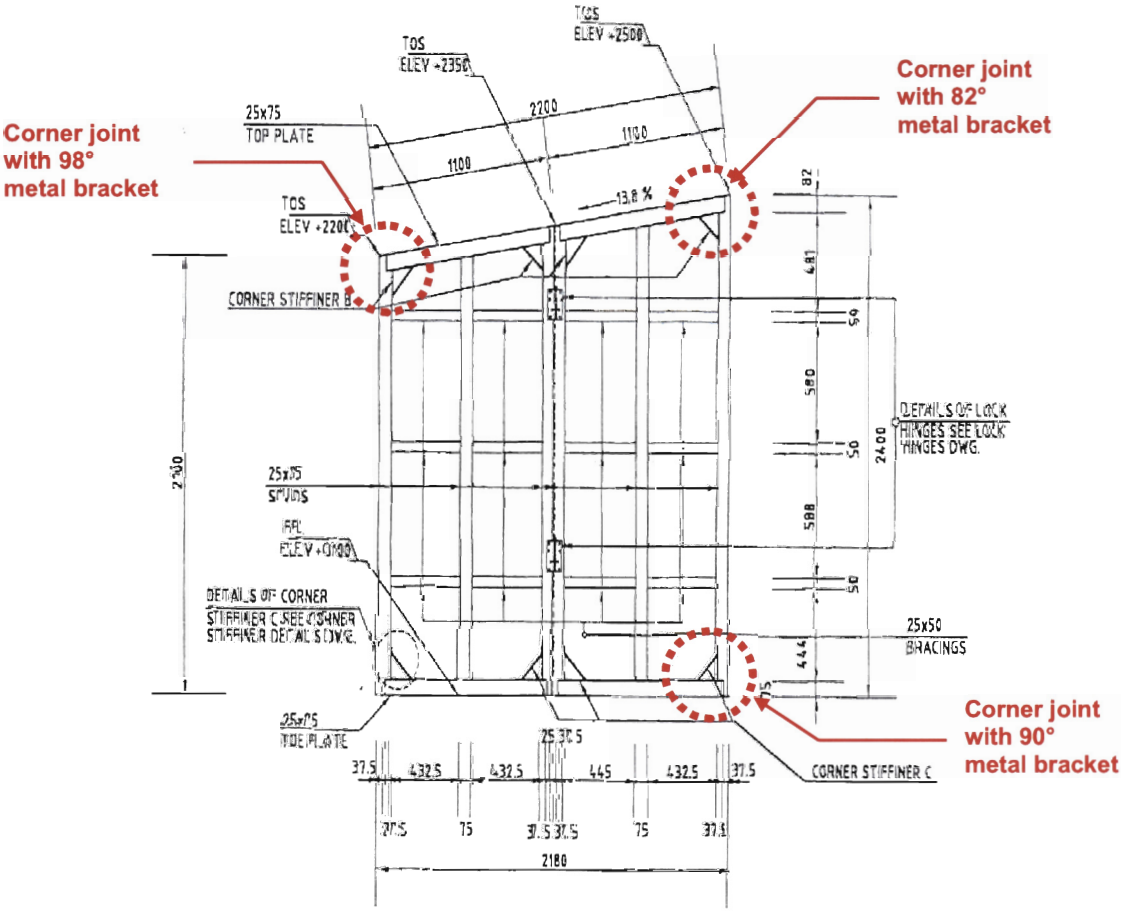

Figure 4.11 Location of the corner metal brackets in the wall frame.

The typical wall corners without an opening have four corner metal brackets. These are two 90-degree angle brackets; one 82-degree and one 98-degree angle, as shown in Figure 4.11. These metal brackets are constructed of 3mm thick steel plate with yield strength of 240 MPa, bent or formed to the desired angle, as indicated above. A 5 mm-diameter diagonal structural steel rod of the same yield strength was fully welded to the bracket to provide stability. Shown in Figure 4.12 are joint corners with the corresponding let-in braces assembled for testing.

Timber frames were made from Apitong and MGP10 Radiata pine. Two sets of test specimens were made; one was Apitong and the other was MGP10 Radiata pine. There were 18 specimens for each species, six specimens for each angle–brackets. Furthermore, a different type of fastener was used for each species. For Apitong, galvanised nails ∅3.39 mm by 25.46 mm in length and bronze-coated screws of Gauge No.6 (2.8 mm in diameter) of 32 mm in length for Radiata Pine were used. No lead holes were provided. Nails were driven manually using a claw hammer and screws were driven using a battery-powered screwdriver. These procedures

were implemented as in the actual construction scenario. Presented in Table 4.2 is a summary of the number of specimens with regard to the type of brackets used.

Table 4.2 Number of replicates for each joint type.

Angle (degree) for the metal bracket	**Timber frame with corresponding type of fastener**		**Total**
	Apitong and nail	Radiata pine and screw	
82	6	6	12
90	6	6	12
98	6	6	12

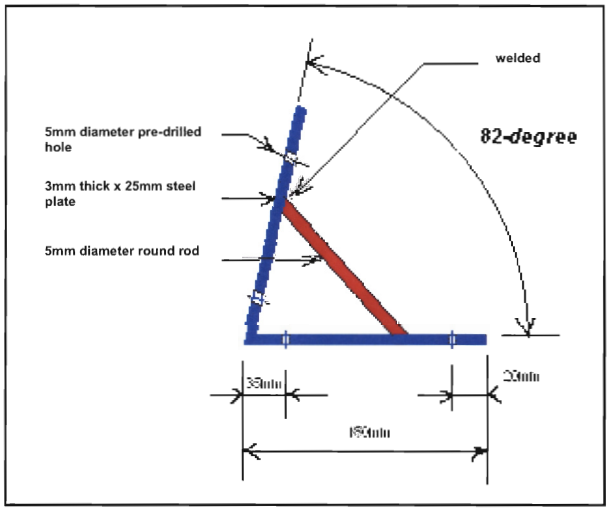

a

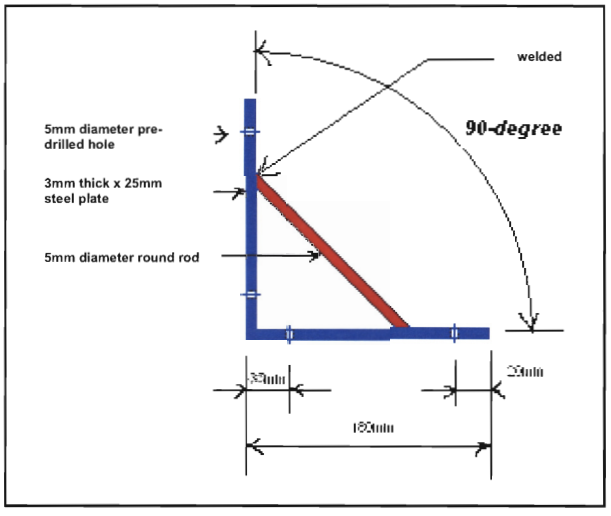

b

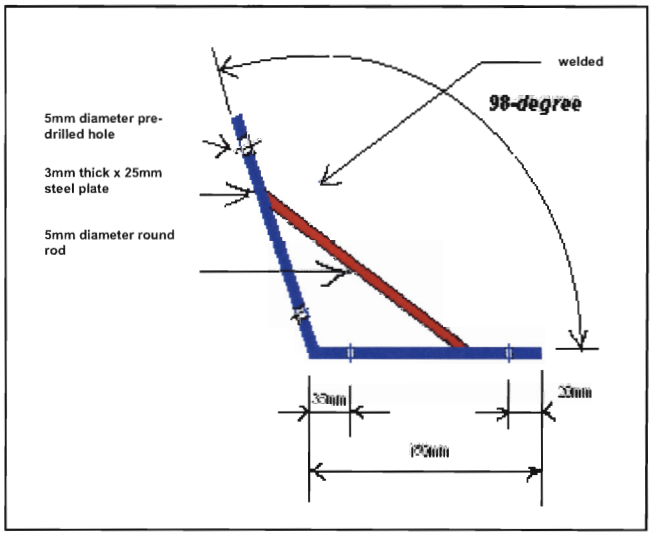

c

Figure 4.12 Schematic diagrams of structural grade corner metal brackets; **a**. 82-degree angle metal brackets, **b**. 90-degree angle metal brackets, and **c**. 98-degree angle metal brackets.

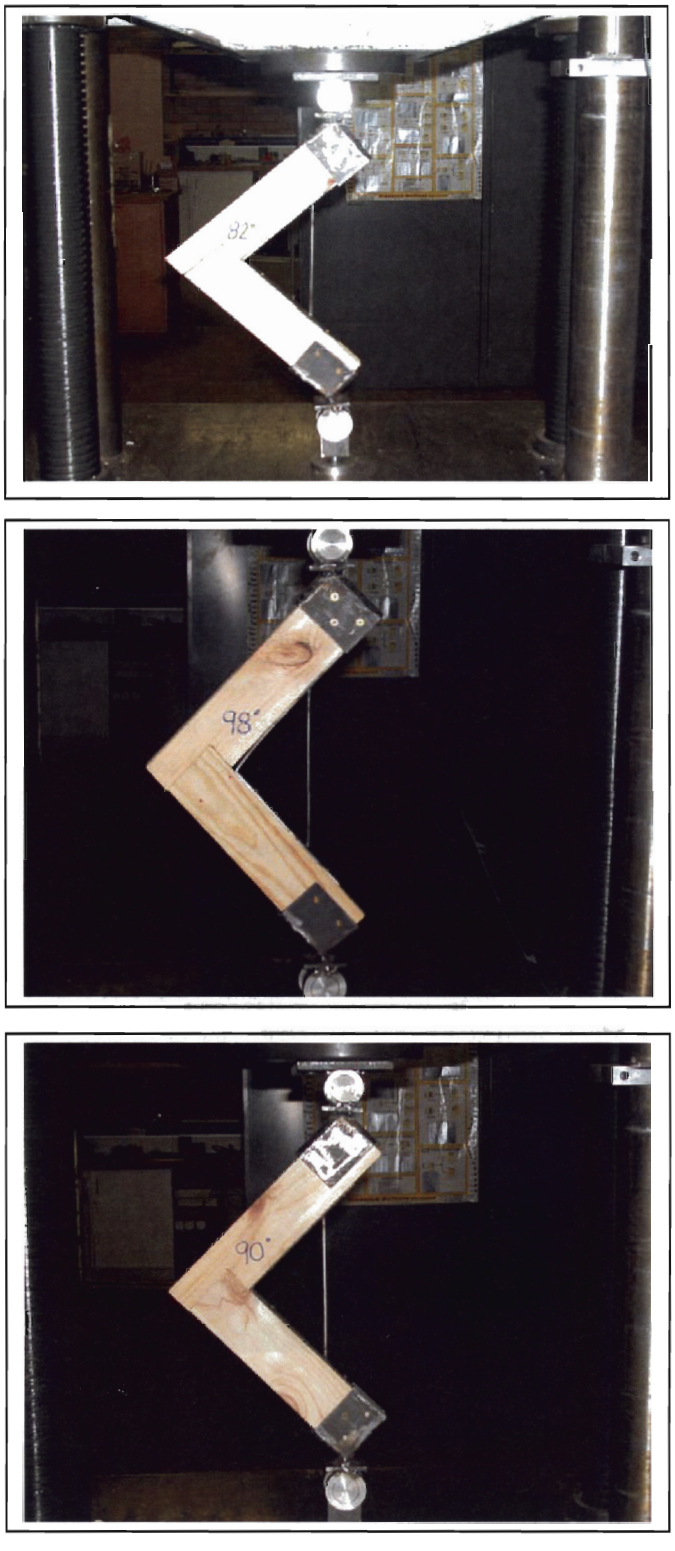

Figure 4.13 Actual wall corner joint specimens with timber frame and metal brackets; **a**. 82-degree corner joint, **b**. 90-degree corner joint and **c**. 98-degree corner joint.

4.3.2.2 Procedure

4.3.2.2.1 Assembly

A 300mm long piece of timber from each tested wall frame was obtained. It was ensured that no damage was present on the piece of timber. Using a hacksaw, each piece was cut in two and formed into 82-degree, 90-degree and 98-degree corner joint fastened with 2-50mm bullet nails. Although this is not recommended as a way of connecting timber frames, especially using nails on the end grain, this was used to temporarily hold the two pieces in place while the metal brackets are connected. Lead holes of Ø2mm were provided to prevent splitting of the timber.

Metal brackets were then fitted inside the corner and connected using either nails for the Apitong frame or screws for the Radiata pine. A claw hammer was used to drive the nails and screws using a battery-powered screw driver.

4.3.2.2.2 Testing

The assembled corners joint were then fitted with specially made connectors (Figures 4.14 and 4.15) to fit the desired type of testing. These connectors were fabricated from 5mm thick metal plates formed into rectangular u-shaped holders. Pre-drilled holes of Ø5mm for screws were provided on the metal plates in staggered location. A lubricated hinge was welded at the base of the u-shaped metal plates to act as a pin connection for the specimen. This type of connection allows rotation on the z-axis of the bottom part of the specimen and rotation on the z-axis and translations on the y-axis of the top connection.

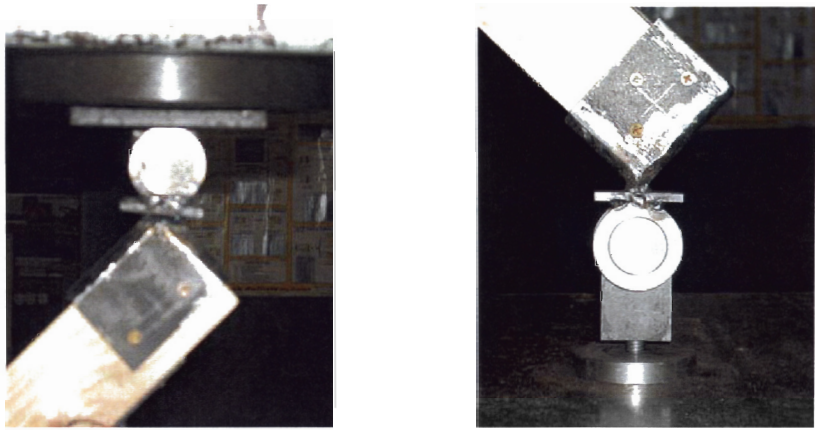

a **b**

Figure 4.14. Connection fittings used for the compression test; **a**. top connection and **b**. bottom connection.

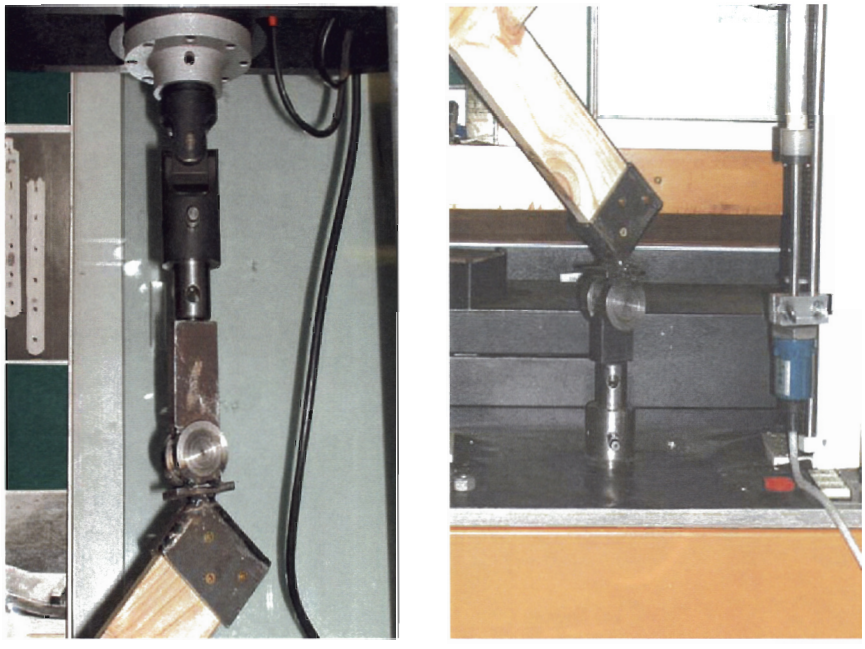

a b

Figure 4.15 Connection fittings used for the tension test; **a**. top connection and **b**. bottom connection.

Two types of tests were conducted. The first was in compressive load and the second was the tensile load. The compressive load was applied using the UTM and the Instron was used for the tensile load. Fittings of the UTM for tensile loading were not available at the time when tensile test was done. The complete test set-up for compressive load test is presented in Figure 4.16. The specimen was fitted in the UTM. Compressive load was applied to the specimen at the rate of 5 mm per min.

The UTM load range was adjusted to the lowest load range of 20 kN to provide more sensitive readings. The machine consists of a fixed frame and a vertically traversing crosshead. The specimen was fitted between the crosshead and the base of the UTM. At the crosshead, an LVDT was fitted to measure deflection of the specimen, as shown in Figure 4.10. An LVDT stopper was fitted to the vertical frame as a reference point for the deflection reading. A 10mm calibration block was chosen because the anticipated maximum deflection of the specimen would be less than 10mm.

Deflection was measured by an LVDT that was connected to the UTM crosshead with a reference point connected to the vertical frame of the machine. The LVDT was calibrated using a 10 mm calibration block. All compression tests were completed first before proceeding to the

tensile tests. Photographs were taken during the experiment to note any significant changes or deformation of the joint system.

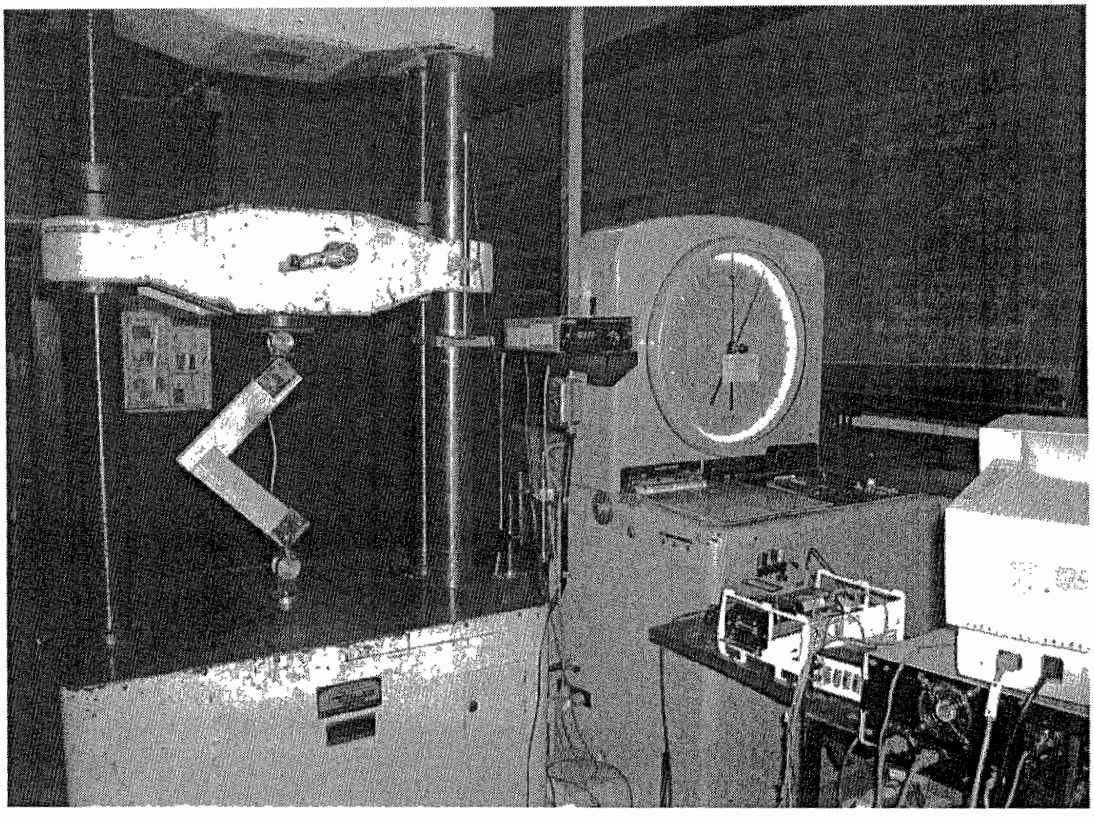

Figure 4.16 Compression test set up on the UTM for a corner joint with a metal bracket.

All tension tests were performed on the Instron model 1026 machine. The test set-up is shown in Figure 4.17. The machine crosshead was gradually raised to obtain the desired height to the specimen. A 5mm per min rate of loading was chosen.

Deflection was measured by an LVDT connected to the UTM crosshead with a reference point connected to the vertical frame of the machine. The same calibration procedure was followed in this test. Photographs were taken during the experiment to assess/evaluate joint deformations.

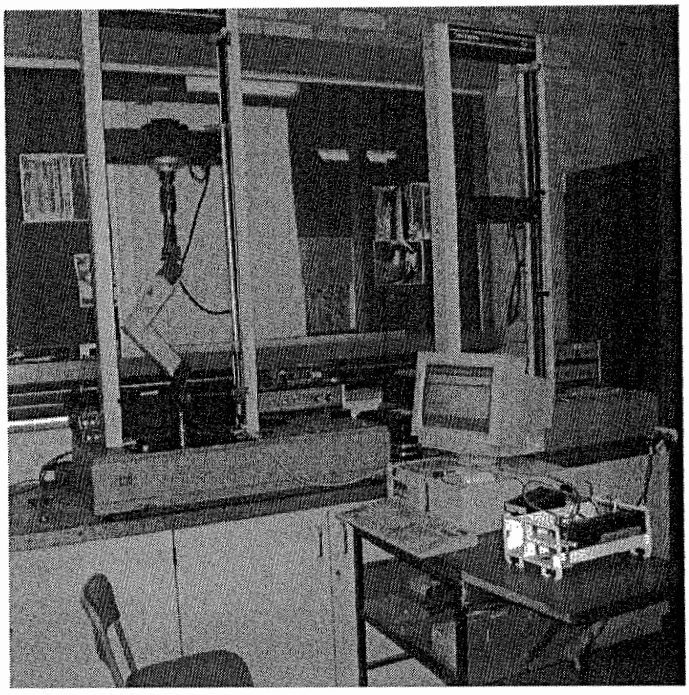

Figure 4.17 Tension test set-up on the Instron for a corner joint with metal brackets.

4.3.2.3 Instrumentation

A similar set-up of the instrumentation was used for the withdrawal test and lateral resistance test for fasteners in Section 4.2 of this Chapter. However, different gripping mechanisms (Figure 4.14 and Figure 4.15) were used to suit these types of experiment. Schematic diagram of the test is similar to Figure 4.5. However, UTM was used for the compression test instead of the Instron machine.

4.3.3 Monotonic test on wall

As mentioned in Chapter 1, the main purpose of this experimental work is to calibrate the non-linear behaviour of the finite element model of the wall, and also to find other alternatives for sheathing. For example, 6mm plywood is used here because of its abundant supply in the Philippines.

This sub-section of the chapter describes the test specimens and testing procedures. A short discussion of the materials, construction details, instrumentation and data acquisition system are also included. This section also identifies the important shear-wall parameters that define the behaviour of the specimen when externally loaded.

4.3.3.1 Introduction

Five wall frames without sheathing and five wall frames with sheathing were tested using monotonic load. Table 4.3 presents a summary of the specimens and corresponding test numbers. Two timber frames were used, namely, the Apitong frame, which is found locally in the Philippines, and Radiata pine. Radiata pine was chosen because of the closeness in density values. The Apitong frame was sheathed with eight pieces of 8mm thick by 600mm by 2,400mm medium-density wood wool cement board panels and the Radiata pine was sheathed with 4 pieces of F11 6mm thick by 1,200mm by 2,400mm plywood panels. The walls were sheathed on both sides. The walls were all trapezoidal in shape and have a dimension of 2,400 mm for height 1, 2,100mm for height 2 and 2,180mm for length, as shown in Figure 4.18. The wall specimens are made up of two wall segments which are assumed to be rigidly connected by 5pieces of 50mm by 160mm by 3mm thick fabricated steel hinges. The other three hinges, located at the back of the frames are not shown in Figure 4.18. As a result, this joint connection is rigid, forming a complete whole section of the wall. The wall frames are either made from seasoned Apitong or Radiata Pine.

Table 4.3 Number of tests and specimen labels for various wall frame.

SPECIMEN	Number of Tests	Specimen label
Apitong wall frame	3	A1,A2 and A3
Wood wool cement board with Apitong frame	3	W1,W2, and W3
Radiata pine wall frame	2	R1 and R2
Plywood (softwood) with Radiata pine frame	2	P1 and P2

Legend: A – Apitong; W – wwcb; R - Radiata pine; P - plywood

4.3.3.2 Specimen

Two types of sheathing materials were used for wall specimens. Although plywood is most widely used in construction, the performance of the wood wool cement board, as FPRDI promotes this as a substitute to plywood sheathing in some applications. A list of the sheathing materials with their respective nail size and nailing schedule is provided in Table 4.4.

Table 4.4 Sheathing materials and nailing schedule

Sheathing		Nails	
Material	**Thickness (mm)**	**Type (diameter x length, mm)**	**Spacing (o.c.)**
Wood wool cement board	8	3.39 x 25.46	150 mm
F11 Softwood plywood	6	2.80 x 25	150 mm

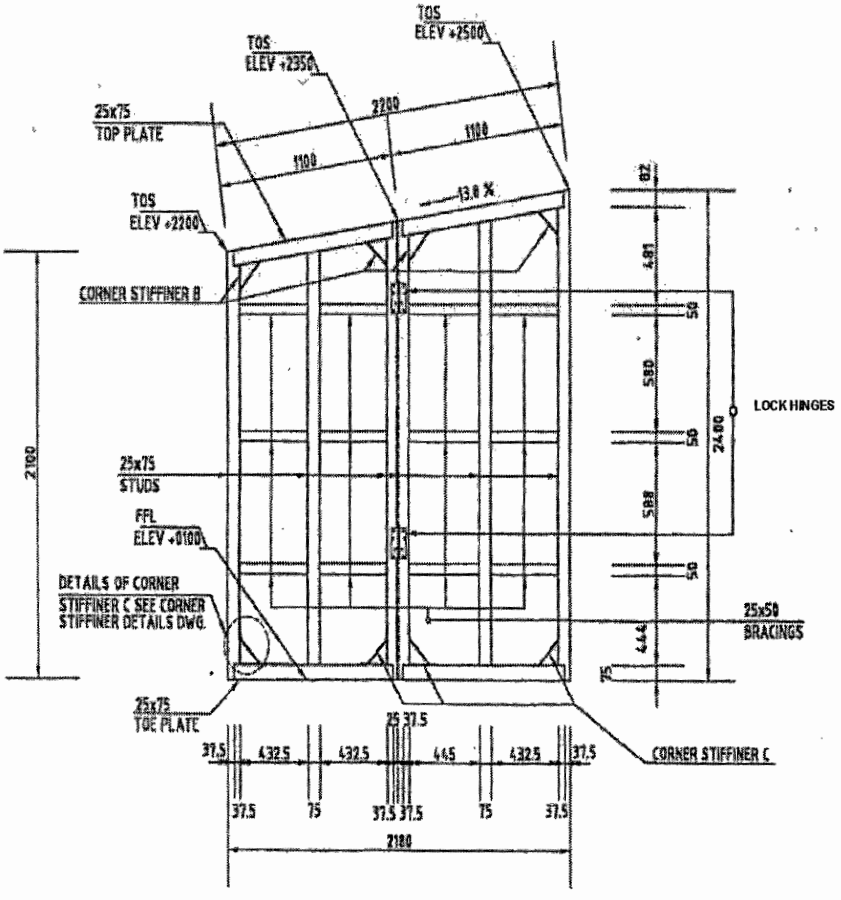

Figure 4.18 Typical wall framing for the wall specimen.

4.3.3.2.1 Sheathing panels

4.3.3.2.1.1 Wood wool cement boards

The most popular Cement Bonded Boards (CBB) in the Philippines is the wood wool cement board (wwcb). This is a panel product made of shredded wood about 30 cm long, ordinary Portland cement and a cement-setting accelerator such as calcium chloride mixed with water to

hasten the hardening of the cement. The wwcb is composed of 45% shredded wood, 55% Portland cement and 5% cement hardening accelerator.

4.3.3.2.1.2 Plywood

Probably the most common structural panel board that is currently used in construction is plywood. In this study we used F11 stress-grade structural softwood plywood. It bears the identification code 7-24-03, manufactured by ECOPLY, Australia. The plywood has a nominal thickness of 7 mm. The veneer surface grades are C on the face and D on the back veneer. The bond type of the glue line is A bond (AS/NZS 2269, 1994).

4.3.3.2.2 Timber framing

4.3.3.2.2.1 Apitong

The Apitong species is classified as M10 with a Modulus of Elasticity (MOE) of 8.75 GPa based on the new lumber grading system formulated by the Forest Products Research and Development Institute (FPRDI) in collaboration with the International Tropical Timber Organization (ITTO) (Soriano *et al* 2004). This timber frame was used with the wwcb panels.

4.3.3.2.2.2 Radiata Pine

A machine-graded pine (MGP) 10 Radiata pine was used as the timber framing for the plywood sheathing. This has an MOE of 10 GPa.

4.3.3.2.3 Frame-to-sheathing connectors

Two types of nails were used in the walls. A 3.39mm by 25.46mm nail was used to connect the wwcb to the Apitong frame, and 2.80mm by 25mm galvanised clouts to connect the F11 plywood to the MGP10 Radiata pine timber.

4.3.3.3 Construction method

4.3.3.3.1 Apitong-framed wwcb

The Apitong-framed wwcb boards was constructed in the Philippines. These were shipped to the University of Technology Sydney, Australia. There were three bare wall frames and three frames sheathed on one side. The purpose of putting the wwcb panels on one side is because of the initial plan to bore a hole in the bottom plate of the wall for the M12 structural bolts. Installation of sheathing on one more side took place in the Structures Laboratory of UTS. All

wwcb panels were pre-cut to size and numbered accordingly to be fitted on a particular frame. The wall was laid on a level floor with ample space to install the wwcb panels. All panels were laid first and were temporarily nailed on four corners. Nails were spaced at 150mm on centre and 25mm edge distance. These spacings were also done during construction.

4.3.3.3.2 Radiata pine framed F11 plywood

The Radiata pine timber-framed plywood construction took place in the wood-working shop of the Structures Laboratory. All frames were planed and cut from a 60 mm by 90 mm by 6,000 mm MGP10 Radiata Pine. It was planed to a size of 23 mm by 70 mm by 3,000 mm.

The wall was assembled into two segments as shown in Figure 4.18. Exterior frames were then temporarily nailed on corners, thus holding the trapezoidal frame in place while connecting the metal brackets. The metal brackets were then screwed to the frame using a cordless drill. The metal brackets were connected one after the other. The middle vertical stud was laid to the trapezoidal frame marked to fit in the frame and then cut. The same procedure was used in installing the horizontal brace. The middle vertical frame and horizontal members were nailed to the main frame at an angle of 45 degrees. There were two 50mm x Ø2.50mm flat-head galvanised nails used at each end of the member.

The two wall segments were then laid down side by side. The wall segments were connected using fabricated hinges made of mild steel plates and steel rods. The hinges were placed in locations specified on the plan, marked and 6mm diameter holes were then drilled on the markings. Each hinge was connected to the frame using 8–5 mm x 75mm long threaded bolts. The bolts were tightened using a torque wrench. Connected wall segments were then flipped on the other side to mark and drill for the fabricated locking pin. The locking pin is made from 8 mm square rod mild steel. These are also connected to the frame by 8–5 mm x 75mm long threaded bolts.

Plywood sheathings were laid under the frame for marking. The plywood was cut using an ordinary hacksaw. Since the sheathing on the opposite side is symmetrical, the cut plywood was used as a reference. The same procedure was followed with the other wall.

A Ø2.80mm x 25mm galvanised nail was used to connect the plywood to the timber frame. The plywood was overlaid on the timber frame, properly aligned and then nailed on the corners. Nails were hammer driven starting from 150mm on centre.

4.3.3.4 Test set-up

The walls were tested for lateral resistance in the vertical position as shown in Figure 4.19 and equivalent schematic diagram in Figure 4.20. Reaction dead weights are carried by the three-tonne crane and then manually adjusted so as to not pinch the specimen. The wall was held in a vertical position using two heavy reaction frames. The specimen was sandwiched by the 6-MGP 12–70mm x 240mm wooden I-beams as shown in Figure 4.19. They were positioned in such a way that no out-of-plane bending or load misalignment would happen during the application of load. Their purpose was to keep the specimens in a vertical position without them touching the specimen. An approximate distance from the specimen was 3mm on each side so that the specimens would be free to move when loaded in the direction of loading.

The bottom plate of the wall was attached to a 35mm x 140mm hardwood base. Eighty per cent of the diameter of the wooden screws was pre-drilled at a distance of 200mm on centre. Wood screws (100mm in length) were used to connect the bottom plate to the hardwood base plate. This was done before erecting the specimen on the test set-up. The specimen was laid on a level ground. Wooden blocks were utilised and put on the bottom to attain a distance of 70mm in height right at the centre of the wall thickness. The hardwood base plate was then laid beside the laid wall. With the 6 mm pre-drilled holes at a distance of 200mm from the near end (in line where the load is applied) on the hardwood base plate, it was redrilled using a 5mm drill bit to put a mark on the bottom plate of the wall. The bottom plate was then drilled with a 6mm diameter drill bit. The wooden screws were driven in using a power drill. The base plate was then fitted to the bolts that were welded on the steel channel section. The channel section had the following dimension: the web was 180mm by 5mm thick and the flange was 72.5mm by 11mm in thickness. All holes in the steel section were drilled 1.5mm larger than the bolt diameter. The M12 bolts were welded on the channel at a spacing of 300mm. The channel was then bolted to the reaction floor to restrain it from moving.

Figure 4.19 Plywood sheathed wall set up for lateral resistance test (see Figure 4.20 for details).

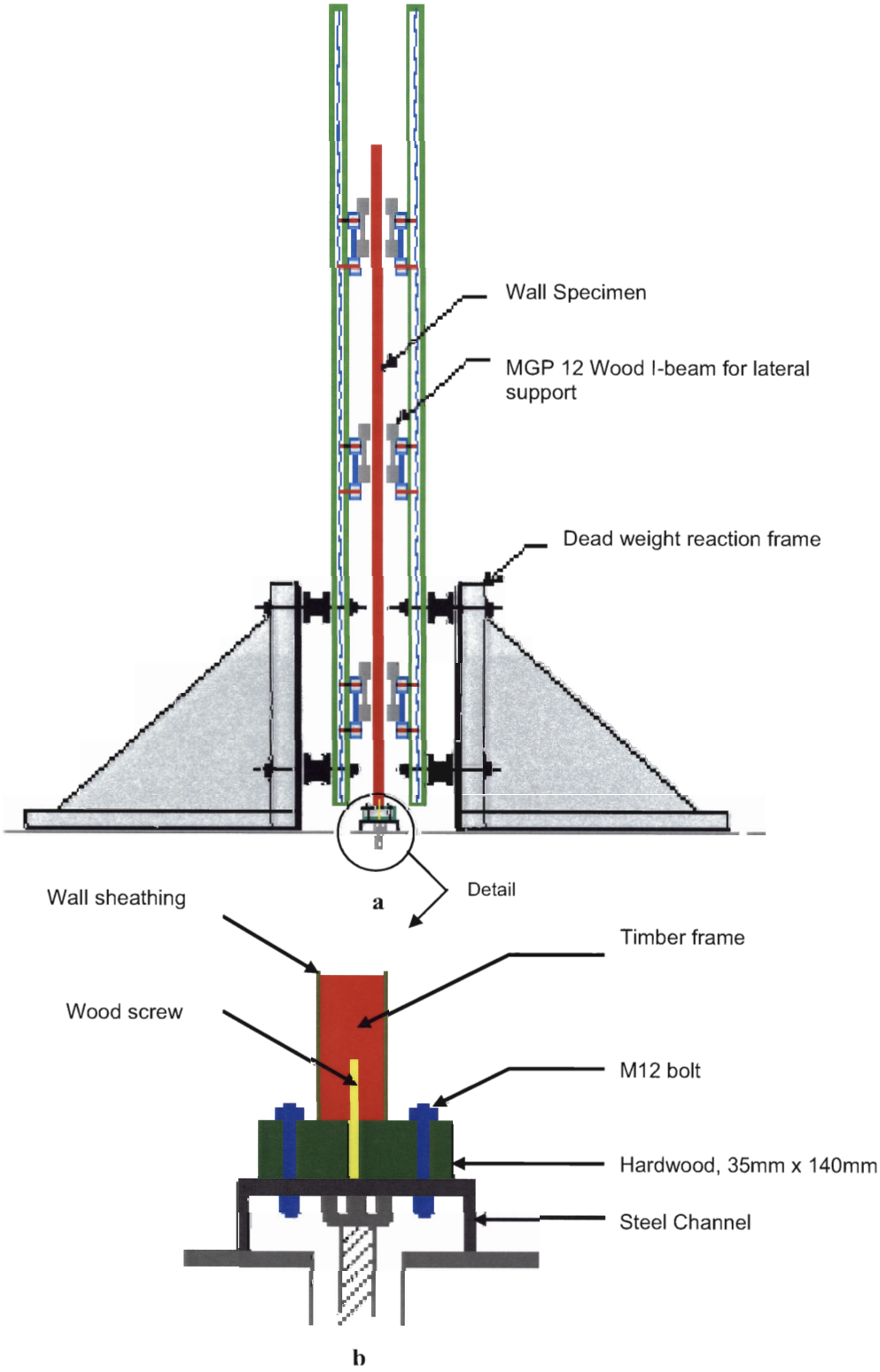

Figure 4.20 Schematic diagram of the wall test set-up;
a. full set-up and **b**. enlarged view of the specimen's bottom.

4.3.3.5 Instrumentation and Data Acquisition

The top of the wall specimen with metal plate was loaded by a controlled hydraulic ram which provided the racking force to the wall. The actuator has a capacity of 20 tonnes with a displacement range of ±300mm. It was secured on a reaction frame, which was set up for this particular test. The actuator was bolted to the reaction frame. The end of the hydraulic rams was fitted with a 20 kN load cell, which records the load applied to the wall. The load cell was also fitted with a roller type end to maintain the horizontal load application and not to restrain the specimen from moving up when the load was applied as shown in Figure 4.21. This movement was anticipated, because no hold downs were used with the wall. A 40 mm x 75 mm by 5 mm mild steel bar was screwed on the top of the wall where the load was applied. Figure 4.22 shows the elevation view of the test set-up. The test utilises two rotary potentiometers and four LVDTs to measure displacements. Table 4.5 presents the channel numbers with appropriate measurements. The rotary potentiometers were used to measure displacement on the top of the wall. This is consistent with the instruments used in the wall frame test. Two LVDTs were located at a height of 882mm to measure middle-span displacements and two LVDTs at the bottom, one on the far end (opposite to the hydraulic jack) to measure horizontal displacement and one at the near end (near the hydraulic jack) to measure vertical movement.

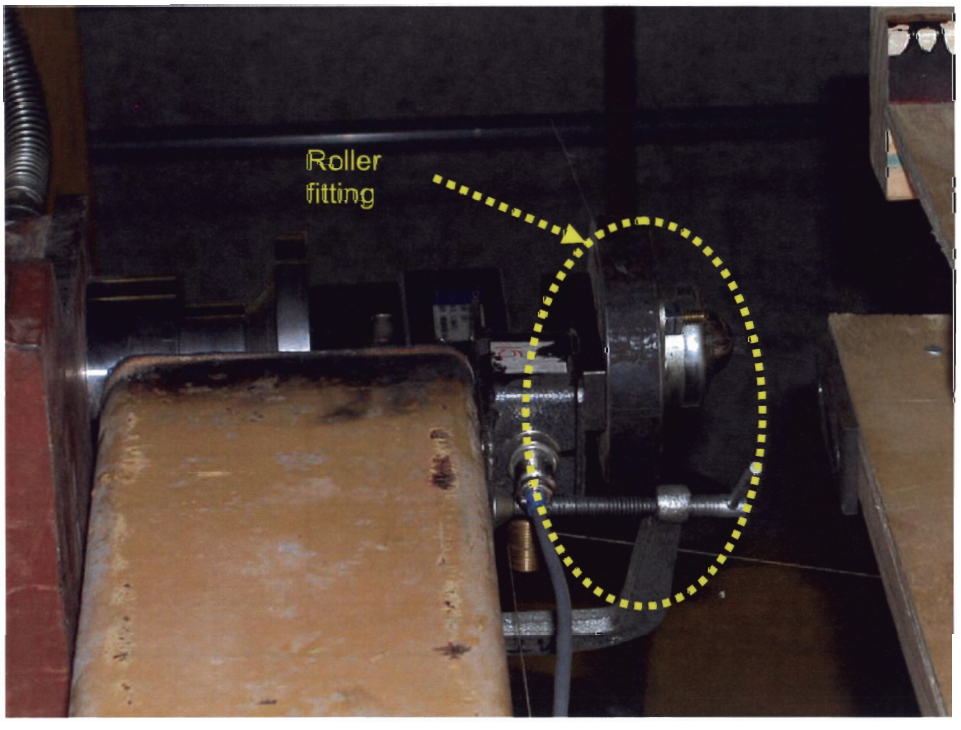

Figure 4.21 Worm's eye view of the hydraulic jack and load cell with attached roller fitting.

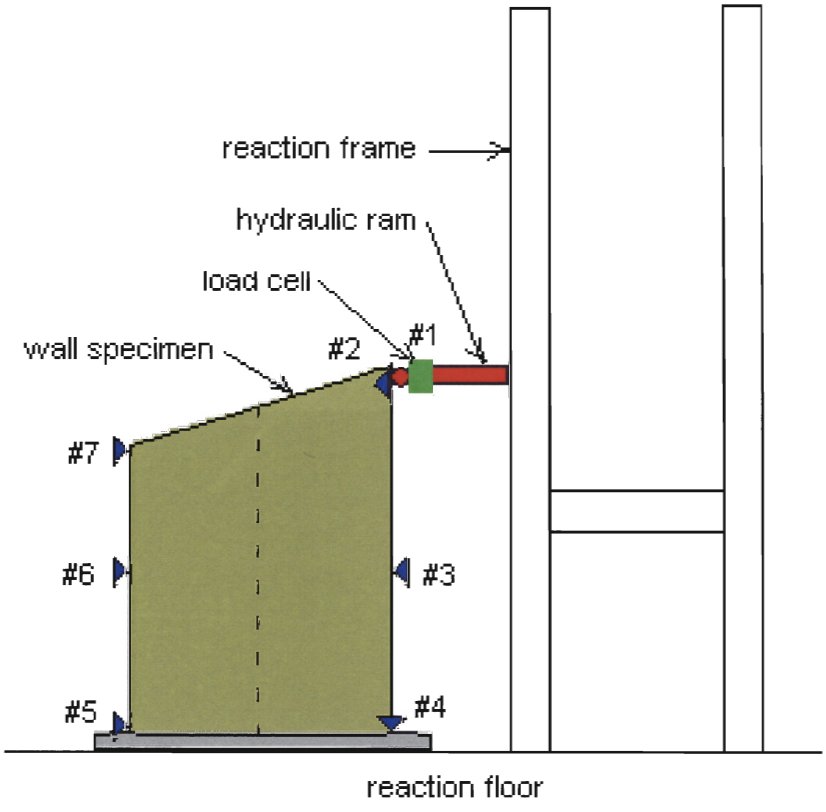

Figure 4.22 Elevation view with instrumentation locations for displacement measurement.

Table 4.5 Channel numbering on data taker with corresponding measurements

Channel #	**Measures**
1	Load
2	Ram/top displacement (Potentiometer)
3	Mid-height displacement at the near end (LVDT)
4	Vertical displacement at the bottom (LVDT)
5	Horizontal displacement at the bottom (LVDT)
6	Mid-height displacement at the far end (LVDT)
7	Top displacement at the far end (Potentiometer)

Instrumentation and recording is crucial for any testing. The test and work details must be properly specified. Figure 4.23 shows the whole set-up for the test. In this study, seven

channels of the data logger were used to take readings on the walls. The numbers and their corresponding measurements are shown in Table 4.5. Rotary potentiometers were utilised for top of the wall displacements. This is consistent with the frame test.

Base displacements were also measured. When the top of the wall was displaced, an overturning moment at the base occurred that caused the wall to lift off the foundation. The uplift of the wall was quite significant because of the absence of hold-downs from both ends of the wall. This measurement is necessary when considering the rigid body motion of the structure.

Figure 4.23 Lateral resistance test set up for the wall.

4.3.3.6 Testing procedure

The monotonic test was a one-directional ramp load test with a rate of 10 mm per min. The data was recorded at a frequency of 18 samples per second. The specimens were pre-loaded thrice with a displacement of 8mm. The hydraulic rams were retracted to zero load each time 8mm were reached. A three-minute relaxation time was allowed for the specimen to be relieved from the stresses caused by the applied load. The fourth load loaded to failure.

4.3.3.7 Shear wall property definitions

4.3.3.7.1 Load-displacement parameters

For every test, a load-displacement curve was produced from the data obtained by channels #1 and #2. Nearly every parameter of the shear wall can be obtained from this graph. The displacement used to generate the graph is the interstory drift, which is the displacement of the top of the wall (channel #2).

The load-displacement graph for the monotonic test, as illustrated in Figure 4.24, is always positive and produces a curved line characteristic of its one-directional loading.

4.3.3.7.2 Wall capacity

The wall capacity, F_{peak}, of the monotonic test is simply the maximum load that the wall can resist during the loading period. The displacement of the wall, δ_{max}, is also recorded at its corresponding loading.

4.3.3.7.3 Wall Failure

The walls tested in this study were considered to fail when the resisted load reached $0.8F_{peak}$ on the descending portion of the load-displacement curve. For light-frame shear walls the failure is rarely sudden, but instead a gradual decline mirroring its increase in load is observed. Since $0.8F_{peak}$ is the arbitrary value for failure, it should be noted that some variation in displacement could result when comparing other parameters based on this value.

The failure displacement is recorded and used to determine the ductility of the structure. The more a structure can deflect before failure and the more loads it can resist at failure are both important to the integrity of the structure.

4.3.3.7.4 Energy dissipation

The amount of energy dissipated by a structure is taken directly from the load-displacement curve. From the monotonic test, it is simply the area under the curve measured from the initial displacement until the failure displacement of the wall.

4.3.3.7.5 Equivalent Energy Elastic Plastic (EEEP) parameters

A light-frame wood construction displays significantly different load-displacement behaviour from other building materials such as steel, which exhibits a nearly perfect elastic-plastic response when loaded. A light-frame wood construction does not have a distinct yield load, and the proportional limit cannot be definitely set.

In order to make comparisons between tests performed on different materials, an equivalent energy elastic-plastic (EEEP) curve, as illustrated in Figure 4.24, is determined for the load and displacement curve of a test.

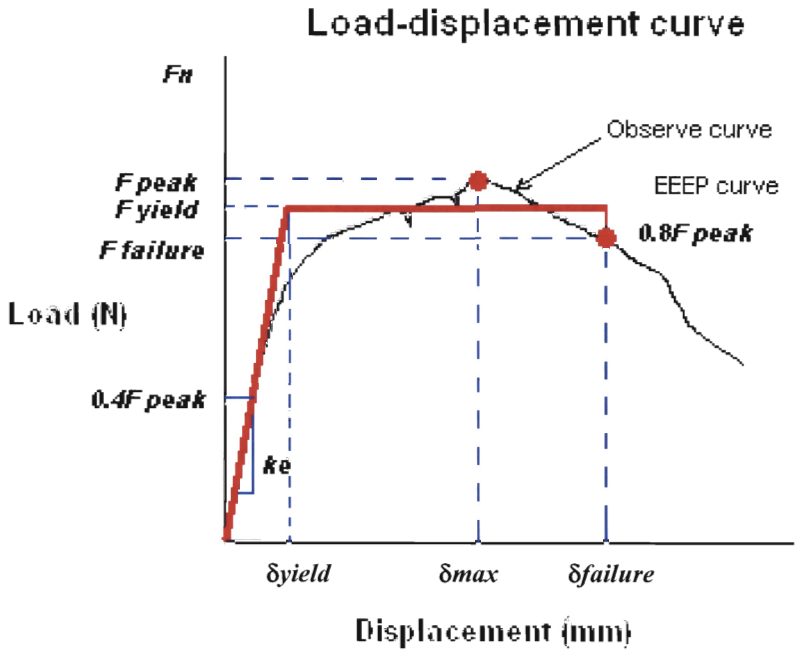

Figure 4.24 Equivalent Energy Elastic Plastic (EEEP) curve (Salenikovich, 2000).

The EEEP curve is a perfectly elastic-plastic representation of the actual response of the specimen. The curve is a function of the yield load and displacement, the failure displacement, area under the observed load-displacement graph, and the elastic stiffness. The EEEP curve encompasses the approximate amount of area as the actual load-displacement curve from the origin to the ultimate displacement. This area is a measure of the toughness of the system. Toughness is the energy that is needed to fail a specimen.

4.3.3.7.5.1 Elastic stiffness

The elastic stiffness, k_e, of the wall is defined as the slope of a line between the origin and a point corresponding to $0.4F_{peak}$ on the load-displacement curve. It is defined by the slope of the secant passing through the origin and the point on the load-displacement curve that is equal to 40% of the peak load, F_{peak}. It is used to find other parameters such as the yield load, yield displacement and ductility ratio.

$$\text{Elastic stiffness} = k_e = 0.4\, F_{peak} / \delta_{0.4\, Fpeak} \qquad \text{equation 4.1}$$

4.3.3.7.5.2 Yield load and yield displacement

The elastic portion of the EEEP curve is determined by the elastic stiffness. It begins at the origin and ends at the yield load and displacement. The plastic portion of the EEEP curve is a horizontal line equal to the yield load and extends until the failure displacement, as illustrated in Figure 4.24. The yield point can be defined in the EEEP curve using different procedures (Foliente, 1996). For this study, using Johnson's (1997) and Heine's (1997), the EEEP is defined as an elastic-plastic curve in which the energy is equal to the energy of the original load deflection curve through failure. This essentially states that the area under the EEEP curve is equal to the area under the load-displacement curve through the point of failure. Load resistance at yield, F_{yield}, is defined as the point at which this equivalent energy curve becomes plastic such that, by definition, $F_{yield} \geq F_{failure}$. Assuming the F_{yield} is a function of the elastic stiffness, the area under the load-displacement graph, and the failure displacement, it can be calculated as follows:

$$F_{yield} = \frac{-\delta_{max} \pm \sqrt{\delta^2_{max} - \frac{2A}{k_e}}}{\frac{1}{k_e}} \qquad \text{equation 4.2}$$

Where:

F_{yield} = Yield load (N)

A = the area (N-mm) under the observed load displacement curve from the origin to the failure displacement ($\delta_{failure}$)

k_e = Elastic stiffness (N/mm)

Once the F_{yield} is determined, the yield displacement can be calculated using the following relationship:

$$\text{Yield displacement } (\delta_{yield}) = F_{yield} / k_e \qquad \text{equation 4.3}$$

4.3.3.7.5.3 Ductility

Ductility is an important feature of a structural system, which enables it to yield and deform inelastically without failure. The ability of walls to bend but not break is crucial when subjected to the sudden and powerful motions of earthquakes. There are several methods that have been proposed to express the ductility of a structure. One accepted measurement of ductility is the ratio of the peak displacement to the yield displacement.

$$\text{Ductlity} = D = \delta_{max} / \delta_{yield} \qquad \text{equation 4.4}$$

This definition considers the structure's ability to yield until reaching its maximum load. The most commonly accepted definition is the ASTM E2126 definition, which defines the ductility factor, μ, as the ratio of the failure displacement and the yield displacement.

$$\text{Ductility factor } = \mu = \delta_{failure} / \delta_{yield} \qquad \text{equation 4.5}$$

This value represents the amount of displacement that a structure can undergo from yielding until failure and assumes that most ductile structures, such as light-frame shear walls, are able to resist loads far beyond $\delta_{max.}$ When the structural component has reached its capacity, it transfers additional load onto other components.

4.4 Summary

This chapter has provided a description of the test specimens used and details on how the experiments were performed in accordance with relevant recognised standards. A nail/screw withdrawal test was performed in accordance with ASTM 1761 (2000), lateral nail and screw resistance tests in accordance with AS 1649 (2001). The joint stiffness test has no standard test available, however, appropriate tests to obtain desired results were conducted, and a quasi-static load on a timber-framed wall, based on ASTM E564.

A discussion of the materials, construction details and instrumentation was included. This section also identified and defined the important shear-wall parameters that define the behaviour of these specimens. When evaluating shear walls, the strength, stiffness, deformation characteristics, energy dissipation and damping are the key parameters.

5 Experimental results

5.1 Introduction

This chapter discusses the results of the experiments performed as presented in the previous chapter. The results from the experimental methods conducted are used to develop the finite element model of the wall. The discussions of the results are divided into two, preliminary tests and monotonic tests on the walls.

All values shown in this chapter are referred to in the previous section. Computations were not shown in detail, however, the equation/formula used is cited.

5.2 Preliminary test

5.2.1 Introduction

This section discusses the experimental results from the withdrawal test, lateral nail resistance test and joint stiffness test. The tests were conducted in accordance with ASTM 1761-88 (2000), AS/NZ 1649 (2001) and 4063 (1992), respectively.

5.2.2 Withdrawal test

5.2.2.1 Nail

Table 5.1 shows that the average maximum nail withdrawal resistance with regard to the Apitong wood prism to which it was connected was 508 N; and a corresponding 1.21mm average maximum displacement and coefficient of variation (COVs) for load and displacement. The maximum load provided by NSCP (2001) is equivalent to 455 N; hence, a 10% difference The reason for this might be the wide variation of values as indicated in Table 5.1, as represented by a COV equivalent to 30%.

5.2.2.2 Screw

The screw withdrawal test failure mode is a result of the withdrawal of the shank from the wood. The screw thread is specially designed to resist shank withdrawal. This is the assumed failure mode in the derivation of withdrawal design values for all screws. Table 5.2 shows peak loads and maximum displacements and COVs based on 10 data sets. It demonstrates that results are more consistent compared to nails fastened to the Apitong prism, as reflected by the COVs of load and displacement.

Table 5.1 Nail withdrawal test results for 10 wood prisms

Test number	Maximum load resistance for 21.5mm penetration (Newtons)	Maximum displacement (millimetres)
Nw1	469	1.35
Nw2	337	0.93
Nw3	595	1.14
Nw4	584	1.56
Nw5	721	0.88
Nw6	705	1.55
Nw7	343	1.08
Nw8	275	1.60
Nw9	588	0.83
Nw10	465	1.16
Average	**508**	**1.21**
COV	**30%**	**24%**

Table 5.2 Maximum loads and corresponding displacements

Test number	Maximum load resistance for 28mm penetration (Newtons)	Maximum displacement (millimetres)
Sw1	3,143	1.75
Sw2	2,161	1.32
Sw3	2,163	1.49
Sw4	2,711	1.41
Sw5	2,910	1.56
Sw6	1,968	1.32
Sw7	3,228	1.59
Sw8	3,008	1.45
Sw9	3,269	1.53
Sw10	2,883	1.44
Average	**2,744**	**1.67**
COV	**17%**	**8%**

5.2.3 Lateral resistance test

5.2.3.1 Nail with wwcb sheathing

Table 5.3 show the number of samples and their corresponding load capacity and displacement. The values shown are for one fastener. The specimens Lw1 and Lw10 have the largest peak load of the data set. Others display almost the same amount of load to fail the specimen. Although it is not unusual to have a coefficient with a variation of 22% for this type of sheathing a large variation in thickness and densities is due to uncontrolled production. The reason behind the increase in load for Lw1 and Lw10 is that wwcb used in these specimens were thicker by 1.13 mm and denser than the other specimens. The modes of failure for these specimens are characterised by pinching of the sheathing material and pulling out of the nails through the timber framing. Almost all remaining specimens failed when the nail head pinched the wwcb, or due to a cross-sectional break or a tear through the wwcb, as shown in Figure 5.1. The COV for the δmaximum at peak load is 42%. This could be attributed to the different density of the Apitong frame and the different density and thickness of the wwcb sheathing.

Table 5.3 Peak loads and displacements (δ) per fastener for wwcb using Apitong timber

Specimen #	Peak load (Newtons)	δmaximum (mm)
Lw1	2,080	1.55
Lw2	1,261	4.84
Lw3	1,250	2.61
Lw4	1,541	3.52
Lw5	1,227	4.12
Lw6	1,460	7.39
Lw7	1,492	3.24
Lw8	1,233	7.26
Lw9	1,691	5.03
Lw10	2,130	5.82
Average	**1,540**	**4.58**
COV	**22%**	**42%**

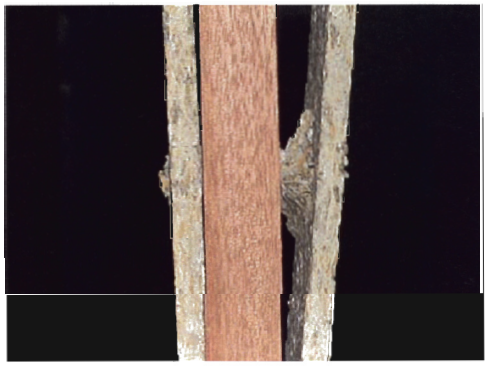

Figure 5.1 Nail tear through the wwcb.

5.2.3.2 Nail with plywood sheathing

Table 5..4 show the number of samples and their corresponding load capacity and displacement. The values shown are for one fastener. Plywood sheathing is far more consistent in thickness and density compared with wwcb, as shown by the results and COVs. The maximum load has a COV of 14% and the COV for maximum displacement at this load is 26%. The coefficient of variation of the plywood sheathing peak loads is smaller by 8% and 16% smaller in displacement as compared to the wwcb sheathing.

The failures of the specimens are characterised by pulling out of the nails from the timber frame and pinching of the nail head on the sheathing as shown in Figure 5.2.

Table 5.4 Peak loads and displacement (δ) for plywood using Radiata Pine timber

Specimen #	Peak load (Newtons)	δmaximum (mm)
Lp1	1,764	7.22
Lp2	1,806	8.61
Lp3	2,326	6.06
Lp4	1,768	7.22
Lp5	1,709	3.95
Lp6	2,206	7.53
Lp7	2,001	7.58
Lp8	2,283	6.24
Lp9	2,399	8.30
Lp10	2,492	11.62
Average	**2,067**	**7.43**
COV	**14%**	**26%**

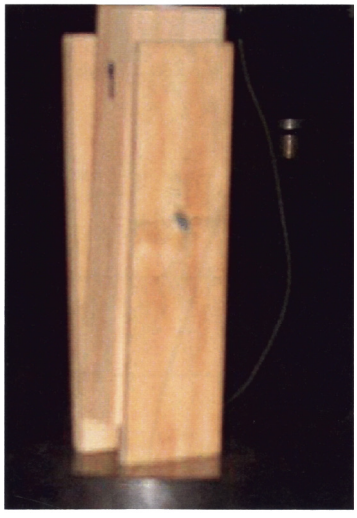

a

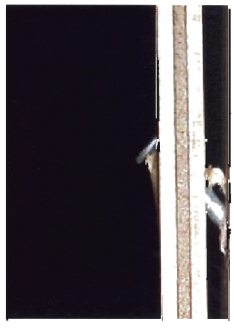

b

Figure 5.2 Mode of failure; **a**. separation from the Radiata pine and **b**. enlarged view of nail pulling out from the frame.

5.2.4 Corner joint testing with metal brackets

5.2.4.1 Apitong framing

The compression test results from on the joints of various angles show consistent values of the average peak load, as illustrated in Table 5.5. This is because of the closeness of the line of load to the diagonal bracing of the joint. The capacity of the frame is dependent on the capacity of the Ø5mm of round steel to carry a compressive load. When the corner metal bracket is applied with tensile force, the maximum capacity is dependent on the fasteners. The fasteners are those connecting the metal brackets to the timber frame. As shown in Figure 5.3, compression and tension tests are compared. Referring to Section 5.2.2.1, the low load capacity of the nail to resist a pull-out force makes it an ineffective fastener for this type of timber.

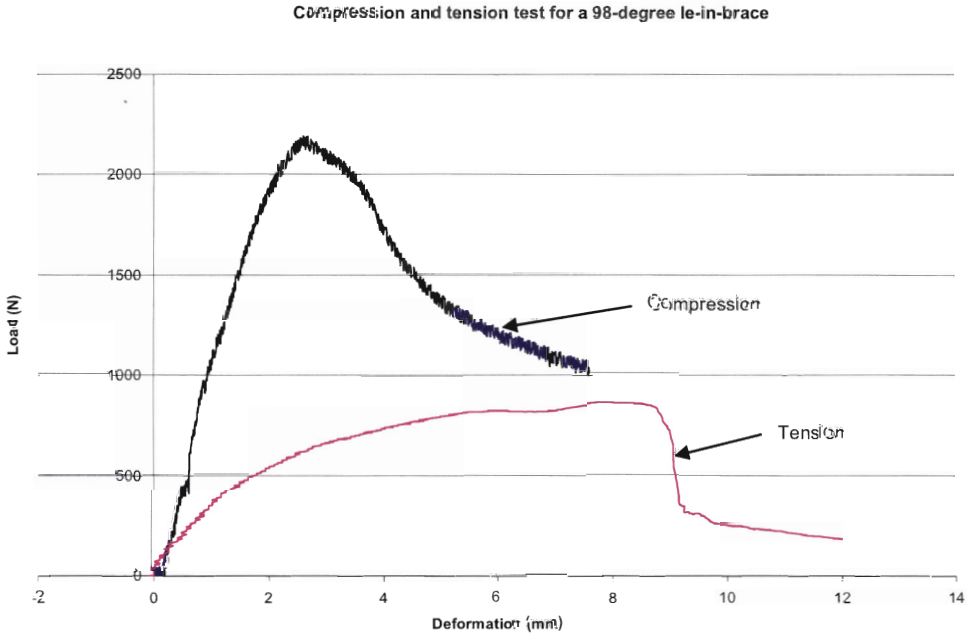

Figure 5.3 Compression and tension test graphs for the 98-degree corner metal bracket.

Because of the end connection of the frame, which is nailed to an end grain, the connection is very easy to separate. The compressive load on the ends acts as a pulling force that causes the nails to withdraw. As shown in Figure 5.4, two nails connecting the 2-timber frame are pulled out. All diagonal braces of the frame are buckled when applied with compression, as illustrated in Figure 5.4.

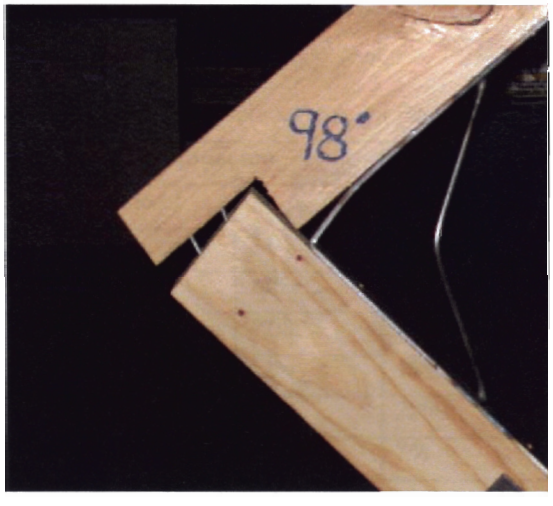

Figure 5.4 Joint separation and buckling of the brace.

Table 5.5 demonstrates that when a tension force is applied to this type of set-up, the frame is weak. The most stressed nail is the one closest to the load. Failure of the joint emanated from this nail's withdrawal. A sudden drop in load occurs when these nails are withdrawn. When the displacement reaches 34% of the length, the capacity begins to drop. The frame is not ductile when compared to the screw-fastened frames.

Table 5.5 Average peak loads and displacements for Apitong framing

Angle	Compression		Tension	
	Peak load (Newtons)	δ_{max} (mm)	Peak load (Newtons)	δ_{max} (mm)
82-degree	1,964	4.57	662	9.40
COV	**21%**	**13%**	**8%**	**13%**
90-degree	2,100	3.65	915	9.40
COV	**9%**	**23%**	**7%**	**4%**
98-degree	2,059	3.59	865	6.95
COV	**10%**	**18%**	**8%**	**18%**

5.2.4.2 Radiata Pine framing

In Table 5.6, the maximum loads on the compression side are comparable to the maximum loads on the tension side. When the diagonal brace starts to buckle, the compressive capacity of the frame is significantly reduced. This ranges from 3–4mm in travel. This is consistent with the results obtained from the compression tests from the Apitong timber.

The general δ_{max} of the screw fastener is greater than the nail fastener. The effective length before reaching its maximum capacity is within the range of 45% of its length. A displacement exceeding this length will decrease its capacity.

Table 5.6 Average peak loads and displacements for Radiata Pine framing

Angle	Compression		Tension	
	Peak load	δ_{max}	Peak load	δ_{max}
82-degree	3,146	3.01	3,030	11
COV	**2%**	**18%**	**15%**	**20%**
90-degree	2,817	4.03	2,369	13.14
COV	**9%**	**12%**	**13%**	**27%**
98-degree	2,702	3.20	2959	11.52
COV	**16%**	**22%**	**7%**	**28%**

The same mode of failure is observed with this type of fastener. In the compression test, separation of the two timber frames is observed on the entire test due to poor connection on the end-grain, as well as buckling of the diagonal braces. In the tension tests, the pull-out of the screw from the metal let-in stiffeners is prevalent.

5.3 Monotonic test on walls

5.3.1 Introduction

A total of 10 monotonic tests were performed on walls. Three wall frames were tested from Apitong and three frames were sheathed with 8mm wwcb. There were also two wall frames made of Radiata Pine timbers, and two were sheathed with 6mm-thick softwood plywood.

The complete data for each monotonic test may be found in Appendices I, J, K and L. A detailed description of the test observations and mode of failures is discussed for each set of specimens in this chapter. Load and displacement graphs are also provided in Appendices D, E, F and G.

5.3.2 Comparison of the two timber-framed walls

This section of the chapter will compare the two timber wall frames with the corresponding corner metal brackets and sheathing materials: wwcb and plywood under monotonic loading. The parameters that were investigated only for the timber frames were ultimate load, elastic stiffness, yield load displacement and failure displacement. The experimental results from the wall with sheathing will also include parametric studies for ductility and energy dissipation in addition to the mentioned parameters for wall frames.

5.3.2.1 Load-displacement relationship

A typical load-displacement curve for the two timber frames tested is illustrated in Figure 5.5. The graph reveals that Apitong with corner brackets fastened four ∅3.2mm x 25mm nails has a higher ultimate load value but a lower maximum displacement value. It shows that these two frames have different peak loads and fail at different load and displacement. Therefore, it is important to look at several different parameters when analysing these two frames.

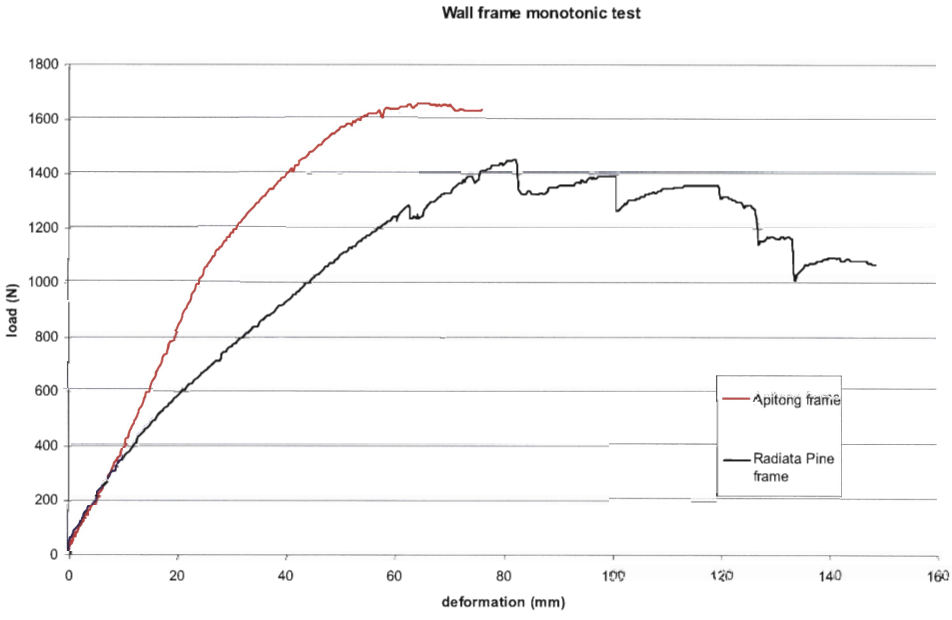

Figure 5.5 Typical load-deflection curve on tested Apitong and Radiata pine timber frame.

5.3.2.2 Ultimate Load

As described in Chapter 4, the ultimate load is the maximum load on the load-displacement graph. Generally, allowable stress design values are determined from the ultimate load, with a factor of safety applied to give a safe design value. A list of ultimate load for each framing material is provided in Table 5.7. For each set of tests, the peak load values were in close agreement. It is observed that the Apitong frame ultimate load is at an average of 1,524N while Radiata pine had 1,378N.

Table 5.7 Monotonic peak loads on wall frames

Specimen label		Peak load (N)	Ave
Apitong frame	A1	1,651	1,524
	A2	1,625	
	A3	1,509	
Radiata pine frame	R1	1,464	1,378
	R2	1,360	

5.3.3 Comparison of the walls with different sheathings

5.3.3.1 Load-displacement relationship

A typical load-displacement relationship for all specimens is shown in Figure 5.6a. The timber frame with plywood sheathing exhibited a higher ultimate load and maximum deflection. Figure 5.6b shows the average values wwcb and the plywood-sheathed timber frames. There were three sets of data for the wwcb wall and two for the plywood wall. The graph reveals that the performance of the wall is highly dependent on the type of sheathing used. This is based on the assumption that the two timber framing materials used have the same strength and stiffness. The Radiata pine was chosen due to its closeness to the Apitong in density value.

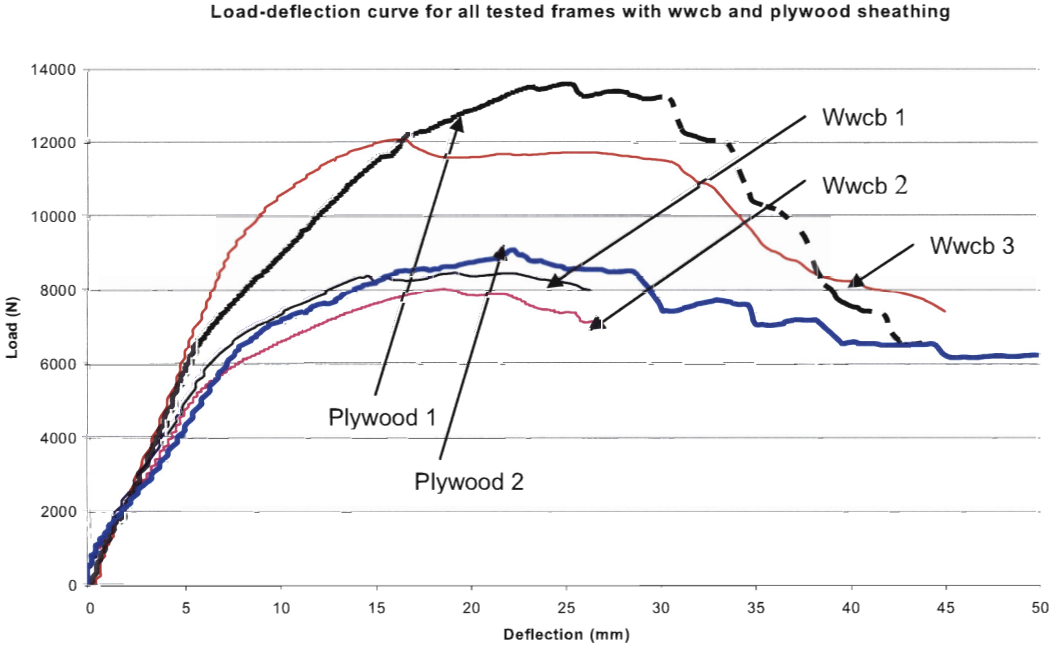

Figure 5.6a Load-deflection curve for wwcb and plywood-sheathed timber frames.

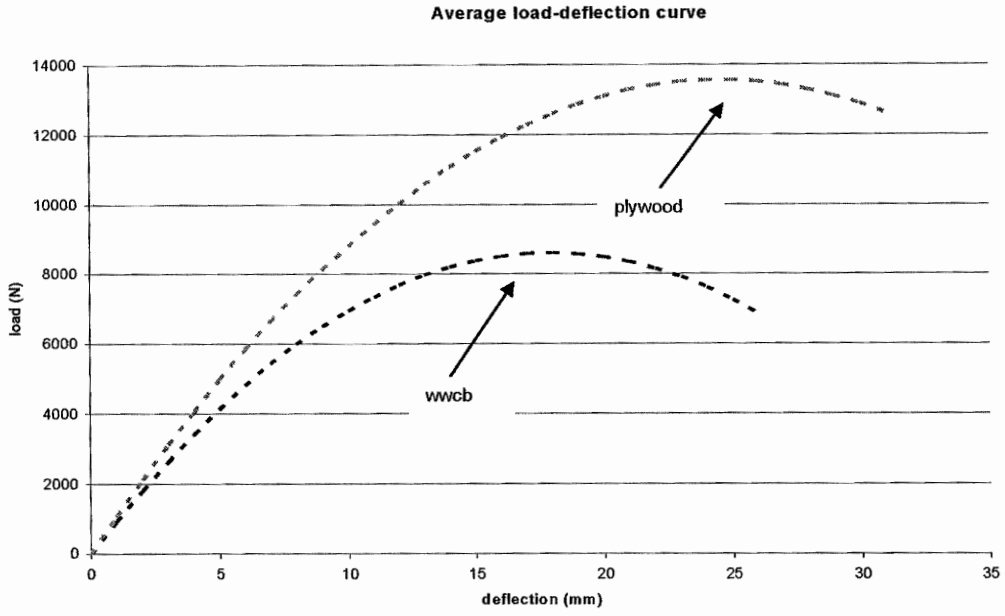

Figure 5.6b Averaged load-deflection curves for wwcb and plywood sheathing.

The average values taken from the wwcb sheathing are the two data sets W1 and W2, as recommended by ASTM E564 (2000). The minimum number of specimens should be two, however, three specimens were tested to verify the initial test results. In the third data set (W3), the ultimate load result increased by 50% from W2. The thickness of the wwcb also contributed to the low maximum displacement of the specimen, causing a shorter penetration of the nails to the timber frame. The reason for specimen W3 attaining this value is that the wwcb panels used were denser and thicker than the other wwcb panels used in specimens W1 and W2.

The same condition applies to the two samples tested for plywood sheathed timber frame. Two sets were tested; however, the P2 specimen was not constructed squarely, thus, only P1 was used. There was dimensional distortion on the second plywood wall specimen, P2. The geometric distortion had an initial gap of 10mm on the far end (Figure 5.7) of the base plate. This was measured using the metric ruler. Note that no force had yet been applied to the bolts to force it to lie flat with the base plate for rigid connection. The gap was reduced to 5 mm when all the bolts on the far end were tightened. When the bolts were tightened, a squeaking sound of the wall could be heard. This could only mean pre-stressing or pre-loading of the wall. Thus, a load was applied even without the force on the hydraulic rams applied on the structure. The author has no means of quantifying the reduction in stiffness, because of the pre-stressing of the wall.

Figure 5.7 A gap of 5 mm on the far end wall.

The load-displacement relationship shows the maximum strength of the specific sheathing materials at a different load, which fails at a different load and displacement. Therefore, it is important to look at several different parameters when analysing the two types of sheathing.

5.3.3.2 Ultimate load

The ultimate load is taken as the highest load on the load-displacement graph. Table 5.8 shows the list of ultimate loads for each wall. The average ultimate load for each type of wall shows that the plywood sheathing is 58% higher than the wwcb sheathing. This result considered the removal of W3 and P2. Furthermore, the value obtained from the second plywood is above the 15% range of values set by ASTM E564 (2000) as explained in Section 5.3.3.1 and pre-stressing of the specimen. Due to time constraints, the author was not able to duplicate the plywood specimen for further verification of the experimental value obtained from specimen P1. The same condition applies for specimen W3; it is 50% above W2. W3 was also discarded as per ASTM E564 (2000).

The ultimate loads of the two types of walls used in this study were compared. There are two variables that were not taken into account with the comparison of the ultimate load. Firstly, the type and size of nails used and timber framing used with the two walls are different. Secondly, MGP10 Radiata pine is the closest to the density of Apitong; therefore the author opted to use it. As with the nails, there were not enough nails that were used with the wwcb walls that could also be used in the plywood wall.

Table 5.8 Monotonic peak load values for the walls with different sheathings

Wall sheathing type	**Ultimate load (F_{peak}) (N)**
Wood wool cement boards (medium density)	
W1	8,463
W2	8,032
W3	12,507
Average (for W1 and W2)	**8,607**
Plywood (F11)	
P1	13,566
P2	9,108
Average (P1 only)	**13,566**

Note that the average values are predicted values from SPSS statistical software. The 50% difference of the test results for W2 and W3 prompted the author to discard W3, as recommended by ASTM E546 (2000). In addition, as a result of pre-stressing the specimen P2, its value was not used.

5.3.3.3 Yield load and displacement

Yield load determination for the walls in this study was an approximation of the first major event, which is the theoretical load and displacement at which the structure starts to deform inelastically. Because wood does not behave in a linear elastic manner, the yield load is only an approximation, determined from Chapter 4. The yield load is a function of the elastic stiffness, failure displacement and the energy dissipated.

As a recap of the elastic stiffness defined in Chapter 4, it is the slope of the secant line that passes through the origin and the load that is equal to $0.4F_{peak}$. There is a wide variation in the elastic stiffness within the individual set of tests. It could probably be due to the initial application of load to the wall; the round pins and rectangular lock pins did not fit exactly to the hinges. Although three repeats of load application up to 8 mm of deformation were implemented, the elastic stiffness still varied.

As shown in Table 5.9, as expected, plywood achieved a higher elastic stiffness compared to the wwcb panels. This is because of the material composition of the wwcb panels which consist of wood excelsior and cement. The average elastic stiffness for the plywood wall was 1018 N/mm, while wwcb wall is 904 N/mm. Due to the reasons mentioned in Section 4.3.3.2, that is, the variation of elastic stiffness in the plywood and specimens W1 and W2, it could still be concluded that the elastic stiffness of the plywood is higher than that of the wwcb panels.

The elastic stiffness of the specimens followed the same pattern as the peak load, with plywood achieving the highest. The yield load per wall specimen is shown in Table 5.10. The yield displacement, which is determined directly by the elastic stiffness and the yield load, is also shown in Table 5.10.

Table 5.9 Elastic stiffness of the walls

Sheathing material	**Elastic stiffness (N/mm)**
Wood wool cement board (Wccb) (Medium density)	
W1	956
W2	852
Average	**904**
Plywood (F11 Softwood)	
P1	1,178

Table 5.10 Monotonic yield load and displacement values

Sheathing material	**Yield load (Fy) (N)**	**Yield displacement (δy) (mm)**
Wood wool cement board		
W1	7,743	8
W2	7,390	9
Plywood		
P1	8,895	8

5.3.3.4 Failure capacity and displacement

As defined in Chapter 4, the failure load was taken to be $0.8F_{peak}$ (that is, when a 20% decrease in resistance occurs) (ISO 1998). Because this is obviously based on the maximum load, the walls with the highest strength will also have the largest load capacity at failure. However, the displacement capacity of a structure is an important parameter to investigate. The ability for the structure to dissipate more energy resulted from it being able to deform without failing.

From Table 5.11, it can be seen that the plywood walls were able to withstand the greatest force; however, the displacement failure is almost the same. The average failure load for plywood is 58% higher than for wwcb panels. The average displacement failure for each wall

material is 35.35 mm for the wwcb and 35.63 mm for plywood, a slight difference of 0.28 mm in displacement at failure values. The reason for this is that plywood uses a different set of fasteners; one is being shorter in length by 0.46 mm and smaller in diameter by 0.39 mm. The full strength and stiffness potential of the plywood was not utilised, as this will be seen in the mode of failure in Section 5.3.3.7.

Table 5.11 Failure load and displacement values

Material	Failure load (N)	Failure displacement (mm)
Wood wool cement boards	6,053	35
Plywood	10,853	36

The failure mode of the walls typically involved the sheathing nails either pulling out of the framing or tearing through the sheathing. When testing the plywood, nails were observed to withdraw from the timber frame with ease, partly due to the length of the nails and the thickness of the timber frame. When pull-out became significant, the sheathing panel could no longer resist shear forces and the wall failed. However, due to the nature of the wwcb material, being a brittle material in the sense that it is mixed with concrete, the typical mode of failure is nail tear-through to the wall sheathing.

5.3.3.5 Ductility

Ductlity values alone do not provide much insight into the performance of the walls. Ductility is a function of the elastic stiffness, yield displacement and failure displacement. As discussed in Chapter 4, the elastic stiffness varies for every type of sheathing material used. The ductility factor used for this study is defined as the failure displacement divided by the yield displacement. The ductility values are listed in Table 5.12.

Table 5.12 Ductility ratios of walls with different sheathing materials

Material	Ductility, μ
Wood wool cement boards	4.44
Plywood	4.40

As mentioned in Section 5.3.3.4, the full capacity of plywood was not utilised due to the size and length of fasteners and the thickness of the timber frame. We can see that the ductility ratios from the experiment for this particular configuration do not differ significantly. The wwcb sheathing exhibited a greater ductility ratio compared to plywood. The full strength of wwcb boards was utilised, whereas plywood's was not.

5.3.3.6 Work to failure or energy dissipation

The amount of work a structure can absorb is very important when considering a material for use as a shear wall. The lateral forces that are exerted on structure and transferred to the shear wall produce large amounts of energy that must be absorbed in order to avoid failure. The energy dissipated during a monotonic test is calculated by determining the area under the load-displacement graph. The limits of the energy dissipation are from the point of zero displacement to the failure displacement, which was taken at displacement equal to $0.8F_{peak}$.

The amounts of energy dissipated are listed in Table 5.13. Plywood was able to dissipate more energy, even though it had not been able to utilise its full strength and stiffness. The data in Table 5.13 show inconsistencies between the results for the wwcb wall-sheathing material. The wwcb energy dissipation coefficient of variation is 8%, this is brought about by the variability of material due to the uncontrolled manual production of wwcb. Only one specimen for plywood was used, due to the pre-stressing of P2. Plywood rapidly reduces its ability to dissipate energy when it has attained its maximum load (F_{peak}).

Table 5.13 Energy dissipation of sheathing materials

Material	Energy dissipated	COV
Wwcb	283	8%
Plywood	471	

5.3.3.7 Wall behaviour and mode of failure

It is generally accepted that the sheathing nail load-slip behaviour is the single most influential factor in the performance of shear walls (Stewart 1987, Dolan 1989). The walls in this study typically failed when sheathing nails either pulled out of the framing or tore through the sheathing. When this happened, the sheathing panels were no longer effectively attached to the framing and the wall was unable to resist any further shear force. Different framing, sheathing and nails, but with the same spacing, were used for the sheathing panels. Generally, the interaction of the nails with the sheathing and framing produced different wall behaviour and modes of failure.

Furthermore, the absence of hold-down or overturning restrains on both ends of the walls renders it vulnerable to base or sill plate and vertical frame separation. It follows then, that when the vertical member of the wall frame is being lifted and the corner metal brace is not able to resist the moment, separation can be seen, as shown in Figure 5.10. The nails connecting the vertical frame and the base are being pulled out. Some failure to this connection is due to splitting of the wood ends. Separation takes place where the load is applied.

5.3.3.7.1 Wall sheathed with wood wool cement board (medium-density wwcb)

Wwcb walls with a standard dimension of 600mm x 2400mm x 8mm thick were used in the walls. They were pre-cut to length for the dimension of the wall. Each wall is sheathed on each side, therefore having eight wwcb panels cut to length. The perimeter nails' spacing was at 150mm from the centre for the main frame and the vertical frame members of the wall. Nail spacing on the horizontal studs were 200 mm on centre. The edge distance spacing was 25mm.

No specimens were provided with hold-down overturning restraints. There were two modes of failure with wwcb sheathing; the first was tearing of the nails through the panels as shown in Figure 5.8, and the second was pulling out of the nails from the timber framing. Figure 5.9 shows separation of the nails from the framing. The reason for this is that on the part where there was tearing, the bonding of the wood excelsior and cement was not good. It was observed that the cement content of this area was less than on other areas of the panel as is expected of manually mixed and formed cement bonded panels. In contrast, the area where the nails pulled out were observed to have more cement. There was bulging effect of the sheathing due to pulling out of the nails through the wwcb panels. As mentioned in the introduction of this section, the absence of hold-down restraints can cause the tendency of the vertical frame to separate from the base of the frame, as shown in Figure 5.10. Nails and corner stiffeners were not enough to hold down the vertical stud where the load was applied. Figure 5.11 shows the deformation and failure of the corner metal brackets of the wall. The corner metal bracket's fasteners at the bottom were pulled out due to uplift.

Figure 5.8 Tearing of the nails through the wwcb panels.

Figure 5.9 Pulling out of the nails from the timber framing.

Figure 5.10 Separation of the vertical frame from the base of the wall.

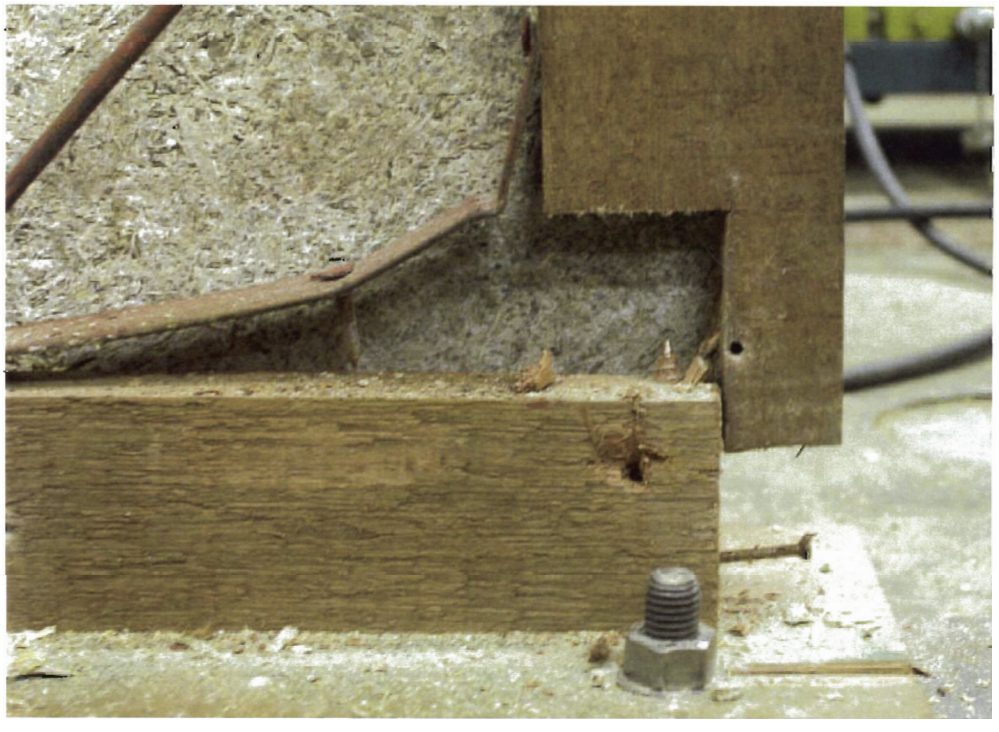

Figure 5.11 End separation with the other sheathing removed.

5.3.3.7.2 Wall sheathed with F11 plywood

F11 softwood plywoods with a standard size of 1,200 mm by 2,400 mm by 7 mm thick were used in this study. The same nailing schedule was implemented with this type of sheathing material. Perimeter nailing is 150 mm o.c., 200 mm o.c on the horizontal members and 25mm to edge distance. Two plywood panels covered one segment of the wall. A total of four plywood panels were used on one wall specimen.

Whereas wwcb nails either pulled out of the framing or tore through the sheathing, the sheathing nails used for the plywood always pulled out of the framing. The nails did not damage the sheathing, as seen in Figures 5.12 and 5.13. This could be attributed either to the smaller diameter and shorter length as compared to the fasteners used in the wwcb panels, or because plywood is denser and more ductile than the wwcb.

As shown in Figures 5.12 and 5.13, nails along the bottom plate were observed to pull out first. Pulling out of the nails from the bottom started from where the load was applied towards the end of the bottom plate. After the sheathing nails pulled out of the bottom plate, the same sheathing nails on the end studs started from the bottom and worked towards the top. This nail pull-out from the vertical frame is noticeable, as with the nail pull-out of the bottom plate. Figure 5.14 also shows the failure with the end connection. The vertical frame tends to pull out the nail connection from the end grain of the bottom plate. The general mode of failure for the plywood walls was the sheathing pulling out of the framing on the bottom plate, allowing the end stud near the hydraulic ram to separate from the top plate.

Figure 5.12 Nail pull-out from the timber framing.

Figure 5.13 Nail pull-out starts from the base where top load is applied.

Figure 5.14 Separation on the nail end grain connection for the vertical bottom plate.

5.4 Summary

This Chapter (5) has provided the results and discussions from the experiments conducted in Chapter 4, starting from the preliminary tests and progressing to the wall tests that are essential in generating the model for the non-linear behaviour of the wall. A full discussion of the non-linear behaviour of the wall based on the experimental procedures and code of standards was presented in this section. Parameters set by the ASTM E564 standard were used to compare the performance of the two type of sheathing materials used in the wall. The EEE parameters were: elastic stiffness, yield load and displacement and ductility. Also covered in this section were the wall capacity, wall failure and energy dissipated by the two timber shear walls. The two sheathing materials used were 8mm medium-density wood wool cement board and 6mm F11 softwood plywood.

The walls have different mode of failures. The wwcb-sheathed wall failure is characterised by a shear or tearing of the sheaths while the plywood sheathed wall is characterised by nail pull-out from the timber frame. Plywood sheathed wall exhibited higher ultimate load, elastic stiffness, yield load and failure load displacement. However, wwcb exhibited larger ductileness as compared to plywood.

6 F-shelter tests

6.1 Introduction

This chapter presents a short description of the F-shelter which has already been described in Chapter 2. The following are contained in this section: construction and assembly, set-up and procedure of the tests and instrumentation.

Two types of tests were performed on one F-shelter: 1) non-destructive test or static tests and 2) destructive test using a simulated earthquake time history reading. Because of financial constraints in producing two symmetrical F-shelters, the author used only one F-shelter for both tests. The purpose of the static test and dynamic test were to observe the behaviour of the structure under lateral load.

Results from the non-destructive and destructive test experiments are presented. Different loadings were recorded and were presented in graphical form; that is, load-deflection graphs. Static loads were only limited to 5kN, so as not incur damage to the structure because the author used only one specimen for both tests. Although incremental damage of the structure is possible when subjected to repetitive loading and unloading, the author saw to it that no damage (visual inspection is taken as a method) was present in the structure. Kobe earthquake and Zone IV earthquake records were used to observe the behaviour of the structure under dynamic loads. Maximum base displacement of the shaker table was limited to 100 mm; that is why full or 100% simulation of the earthquake intensities was not possible. For the Kobe, the author used just 70% and for Zone IV only 80% intensity.

6.2 Full-size F-shelter testing

This section describes the physical testing of a full-scale test of the F-shelter. A description of the structure will be discussed. Details of how the structure is actually set up in the field is shown in Appendix A in picture form, to illustrate the structure when erected and not erected.

6.2.1 The F-shelter for testing

The structure was built differently from traditional/conventional shelters. The intercomponent connections were fabricated hinges and steel plates; whereas nails are used to rigidly connect house components in residential houses. Design and specifications were prepared by the Structural Design and Engineering Section of the Forest Products Research and Development Institute (FPRDI), Philippines. The shelter was intended for emergency shelters during calamities caused by typhoons, floods, earthquakes and volcanic eruptions. The structure was designed to rest on adjustable footings to make it adaptable to uneven terrain. For the purposes

of this experiment, the base or the perimeter floor framing was bolted. This experiment aimed to load the F-shelter to attain its maximum capacity by fixing its base when subjected to dynamic load.

The prototype F-shelter was constructed using Apitong timber frames. The wall's structural frame, vertical studs and horizontal braces are 25mm x 75mm. Metal plates connect the floor and wall.

The main sheathing used in the structure is wwcb of various thicknesses and densities, i.e., 8mm medium density (600 kg/m^2) wwcb for the walls, 12mm medium density wwcb for the casing, 25mm high-density (750 kg/m^2) wwcb for the floors and 8mm low density (450 kg/m^2) roof that serves as a horizontal diaphragm. The roof sheathing is overlaid with asphalt shingles fastened to the wwcb sheathing of the roof with 25mm aluminium rivets.

6.2.2 Construction and Assembly

A steel base frame was utilised to position the F-shelter on the shaker table. To facilitate the set-up for both the static and dynamic tests, the structure was set up on the shaker table using this same connections. This base frame was bolted to the shaker table. A cross-section of the frame is shown in Figure 6.1. Two 205mm x 9mm I-beams were used as base frames. Pre-drilled holes of Ø13.5mm were provided at a distance of 800mm on centre for the angle bars to be bolted. The angle bars connected to the I-beams were used to clamp the RCHS 45mm x 90mm.

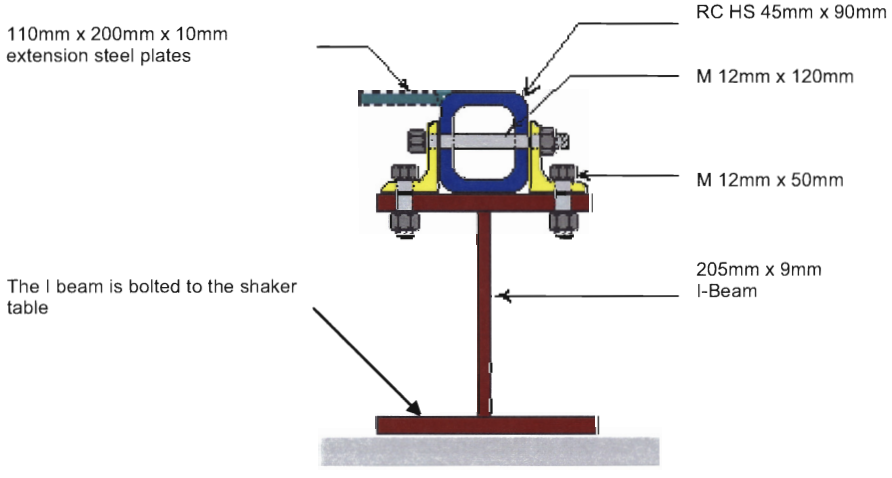

Figure 6.1 Base of the structure for testing.

With the base frame assembled on the shaker table, the floor of the structure was laid on the base frame. The north end of the floor was flashed at the end of the RCHS. At a distance of

150mm from the north end, bolts were spaced at 300mm. Holes were drilled on first, making sure that there was a mark or dent left on the RCHS to attain the same locations of the holes. The markings made on the RCHS were then drilled at Ø11.5mm holes for Grade 5, 10mm x 115mm plain finish bolts. The holes were then tapped for a UNF thread. Figure 6.2 shows a finished assembly of the floor base. The figure shows the south end of the structure. The same procedure was implemented at the other side of the wall. The floor was fastened using 10mm x 115mm Grade 5 bolts threaded to the tapped holes.

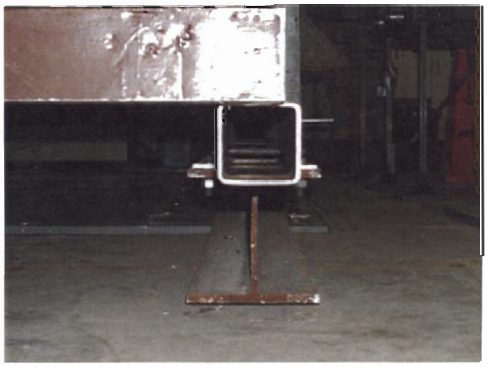

Figure 6.2 Floor fastened to the steel base frame.

The bottom piece of the casing was similarly connected to the floor. After the bottom part of the structure was assembled, the walls were erected one after the other.

The exterior of the casing, which holds the entire wall and roof component in place, was erected first. The bottom 50mm x 100mm wood frame of the casing side walls was drilled with Ø15 mm holes. The base was bolted to the extension plate shown in Figure 6.1. The walls of the casing were attached to the steel base frame with two M12 bolts for each side. The walls were plumbed to establish the proper fitting of the walls when placed. Fourteen screws of type 17 Buglebatt CL2 (10mm x 100mm) were used to connect the side wall to the bottom part of the casing.

Walls number 2 and 6 (refer to Figure 2.4) were first connected to the casing of the centre piece. Walls number 2 and 6 were folded inwards to provide additional balance and stability. The walls can stand on their own if wall number 1 is connected to walls 2 and 6. As shown in Figure 6.3, two side walls were already connected to the north side of the structure. The walls were put in position and then the pins were placed in place on the hinges connected to the side wall of the casing. Once the side walls number 2 and 6 were erected, wall number 1 could easily be connected to walls 2 and 6. The same procedure was applied, putting the pins in place in the hinges on walls 2 and 6. The roof of the casing was connected next. A temporary bracing was nailed on the side casing to maintain its plumpness while the casing's roof was

being prepared to be connected to the side walls. Gradually the roof was lowered down while adjustments were being made on the side wall of the casing. Both sides were fastened with fourteen screws type 17 Buglebatt CL2 (10mm x 100mm), using a battery-powered drill.

Figure 6.3 Side walls 2 and 6 were erected.

Walls number 3 and 5 were then erected. Wall number 4 was connected to walls number 3 and 5 in the same way. With all the walls erected, the walls were then connected to the roof of the casing. The walls on the south end of the structure were folded inwards to provide enough room to install the roof, leaving the north end wall partially open to provide additional structural stability.

Although a forklift carried the roof, installation was performed manually. The roof was then carried across the floor, since a limited area was available for the forklift to manoeuvre the roof in place. Two staff held the roof in a slanting position with the hinges approximately in the positions of the casing roof hinges. The base of the roof was adjusted accordingly until the hinges were fitted nicely to the hinges on the casing's roof. After the installation of the roof, the roof was lifted using a forklift. The roof was lifted at a height approximately the same as with wall number 4 but higher. This is to give way for the wall to be unfolded completely. The folded walls were then unfolded, extended and aligned with the roof. The same procedure was adopted for the opposite side of the structure. Due to the obstruction made by the reaction

frame on this side, a chain block was used to lift the roof while unfolding the walls and putting them in place.

6.3 Monotonic test

This section summarises the procedures conducted on the F-shelter. The structure was set up on the shaker table, using 20-tonnes capacity hydraulic jacks positioned at exactly 1.9 metres from the floor level on both corners of the wall on the north end, as shown in Figure 6.4. The distance of the hydraulic jacks from the floor was limited to only 1.90m in consideration of the clearance needed for the hydraulic jacks that would be put in place horizontally.

Figure 6.4 Location of two hydraulic jacks.

6.3.1 Set-up and experimental procedure

Two static tests were conducted on the structure. The first one was the test with reinforcement plates. These 3mm x 100mm x 100mm and 3mm x 100mm x 160mm steel plates were used to reinforce the connection between the roof and the wall and the wall to the floor (Figure 6.5). The second test was conducted without the reinforcement plates, which is the true or actual condition of the structure. It is only connected on the mid-length of the wall and the ends of the wall connecting the roof and floor.

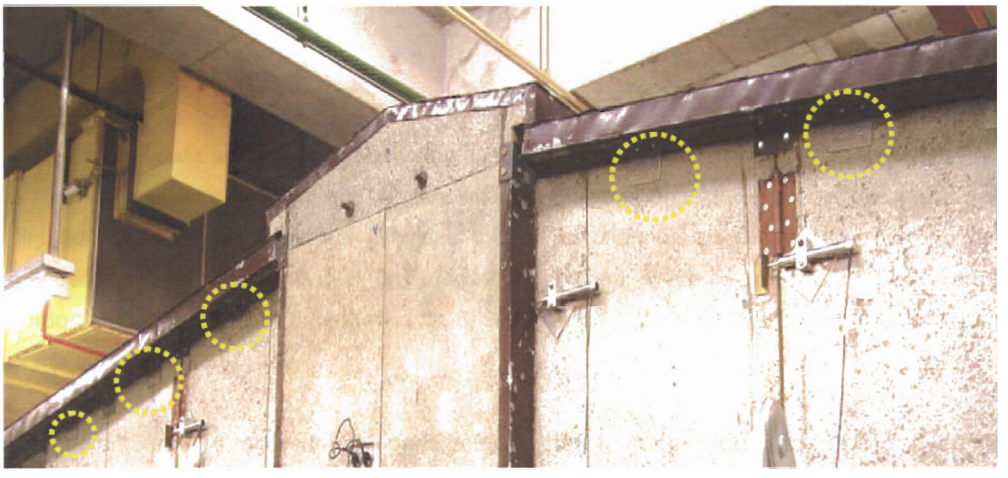

Figure 6.5 Reinforcement plates used to connect the roof and wall

The same hydraulic rams/jacks were used in both tests. The hydraulic rams have a capacity of 20 tonnes with a maximum displacement range of 300mm. These two actuators are connected to the reaction frame located on the north end of the structure, as shown in Figure 6.6. The rate of loading applied was 36N/sec. The F-shelter should be able to withstand a 5 kN load at each actuator since this is the designed load (refer to Section 2.3 of Chapter 2).These are fitted with a 20 kN range load cell and a spherical seat to keep an even loading. A 5mm x 45mm x 75mm steel plate was glued on the structure as the loading point of the hydraulic rams to the structure. Walls 2 and 6 were loaded at the top, using the two hydraulic rams under a load control.

Figure 6.6 Hydraulic rams connected to the reaction frame.

6.3.2 Instrumentation

A 16-channel data acquisition system was used. Location of the channels is illustrated in Figure 6.7. Displacements of the structure were measured in one principal direction, the x-axis or the direction of loading. Table 6.1 provides the list of channels used and their corresponding measurements. Numbers 3, 4, 5, 6, 7, 11, 12, 14, 15 and 16 are instruments located at the top portion of the structure and numbers 1, 2, 8, 9, 10, and 13 are instruments located at the bottom of the structure.

Channels 15 and 16 represent the loads being applied from the hydraulic rams to the structure. They are located on the top end of the structure on the north end side. Channels 1 and 9 represent LVDT #1 and #9 to measure the uplift movement of the floor. Channels 2 and 10 represent LVDT #2 and #10 that are used to measure horizontal distances at 2m high away from the load. Channels 3, 4 and 5 represent LVDTs # 3, #4 and #5 that measure the relative movement of the hinges or the connection of the components. Channels 3 and 11 represent LVDTs # 3 and #11 which measure the horizontal travel of the wall where the load is being applied. On the opposite side are channels 7 and 14 for LVDTs #7 and #14, used to measure the displacement of the structure opposite of the load. Channels 13 and 8, representing LVDTs # 13 and #8, measure the horizontal displacement of the structure at the bottom. Lastly channel 12 for LVDT #12 measures any change in angle on the opening for the applied load.

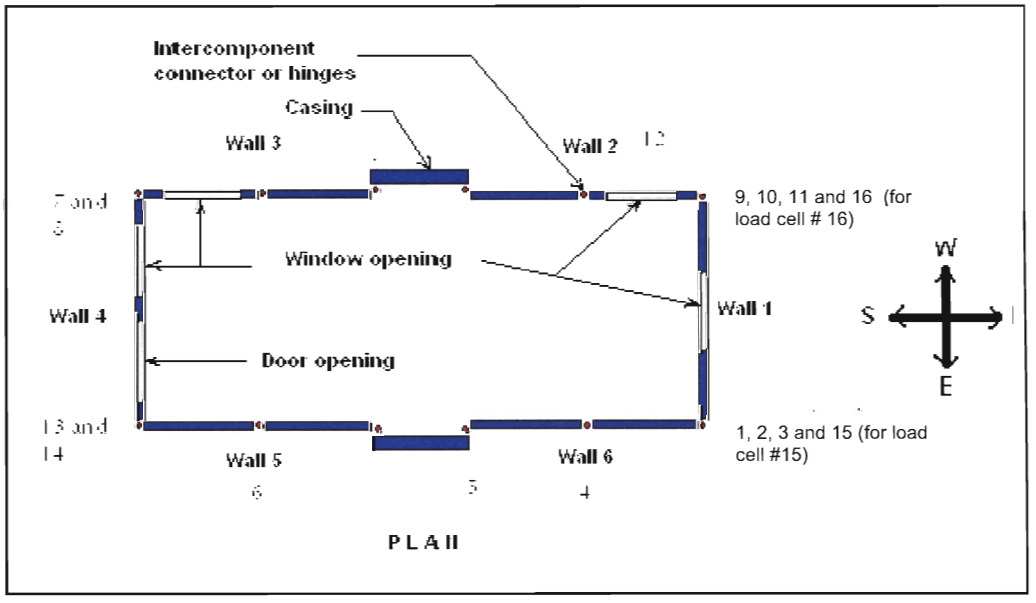

Figure 6.7 Location of instrumentation channels for non-destructive monotonic test.

Table 6.1 Summary of channels and measured displacements

Channel #	LDVT represented	Range (mm)	Measures
1	1	25	Uplift movement of the floor
2	2	25	Horizontal movement of the wall
3	3	50	Displacement of the top of the wall
4	4	25	wall to wall displacement
5	5	25	wall to casing displacement
6	6	25	wall to wall displacement
7	7	50	Displacement of the top of the wall
8	8	25	Horizontal movement of the wall
9	9	25	Uplift movement of the floor
10	10	25	Horizontal movement of the wall
11	11	50	Displacement of the top of the wall
12	12	25	Change in angle for the opening
13	13	25	Horizontal movement of the wall
14	14	50	Displacement of the top of the wall
15	Load cell #1	20kN	Load applied right of the north end
16	Load cell #2	20kN	Load applied left of the north end

The data acquisition system that was used in this test was LabView. The data for load and displacement were logged to a computer. The 16 channels of data that were logged during the experiment to capture the load distribution and displacement responses of the structure during the experiment were sufficient to describe the structural behaviour of the structure. Readings were taken at 12 a rate of points per second which is sufficiently fast, given the slow rates of loading. The two load cells are connected together by separate RS485 lines which were then read into the serial port of the PC via RS232 converters, while the digital gauges were connected directly with an RS232 to the computer. The static and dynamic test flow is shown in Figure 6.8, which also indicates the flow of the work done on F-shelter structural testing.

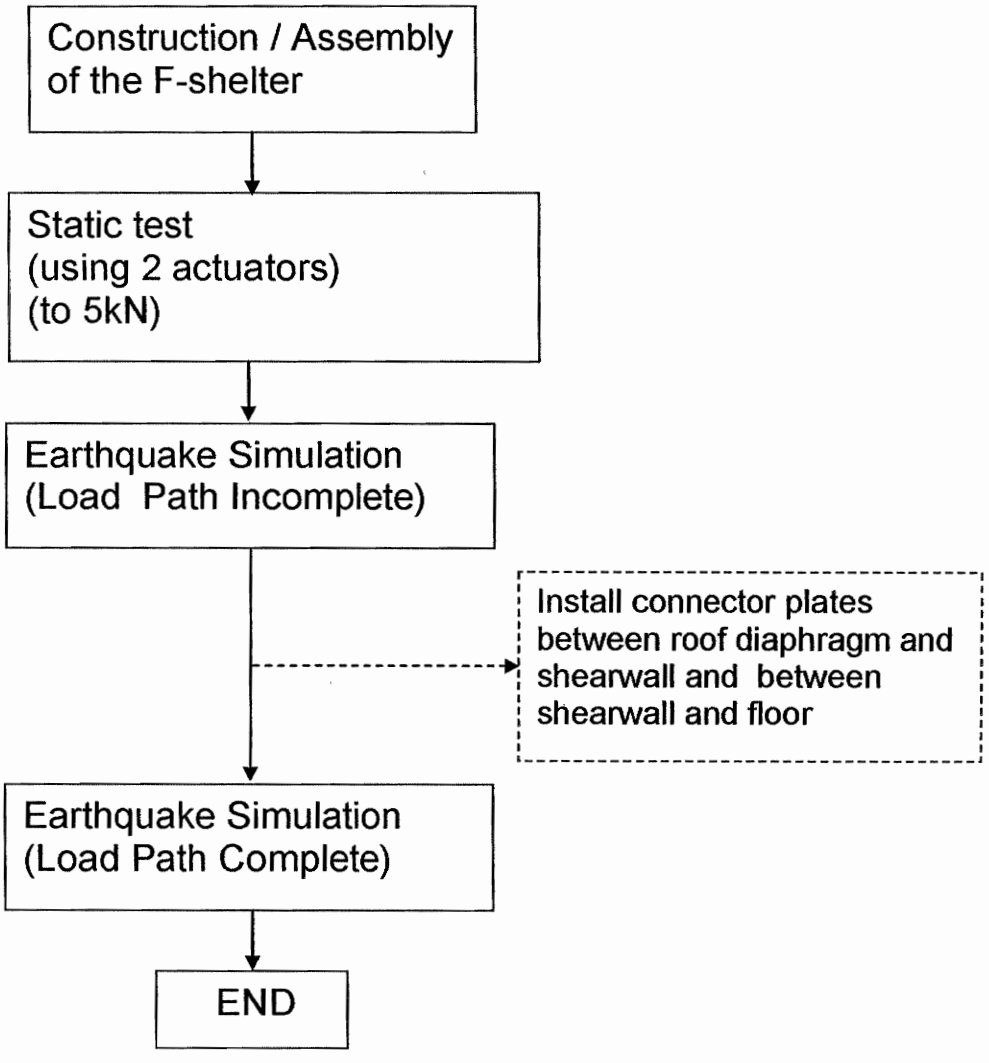

Figure 6.8 Flow of testing activity for the F-shelter.

6.3.3 Results and Conclusions

The static test presents two conditions: (1) the F-shelter with additional metal plate reinforcement and (2) the F-shelter without reinforcements. The destructive dynamic test will present results from the simulated Kobe and Armageddon earthquakes.

The test performed on the non-destructive test was limited to 4,000 N and 5,000 N loads for the F-shelter with metal plate reinforcements and without reinforcement, respectively. This was to make sure that the structure would not suffer any damage in preparation for the dynamic test. It was observed that at 5 kN load, the joints produced squeaking sounds that could be detrimental to the structure's stability.

6.3.3.1 F-shelter with metal plate reinforcements.

The additional reinforcements were incorporated in the design to permit proper distribution of the loads applied to the structure or complete load path. Although this would make the structure more rigid, this precaution was implemented due to the possibility of the structure failing at its joints.

For each load, the structure was loaded and unloaded three times. This was carried out to eliminate lagging, gaps and unevenness in the thicknesses of the sheathing that would cause displacement offsets on the results of the structure. An example of the loading and unloading or the hysteresis of the load is presented in Figure 6.9. Test 1-4kN on the graph shows the maximum offset for a 4 kN load, that is, 1 mm. The second and the third tests have significantly reduced the offsets of the succeeding loads by 0.3mm and 0.2mm respectively.

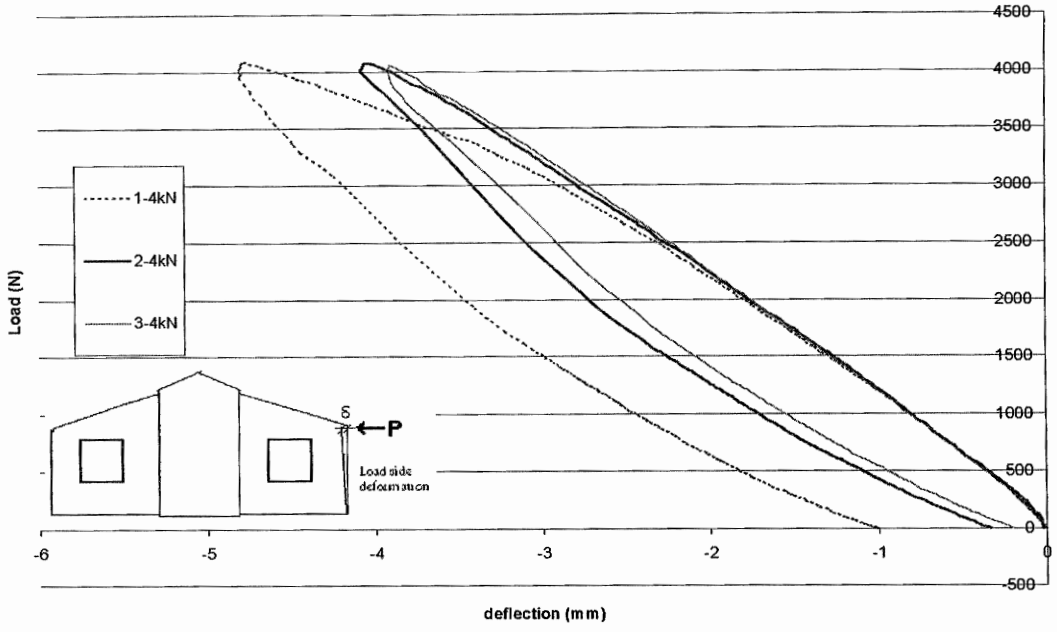

Figure 6.9 Hysteresis loops at 4 kN maximum load on the side with opening.

On the other hand, the side with the opening is graphically illustrated in Figure 6.10. The offsets registered are almost the same as the side with opening. A 1.1 mm, 0.3 mm and 0.2 mm offset was observed for tests 1, 2 and 3 respectively. We can also see that the initial loads for the three tests did not start with zero (0). We have 350 N, 330 N and 310 N as the starting loads for tests 1, 2 and 3 with a corresponding deformation. Because of the presence of gaps in the intercomponent connections and or deformed and elongated bolt holes, initial loads push or compress the components to get rid of such gaps before these start to absorb the loads.

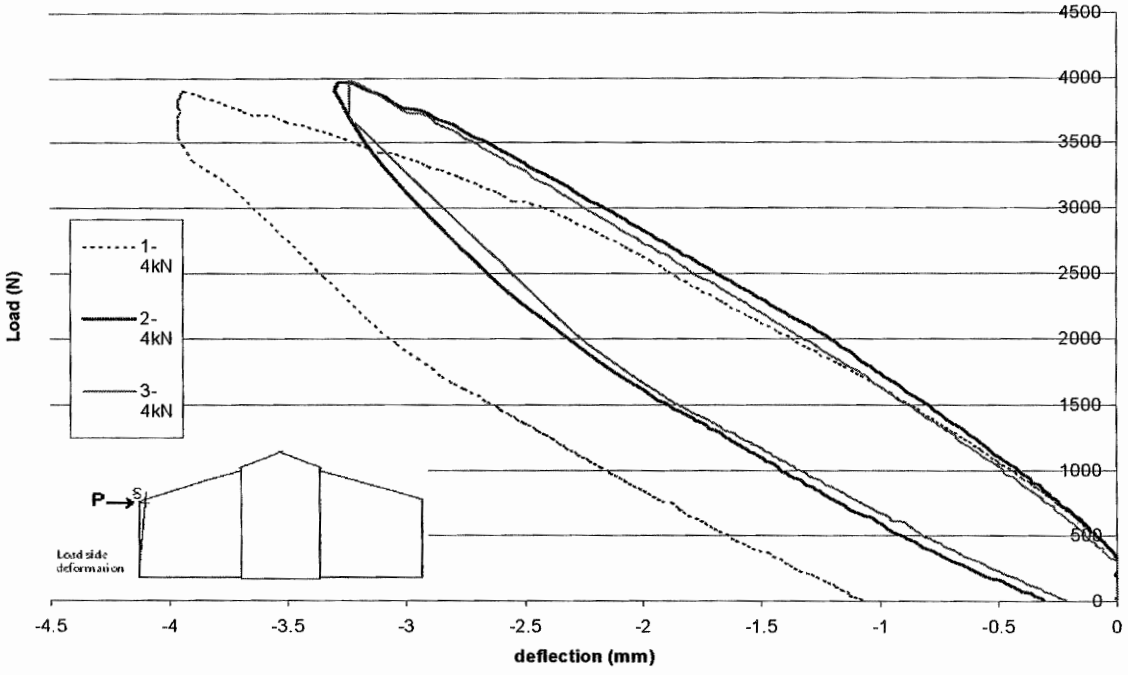

Figure 6.10 Hysteresis loops at 4 kN maximum load on the side without opening.

The side without an opening has an average deflection of 3.3mm, while deflection on the other side is 4.0mm. This result disregards test no.1 for each of the hysteresis curves.

6.3.3.2 F-shelter without metal plate reinforcements

The removal of the metal reinforcements simulates the actual condition or the type of connection in the F-shelter in service. A different approach to the testing was employed. An increasing load, starting from 1.5 kN to 5 kN was applied. The maximum loads applied to the structure are presented in Figures 6.11 and 6.12. Each figure presents deflections on the loaded and the opposite sides with and without opening, respectively. The deformations showed that the structure has twisted, due to unequal stiffness of the side walls. The side walls without opening showed less deformation compared to the side with the opening.

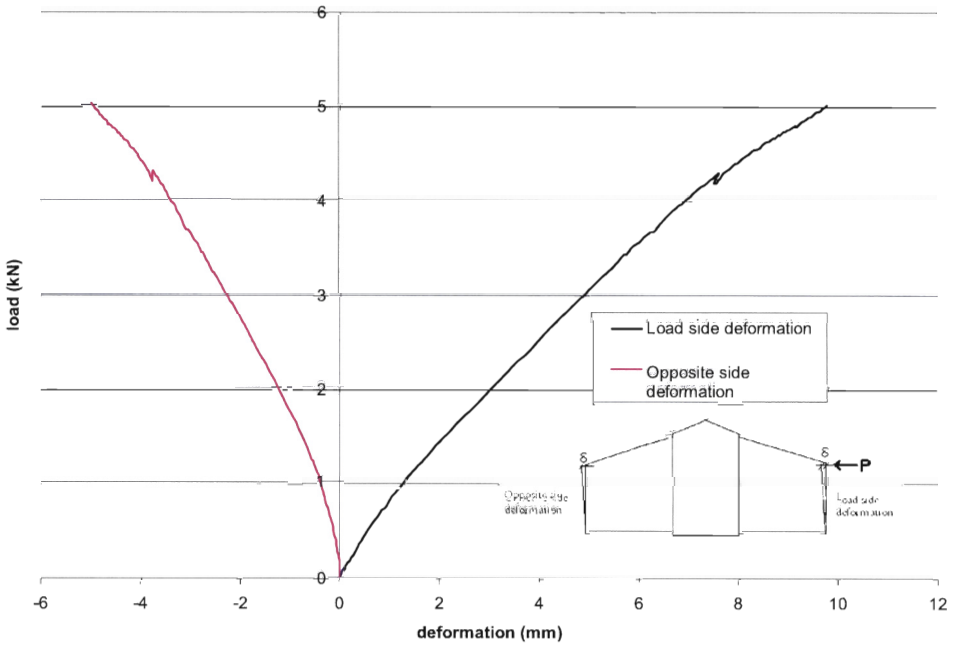

Figure 6.11 Deformation on the side without window opening.

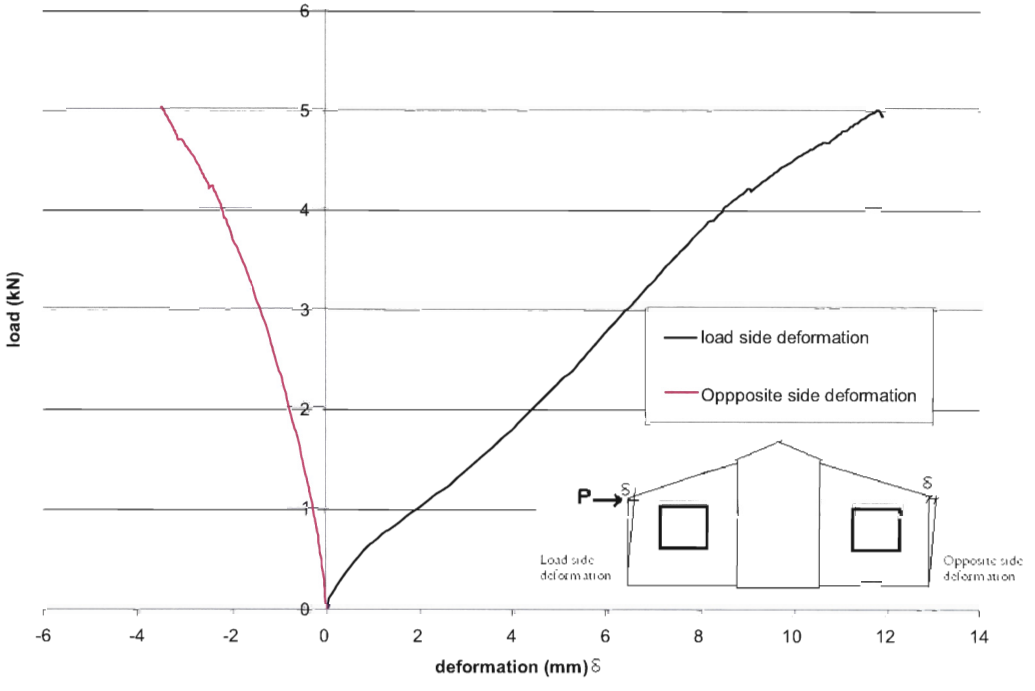

Figure 6.12 Deformation on the side with window opening.

The summary of the test results for deformations and corresponding loads are tabulated in Table 6.2. Based on the results, the F-shelter without metal reinforcements has attained bigger values of deformation. The tabulated deformations on this table represent movements on the loaded side.

Table 6.2 Summary of deformation (mm) for static test

	With metal reinforcements			**Without metal reinforcements**		
Load (N)	With opening (a)	Without opening (b)	Ratio (a/b)	With opening (a)	Without opening (b)	Ratio (a/b)
1,500	0.8	1.8	0.4			
2,000				4.8	4.4	1.1
3,000	2.3	2.8	0.8	6.7	5.6	1.2
4,000	3.9	3.2	1.2	8.3	7.0	1.2
5,000				9.8	5.0	1.9

At 4 kN, the elastic stiffness of the F-shelter with metal reinforcements is 115% higher than the stiffness of the structure without metal stiffeners on the side with openings, while on the other hand, the elastic stiffness of the F-shelter with metal reinforcement is 124% higher than the stiffness of the structure without metal stiffeners on the side without openings.

The elastic stiffness of the F-shelter, comparing the side with opening and the side without opening is, 18% and 16% higher for both structures with metal reinforcements and without metal reinforcements, respectively.

6.4 Dynamic test through the Shaker table

This sub-section presents a detailed procedure on how the shaker table test was conducted. Earthquake history readings were taken from two prominent earthquake records: one from the Kobe (1995) earthquake and the second from the Zone IV earthquake simulation that is used to test electronic casing devices. This Zone IV record reading is a compilation of the strongest earthquakes in history.

The structure was also tested under two conditions, as was the case in the static test. The first was with metal connectors to establish the proper transmittal of loads from the wall to the roof, floor and casing. The second was without metal connectors, as it represents the actual construction of the F-shelter.

The following subsection will present a brief description of the Kobe earthquake and the Zone IV earthquake in terms of time-acceleration readings and relevant information. In addition, the procedures performed in the conduct of the shaker table test are described.

6.4.1 Ground Motion Simulation

Simulated earthquake motions are used when strong motion recordings are not available for a particular earthquake engineering application. This can occur for particular geographical regions where recordings are sparse or for particular magnitude and distance ranges that may be of interest for a project. In either case, simulated earthquake motions represent synthetic data that can be used to supplement or supplant recorded motions. The two applications of simulations that have been common in engineering design practice are: (1) to provide design ground motion for structural or geotechnical response analyses for a particular project or site; and (2) to provide synthetic data for regions (geographic area, magnitudes and distances) of sparse data to supplement or supplant recorded motions in developing attenuation relations or design ground motions. For this particular project the Kobe and Zone IV earthquake ground motion recordings were used.

6.4.1.1 Kobe Earthquake ground simulation

The Hyougo-ken Nanbu earthquake, or Kobe earthquake, that happened on the 17th of January 1995 had a magnitude of 7.2 (http://nwn.ege.com 2004). It struck the region of Kobe and Osaka in south central Japan. An example of the ground motion recording is illustrated in Figure 6.13. Strong ground motion/shaking lasted for about 20 seconds, equivalent to an acceleration of 0.85 cm/s^2 and a maximum displacement of 125 mm that caused severe damage over a large area. The shock occurred at a shallow depth on a fault running from Awaji Island through the city of Kobe. Strong ground shaking lasted for about 20 seconds and caused severe damage over a large area (http://www.ege.com/publications 2004).

Nearly 5,500 deaths were confirmed, with the number of injured people reaching about 35,000. Nearly 180,000 structures were badly damaged or destroyed.

Damage was recorded over a 100-kilometre radius from the epicentre, including the cities of Kobe, Osaka and Kyoto, but Kobe and its immediate regions were the areas most severely affected. Damage was particularly severe in central Kobe, in an area roughly five kilometres by 20 kilometres parallel to the port of Kobe. This coastal area is composed primarily of alluvial soils and artificial fills, a type of soil common or similar in the Philippines (NSCP 2001).

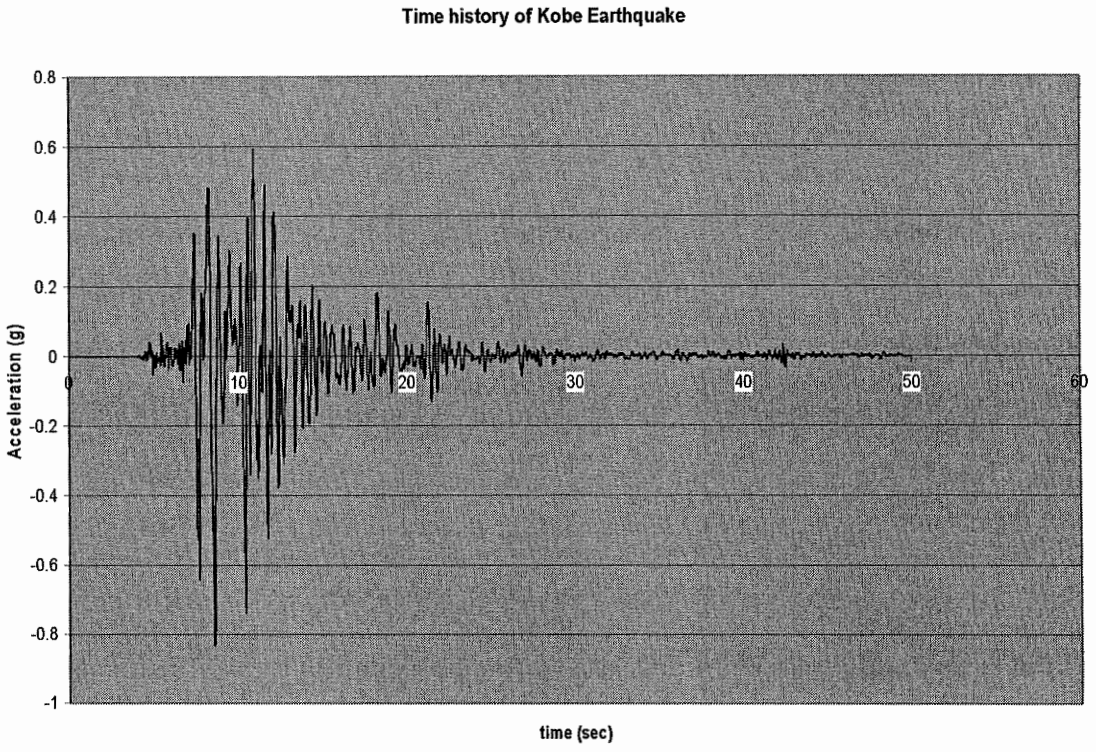

Figure 6.13 Time history record for Kobe earthquake.

6.4.1.2 Zone IV earthquake ground simulation

Little is known about the time history record of this earthquake simulation. This type of earthquake ground simulation is used primarily to test the casings of electronic devices that are sensitive to vibrations. The Zone IV earthquake was opted as there are no other time history record stronger that is available at the laboratory at the time of testing. This synthetic earthquake data represents a compilation of strong records of earthquakes such as the Hachinohe, El Centro, Kobe and others.

An example of the time history record of the Zone IV earthquake has been provided in Figure 6.14: a strong earthquake record that lasts for about 20 seconds, attaining a maximum acceleration of 1.4 cm/s^2.

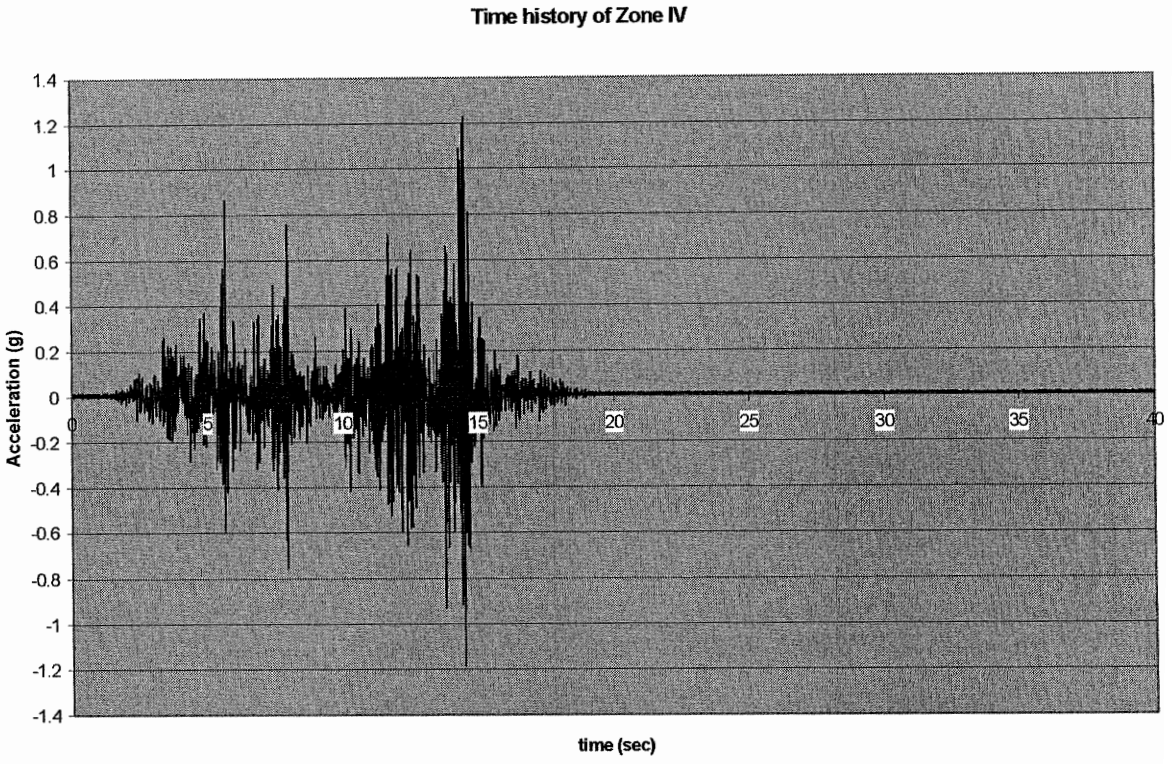

Figure 6.14 Time history record for Zone IV earthquake.

6.4.2 Set-up and instrumentations

This experiment is a continuation from the static test. The steel base frame, the shaker table connection, the floor of the structure, the steel base frame connection were checked. All connections from the base of the structure to the floor were rigidly connected. This ensured that there would be no incidental movement or slippage coming from the structure when loaded.

Dynamic LVDTs were used instead of the static LVDTs that were used in the static test. Two dynamic LVDTs were used in the north end of the structure and two static LVDTs were used in the south end of the structure. These LVDTs were positioned in exactly the same place as for the previous static test. Locations of the LVDTs are shown in Figure 6.15. Five PCB type accelerometers were also used to record acceleration on different locations on the structure. Locations of the PCB 393C accelerometers is shown in Figure 6.15.

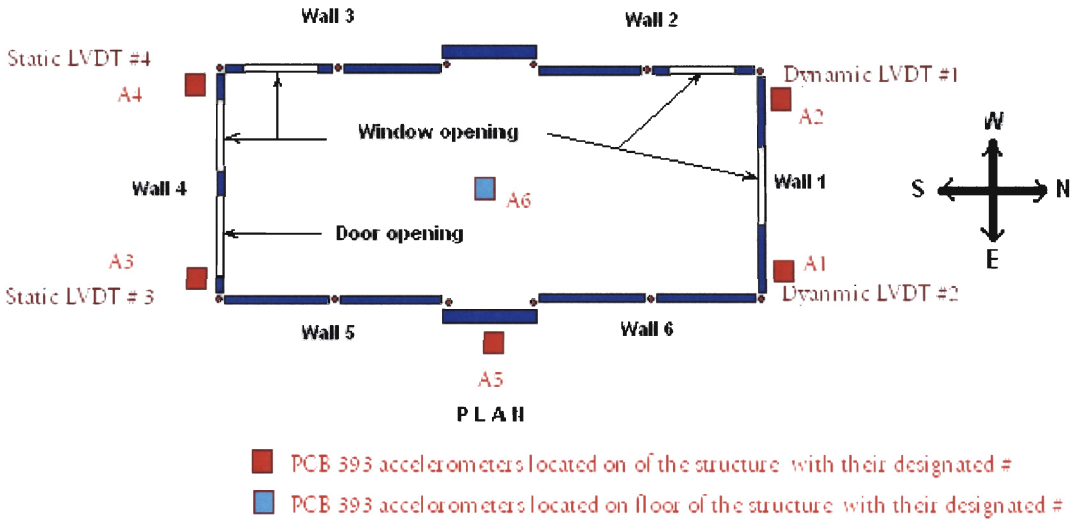

Figure 6.15 Locations of PCB 393C accelerometers and LVDTs.

Furthermore, three video recorders were set up in different locations to assist us for future evaluations. Figure 6.16 illustrates the location of the recorders.

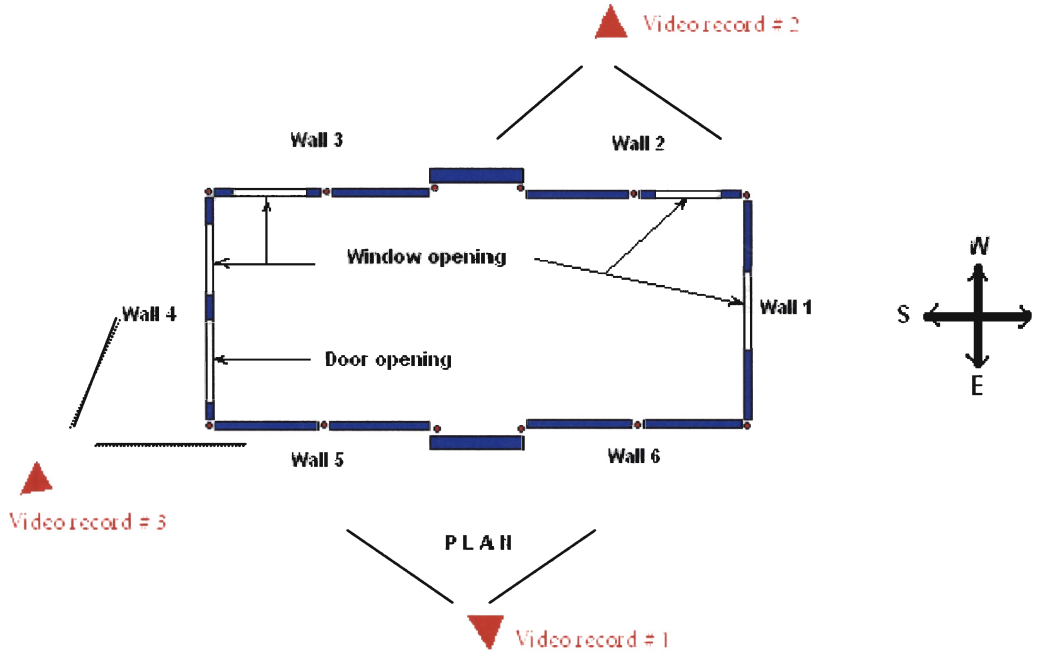

Figure 6.16 Locations of the video camera recorders

6.4.3 Experimental procedure

Before the installation of the walls and the roof, a preliminary testing was conducted to make sure that connections between the shaker table plate and F-shelter's floor (Figure 6.2) were rigid. Similar tests were performed to observe whether the floor restraints were enough to resist the magnitude of the dynamic load, to control if the two connections of frames that were connected to the shaker table were rigid, and to observed any load eccentricities when load is applied – thus depending on the bolt tightness – on the floor frame and on the steel base frames connected to the shaker table.

Warming up the machine, a 1 Hz frequency was selected in a sine waveform. A displacement of 10 mm on each side was selected. After warming up, an assessment of the connections was carried out to see if they are loose.

In addition, a simulation of the Kobe earthquake was tested, for the same purpose as enumerated above and to ensure that the shaker table could exactly simulate the time history readings of the Kobe earthquake. Simulation started at 20% of the full-scale time-displacement reading of the Kobe, and was then followed by 50% and lastly 70%. The shaker table cannot accommodate an 100% full-scale record of the Kobe earthquake, since maximum displacement of the table is only limited to 100mm on each side, whereas, the Kobe earthquake has a maximum of 125 mm.

On the actual experiment of the F-shelter, a 1 Hz sine waveform was also implemented to warm up the machine, followed by the designated percentage of loads to be induced on the structure as follows, as shown in Table 6.3.

Table 6.3 Load percentage applied to the structure for a particular earthquake simulation

Dynamic tests	
Kobe earthquake simulation	**Zone IV earthquake**
5%	50%
15%	80%
30%	
40%	
50%	
70%	

For every test, a close visual inspection of the structure was implemented. Findings were also verified by other staff present.

A block diagram showing the steps taken and the flow of activities for this particular experiment is presented in Figure 6.17.

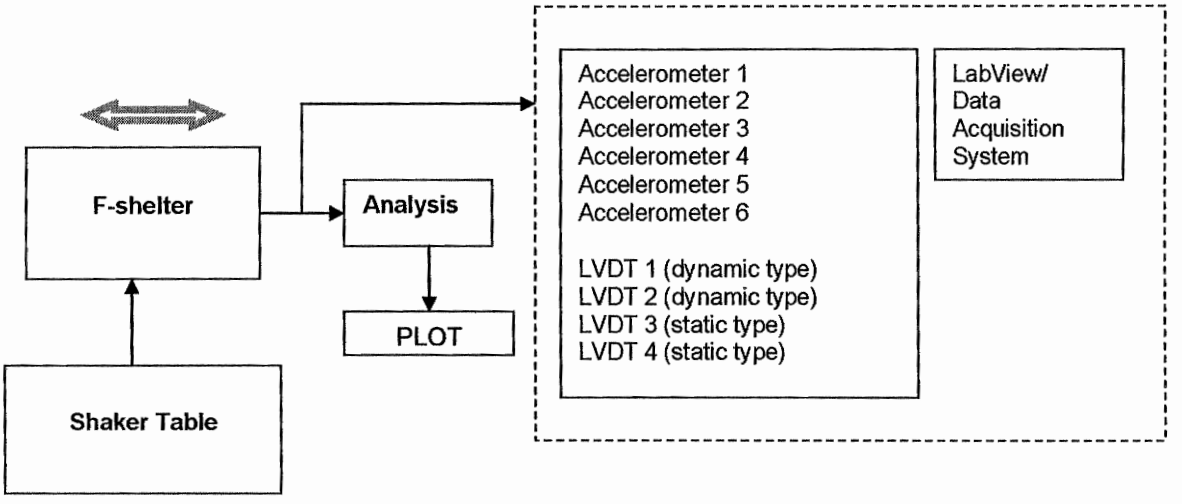

Figure 6.17 Schematic diagrams of activities for the dynamic test of F-shelter.

6.4.4 Results and conclusions

The performance-based seismic design approach has advanced for some types of structures, such as reinforced concrete buildings and bridges, to the point where it may be ready for incorporation into future generations of building and bridge codes; however, its application to wood-framed buildings remains largely unexplored. Current seismic provisions for wood-framed buildings are based on the traditional force-based design procedure, which is mainly concerned with providing what is considered an adequate lateral strength to the structure under seismic hazard level (NSCP, 2001). The strength of a structure does not guarantee safety, nor does it ensure damage control for multiple hazard levels. A large portion of the costly damage to wood-framed buildings during recent earthquakes has been related to performance levels other than life safety, such as excessive drifts causing cracking to interior and exterior wall finishes and high accelerations inducing damage to unsecured building contents (Filliatrault and Folz, 2002; Soriano, 2000).

It is also the aim of this experiment to observe the performance of the F-shelter under specified ground motions such as the Kobe and the Zone IV earthquakes.

Two earthquake loads were applied to the F-shelter. A 70% simulation full-scale displacement of the Kobe earthquake and 80% for the Zone IV earthquake was induced to the structure. The

purpose of this test was to observe the resistance of the structure when subjected to this type of earthquake. As mentioned, full-scale simulation of each earthquake was not possible, due to the limitation of table displacement being only 100mm, enough only to accommodate displacements at 70% and 80% for the Kobe and Armageddon earthquakes. The results shown in this section are presented for the F-shelter with and without the metal plate reinforcements.

The readings of the Kobe earthquake or the Zone IV earthquake are not presented in this section; however, they can be viewed at Appendix M. The Armageddon earthquake was simulated to verify whether the structure could still resist a stronger simulated earthquake. Table 6.4 shows the visual inspection made in the conduct of the Armageddon earthquake, together with the Kobe earthquake.

6.4.4.1 Acceleration comparison

PCB 393C type accelerometers were positioned in strategic locations on the F-shelter; four on the corners of the structure, one on the top side and one on the base. At 50% of the full-scale displacement Kobe earthquake, accelerometer readings on the four top corners of the structure were compared. In Figure 6.18, the structure with metal reinforcements has a maximum acceleration of 0.76 g on the side with opening, while on the other side it is 0.43 g. The maximum accelerations on the opposite side are both 0.49 g (Figure 6.19) on the side with and without opening. The acceleration on the side without opening is 76% higher than the acceleration on the side with opening on the loaded side, and 12% lower on the side without opening.

A difference of 55% is observed for the acceleration between the loaded and the unloaded sides on the wall without opening. This means that the structure had incurred twisting moment while subjected to ground simulation. This means that the casing of the structure had slowed down the acceleration on the unloaded side and also accounted for the reduction of wall stiffness due to the presence of wall openings.

The removal of the metal reinforcement has caused the accelerations to be lower than the acceleration on the structure with metal reinforcements on the loaded side. However, the maximum acceleration at the opposite side is higher than the maximum acceleration on the structure with metal reinforcements. At 50% of the Kobe earthquake, the maximum acceleration of the structure without reinforcement is 1.19 g on the side without opening at the opposite side, and 0.50 g on the side with opening (Figures 6.20 and 6.21).

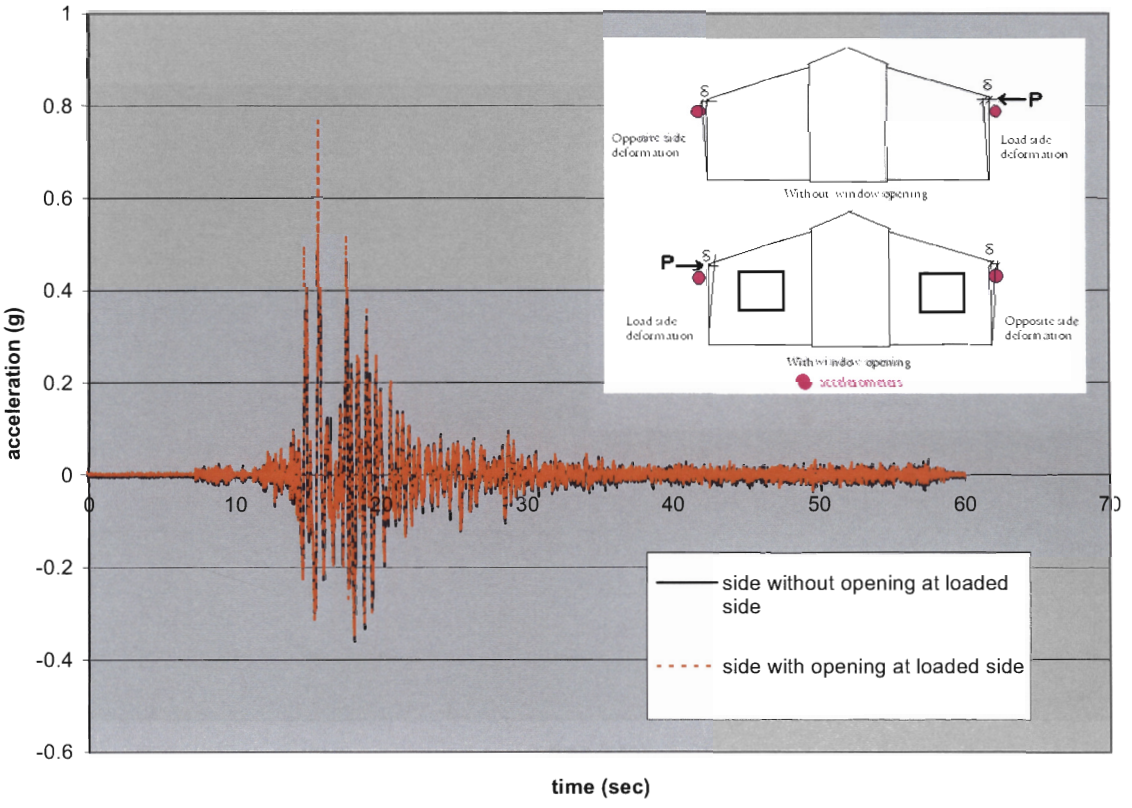

Figure 6.18 Acceleration @ 50% Kobe on the loaded side; with metal plates.

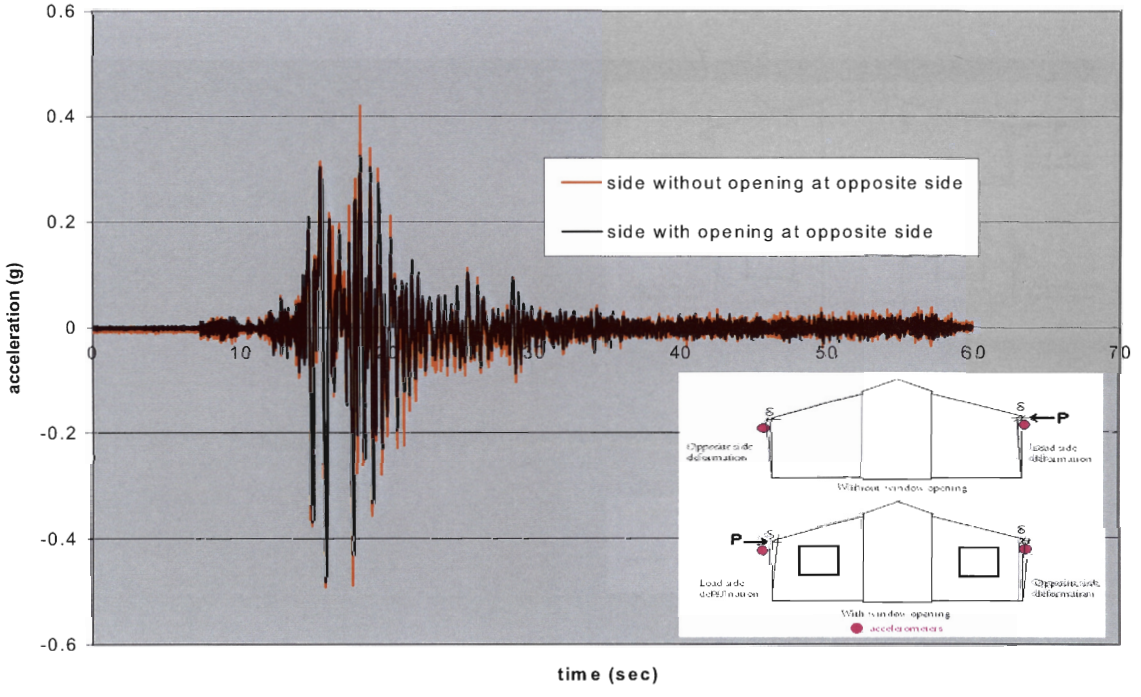

Figure 6.19 Acceleration @ 50% Kobe on the opposite side; with metal plates.

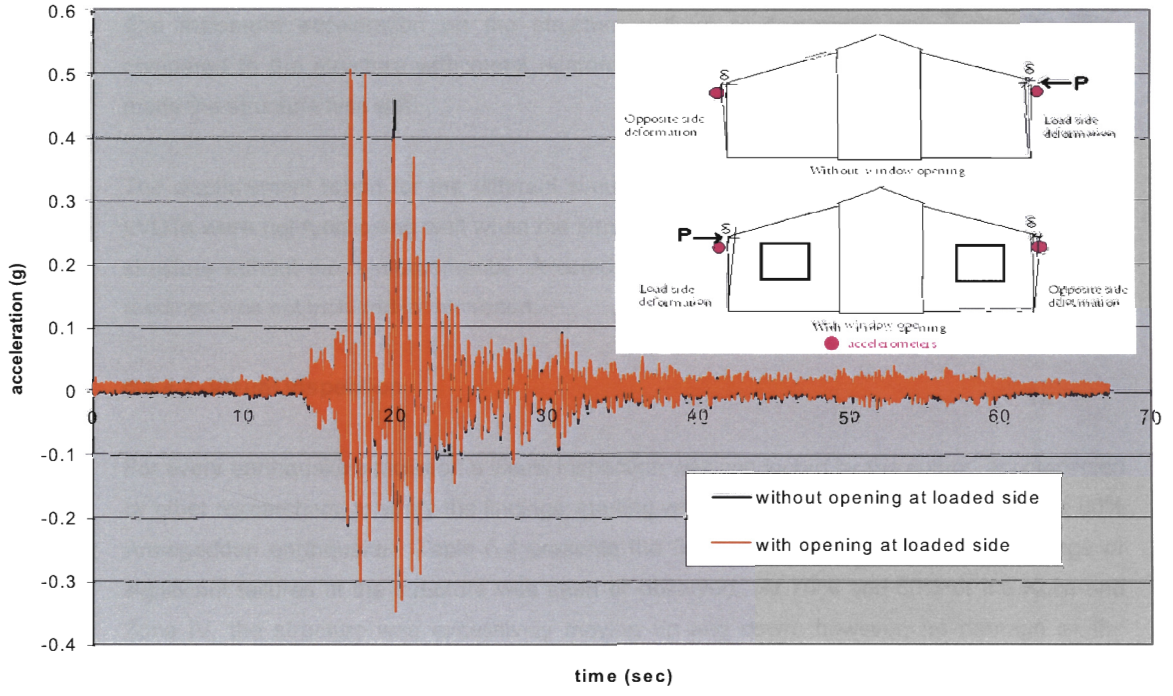

Figure 6.20 Acceleration @ 50% Kobe on at the loaded side; without metal plates.

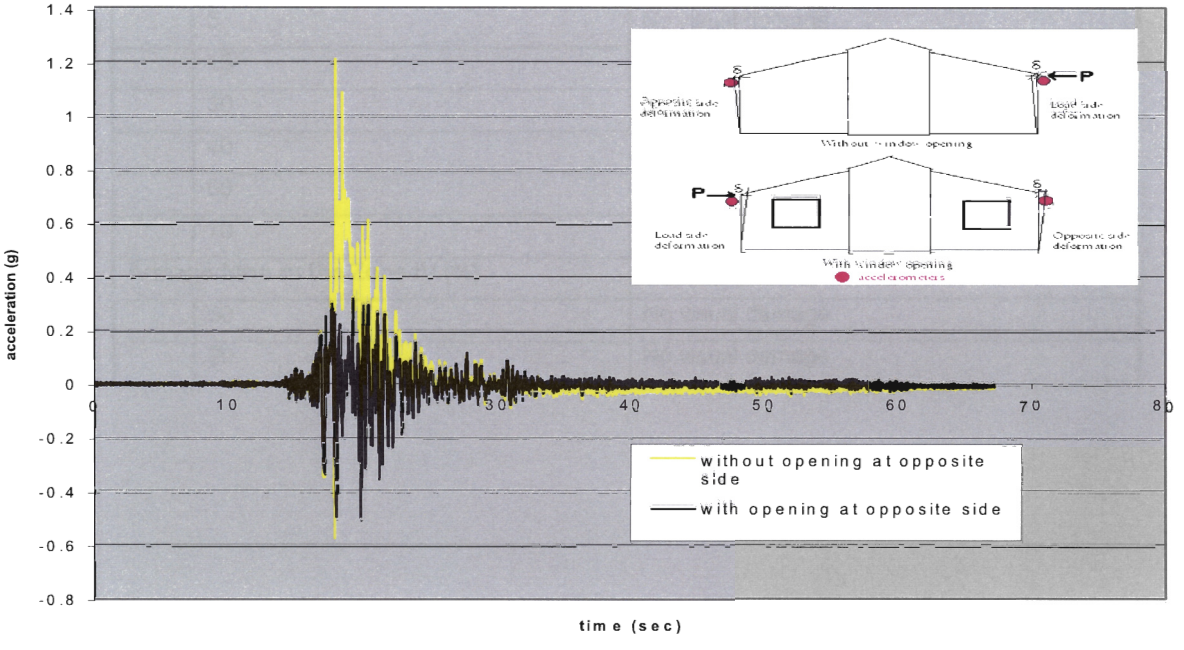

Figure 6.21 Acceleration @ 50% Kobe on the opposite side; without metal plates.

The maximum acceleration on the structure without reinforcement was higher by 56%, compared to the structure with metal reinforcement. The removal of the reinforcement has made the structure less stiff.

The displacement report for the different simulation was not recorded properly. The dynamic LVDTs were not functioning well when the simulation of the earthquake was undertaken on the structure without the reinforcements. A comparison of both tests with regard to the deflection readings was not included in this report.

6.4.4.2 Visual inspection

For every earthquake simulation a visual inspection was conducted by the author, accompanied by other researchers, to verify the findings, starting with 15% of the Kobe earthquake to the 80% Armageddon earthquake. Table 6.4 presents the findings of the inspection. No damage or significant failures of the structure was seen or observed. At 70% and 80% of the Kobe and Zone IV, the structure was excessively moving up and down, however, no damage on the structure was seen.

Table 6.4 Visual inspection report

Excitation		**Inspection damage report**
Kobe earthquake (%)		
	5	No visual damage
	15	No visual damage
	30	No visual damage
	40	No visual damage
	50	No visual damage
	70	No visual damage
Armageddon or the Zone IV (%)		
	50	No visual damage
	80	No visual damage

6.5 Summary

This section briefly described the prototype subjected to test in this experiment, as well as the procedures in this study. The construction method for the prototype was presented. The static and the dynamic tests were also discussed. The static load was limited to 5 kN on each side; this was to ensure that no damage be imposed on the structure. A maximum of 70% full scale displacement record for the Kobe earthquake was induced to the structure, since the maximum displacement of the shaker table was only 100 mm, compared to the Kobe earthquake, that is 125 mm. This applies also for the Zone IV earthquake; only 80% was taken from the full-scale displacement readings.

Results from the experimental work on the F-shelter were also presented. The structure was subjected to both static and dynamic loading. The static test was a non-destructive type, while the dynamic or ground simulation test was a destructive type.

The structure developed a twisting moment when equally loaded on both sides. Maximums of 3.9mm and 9.8mm deflection were recorded for structures with and without metal reinforcements, respectively. This is because of the unequal stiffness on the side walls. The side walls were divided into two parts, one wall without a window opening and one wall with a window opening.

The acceleration readings for the F-shelter without reinforcements were higher by 56% compared to the structure with metal reinforcements. Due to incorrect readings obtained from the dynamic LVDTs, the deflection readings and analysis were not included in this report.

No damage was incurred by the F-shelter when subjected to ground simulation equivalent to 70% of the Kobe earthquake and 80% of the Zone IV earthquake. The structure performed well under these two earthquake simulations.

The next chapter will present finite element modelling techniques for the two-dimensional analysis of the non-linear behaviour of the timber-framed wall. The results obtained from experimental works serve as data to verify the results for the finite element model.

7 Finite Element Modelling of the non-linear behaviour of the timber-framed wood wool cement board (wwcb) and plywood sheathing

7.1 Introduction

Due to the relatively high cost of full-scale testing of the F-shelter, it was only possible to test a small number of specimens within the scope of this thesis. However, in order to parametrically study the behaviour of specimens with different configurations, finite element analysis was considered as a means of complementing the experimental work on the F-shelter. Furthermore, the applicability and validity of the finite element model would be established by comparing the results from the experimental works.

A calibrated finite element model (FEM) would reduce experimental expenses and time. However, generation of a detailed FEM would require a high initial cost to arrive at a desired calibrated model. Therefore, within the scope of this thesis, the use of FEM was limited to obtaining qualitative results and to analysing critical areas in the design of the shelter such as the wall and the corner brackets. Structures essentially exhibit non-linear behaviour if loaded up to failure. Hence, knowing that most structures in the Philippines suffer damage due to strong tropical typhoons and earthquakes, structures perform and exceed the linear designed capacity. There is a need to analyse the non-linear behaviour of the F-shelter to cater safely to the dwellers and structural soundness when dynamic loads are applied.

Two separate FE models were completed:

1. A non-linear model of the corner bracket, which was calibrated against the experimental results.
2. A two-dimensional model of the wall, whereby the calibrated model of the corner bracket was integrated into the wall model.

The two models are now discussed in detail.

7.2 Modelling the corner metal bracket

A two-dimensional model of the corner bracket was prepared using ANSYS finite element software. The timber frame and flat bar are assigned as BEAM 3 elements, and the nails and the round bar stiffener are assigned as LINK1 elements, as illustrated in Figure 7.1. The elements mentioned in this section are described in detail in Section 7.3. The model shown was calibrated through the tension test. The distance of the nail from the figure is the distance from the centroid of the timber frame to the flat bar. The non-linear input property of the nail and screw are taken from the averaged nail/screw withdrawal tests that are conducted in accordance with ASTM 1761.

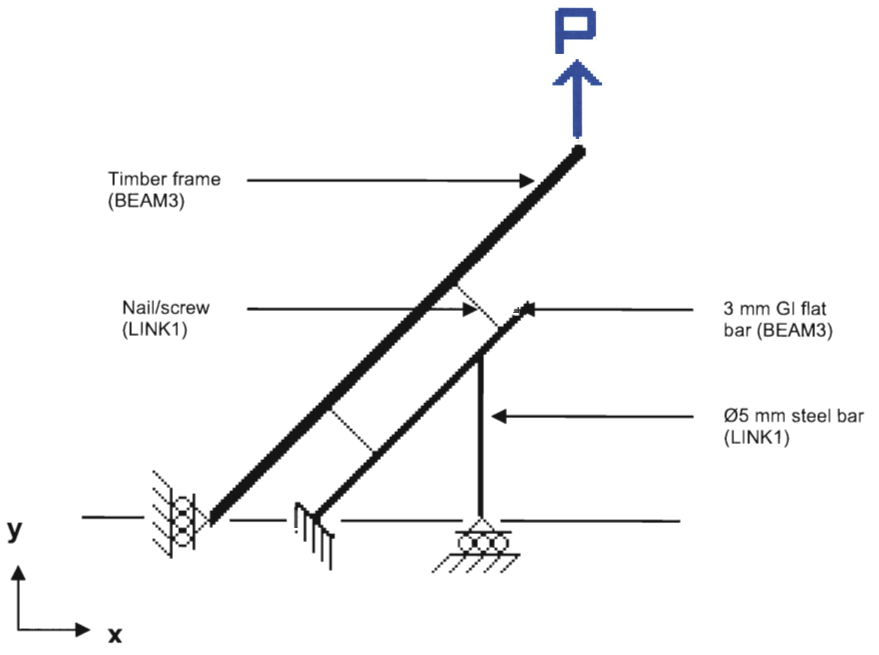

Figure 7.1 Schematic diagram of FEM for the corner bracket.

The corner joint was cut in half because of symmetry along the x-axis, as shown in Figure 7.1. The input properties of the model are listed in Table 7.1.

Table 7.1 Input properties for the corner bracket model

Corner joint part	Equivalent element	Area (mm^2)	MOE (GPa)	Poisson's ratio (ν)
Timber frame (Radiata pine/Apitong)	Beam 3	1875.0	10/7.3	0.29
Flat bar	Beam 3	75.0	200	0.3
Nail/Screw	LINK 1	7.0	200	0.3
Round bar	LINK 1	19.6	200	0.3

The failure of the corner bracket is dependent on the capacity of the nail or the screw to resist pull-out forces. Hence, an experimental work was conducted to obtain the non-linear reaction of the nail when subjected to a withdrawal load. Figure 7.2 shows the load and deflection curves form the withdrawal tests of the nails and the average value. The average value was then used as an input property of the nail as a LINK 1 element, as shown in Table 7.2.

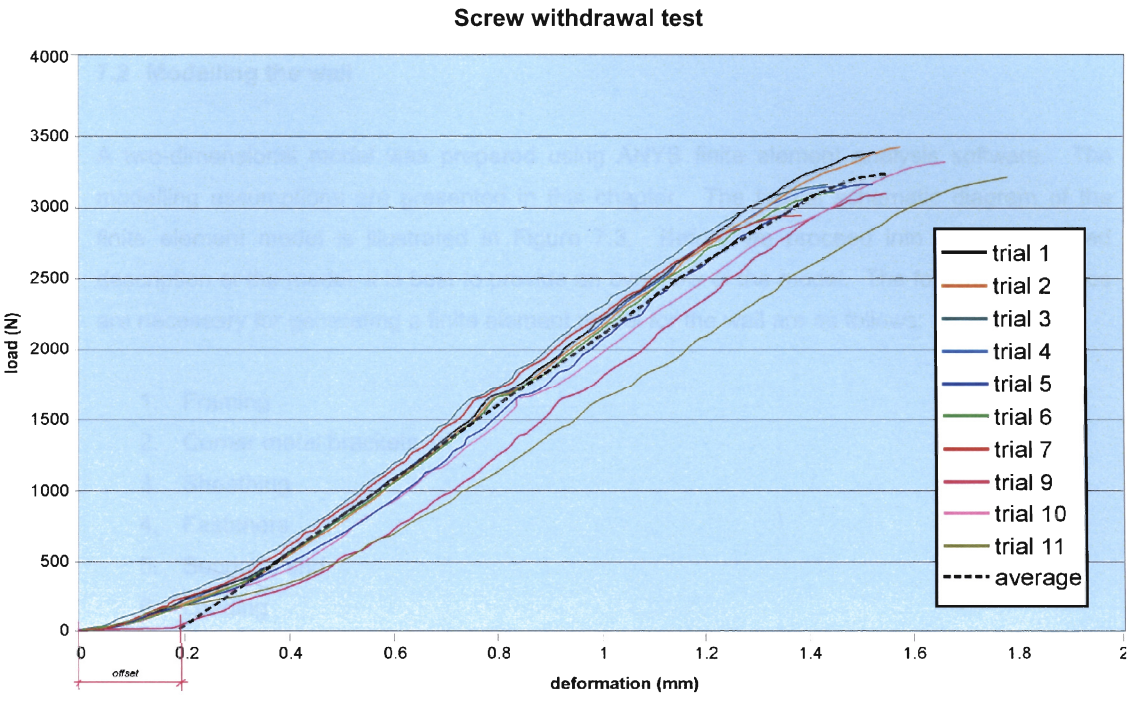

Figure 7.2 Load and deflections curves of the screw withdrawal tests.

Table 7.2 Input property for the LINK 1 element for screw

Stress (σ)	Strain (ε)
0	0
396	0.0281
424	0.0305
449	0.0329
459	0.0351

As shown in Figure 7.1, a tensile load applied on the top end part of the corner bracket in the model represents the load from the universal testing machine. To obtain the non-linear response, the load was input incrementally. The first load was 500 N, which was still in the elastic region of the load-deflection curve. At each load increment, the analysis was allowed to iterate until convergence to an equilibrium state was achieved. The analysis was terminated when convergence was no longer possible. Non-convergence was an indication that the ultimate load-carrying capacity of the structure was being approached.

The calibrated model of the corner bracket was integrated into the wall model. The stress and strain inputs are summarised in Tables 7.5 and 7.6 for the Radiata pine and Apitong timber frame, respectively.

7.2 Modelling the wall

A two-dimensional model was prepared using ANYS finite element analysis software. The modelling assumptions are presented in this chapter. The typical schematic diagram of the finite element model is illustrated in Figure 7.3. Before we proceed into a more detailed description of the model, it is best to provide an overview of the model. The following subtopics are necessary for generating a finite element model for the wall are as follows:

1. Framing
2. Corner metal brackets
3. Sheathing
4. Fasteners
5. Supports and
6. Loading

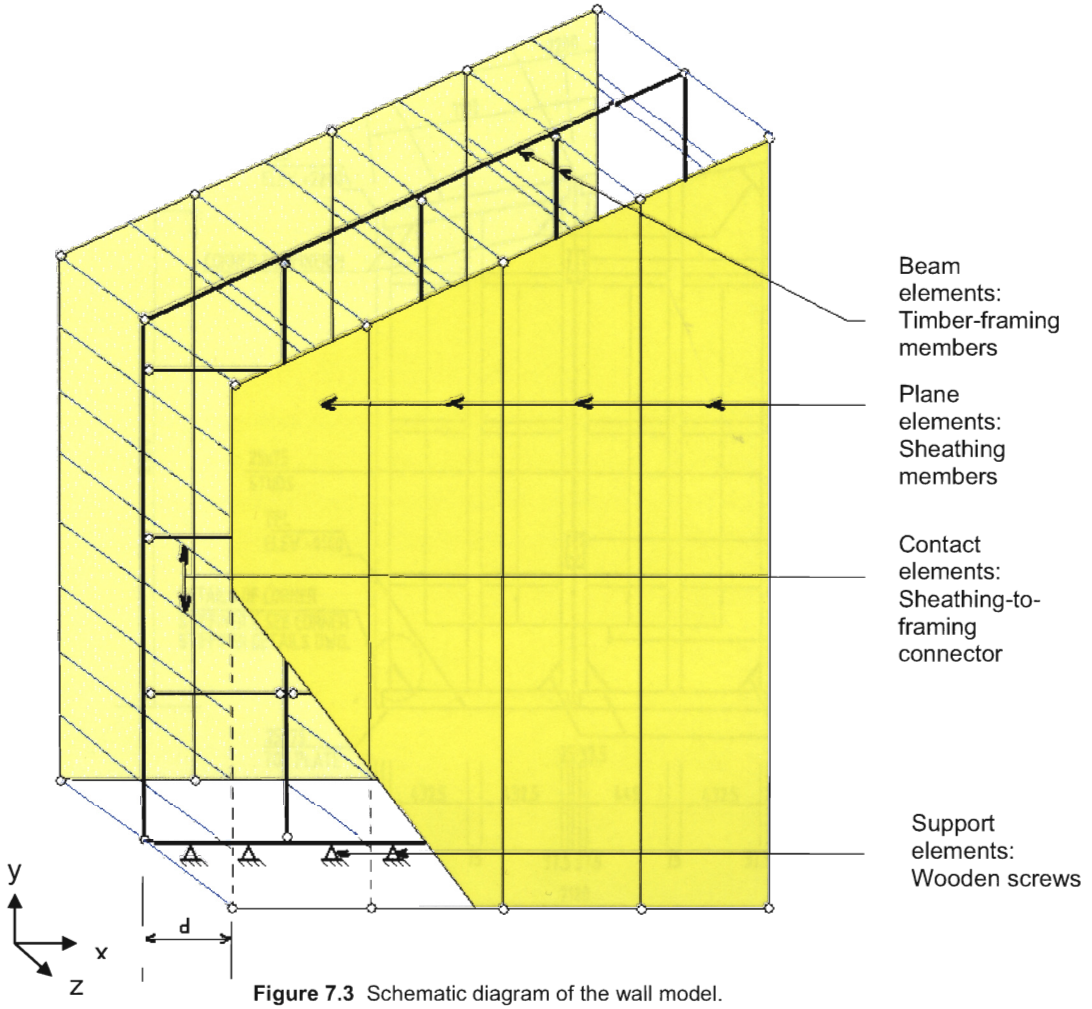

Figure 7.3 Schematic diagram of the wall model.

7.3.1 Framing

A more detailed description of the framing members is presented in Chapter 4, Materials and Methods. Figure 7.4 shows the typical geometry and composition of the timber-framed panels. The perimeter framing and middle vertical studs (25mm x 75mm) serve as the main structural elements of the wall. The typical spacing is 432.5mm (17 in) on centre. The horizontal bracing spaced at 444mm, 588mm and 580mm serve to prevent in-plane bending of the panels, especially the wwcb's that have a low bending capacity.

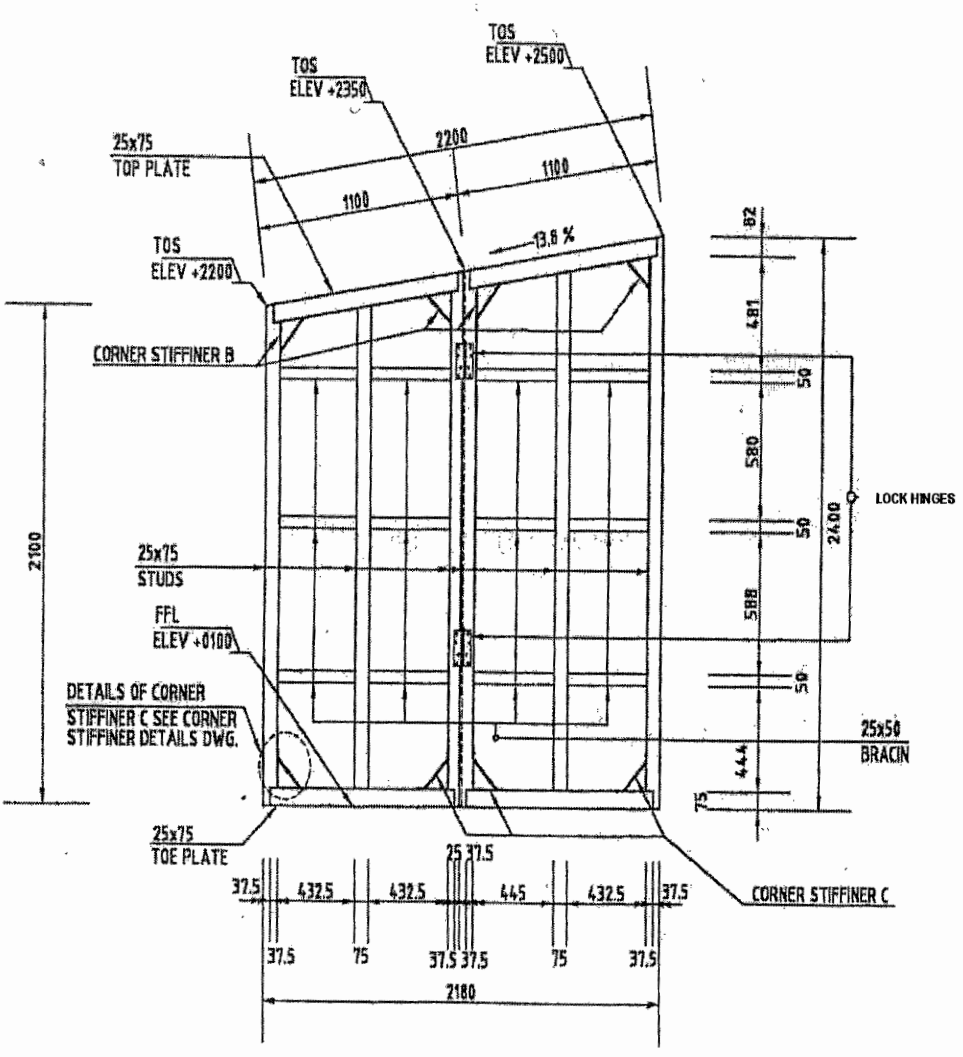

Figure 7.4 Geometry of the timber frame (dimensions are mm).

As depicted in Figure 7.3, the framing members are located in the x-y and z=0 global plane. They are modelled in ANSYS using two-dimensional elastic beam elements (BEAM 3). These elements have three degrees of freedom at each node; rotation about the nodal z-axis and translation in the x and y directions. Figure 7.5 shows the element geometry.

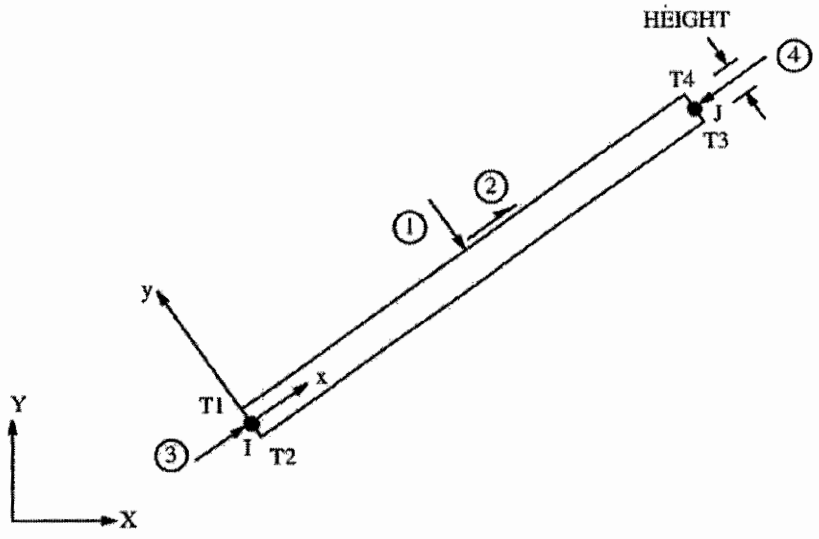

Figure 7.5 BEAM 3; 2D Elastic Beam (ANSYS 1998).

All framing members connected at the ends by nails were modelled as pin-ended members, because nailed connections have little or no moment resistance. In ANSYS, pin connections are typically modelled using two coincident nodes which are rigidly linked in displacement only (Figure 7.6) and hence enable the nodes to rotate freely relative to each other.

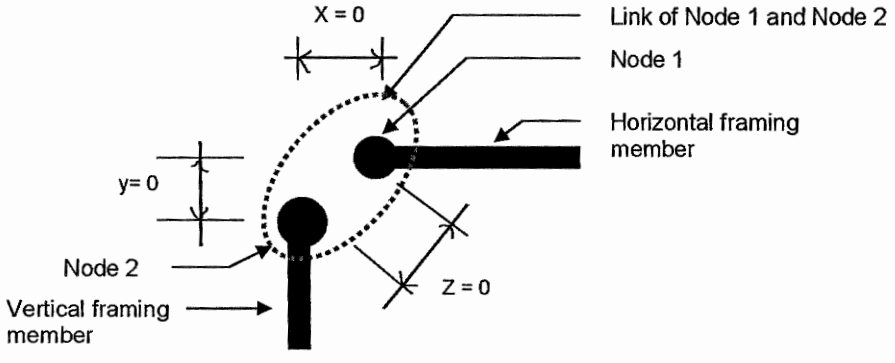

Figure 7.6 End connection for coincident nodes.

Figure 7.7 shows the 2-D frame model. All short diagonal elements at the corners and middle studs are also modelled as being pin-ended.

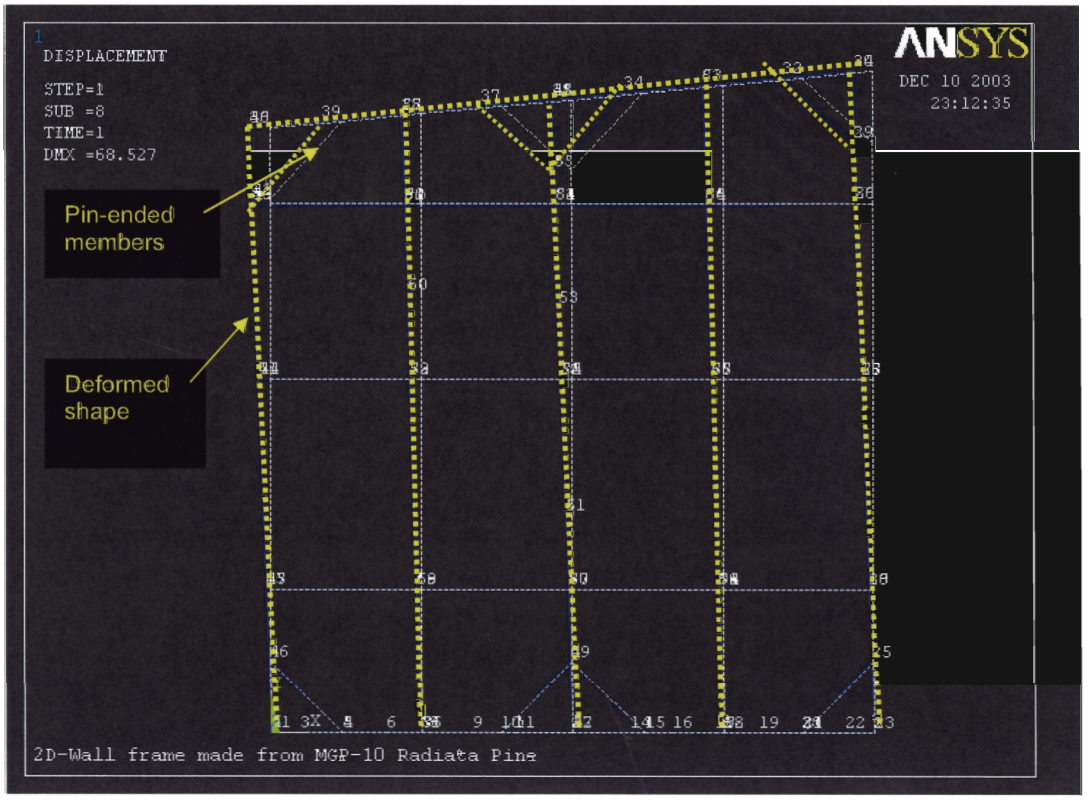

Figure 7.7 BEAM 3 elements for the timber framing.

Member properties of the BEAM 3 element used in the FE model were defined in Table 7.3. The diagonal member (LINK 1 element) is defined in the next section. **A** represents the cross-sectional area in mm^2, **Iy** is the moment of inertia in mm^4 along the y-axis, **MOE** represents the modulus of elasticity, and ν is the Poisson's ratio.

Table 7.3 Input properties for BEAM 3 element

Member	A (mm^2)	Iy (mm^4)	MOE (GPa)		ν
Perimeter and vertical studs, except the middle stud	1,875	878,906	Apitong (NSCP 2001) 8.75	Radiata Pine (AS4063 1992) 10.00	0.29
Middle stud	3,750	7,031,250			
Horizontal brace	1,250	260,416			

The middle stud, which serves as a connecting member for the two segments of the wall, has two 25 mm x 75 mm vertical members. The author assumed these two studs as one stud, since the connections were rigid enough that deformation will have the same value for each section.

7.3.2 Corner joint with metal brackets

To establish the effective load-deformation behaviour of the corner diagonals, the calibrated FEM results from the individual corner joints were used to define the non-linear load deformation curve of certain elements in the finite element model (LINK 1 element).

The composite reactions of the metal let-in brackets, together with the timber framing, were modelled using the LINK 1 element from the ANSYS. The element is capable of modelling the non-linear behaviour for tension and compression loading for the corner joint and offers no moment resistance at each node. ANSYS has the capability of modelling the non-linear load-deflection behaviour of the link element to be entered directly as a set of points on a multi-linear load-deflection curve.

The location of the nodes for the LINK 1 element is based on the distance of the timber frame from the projection of the line of loading to the centroidal width of the timber frame. As shown in Figure 7.8, the centre from the corner to the intersection of the centre line of the timber to the projected line of loading was the distance used in the model for a 90-degree angle corner joint. The same distances were attained for the 82-degree and 98-degree corner joints. Only the element lengths had different values.

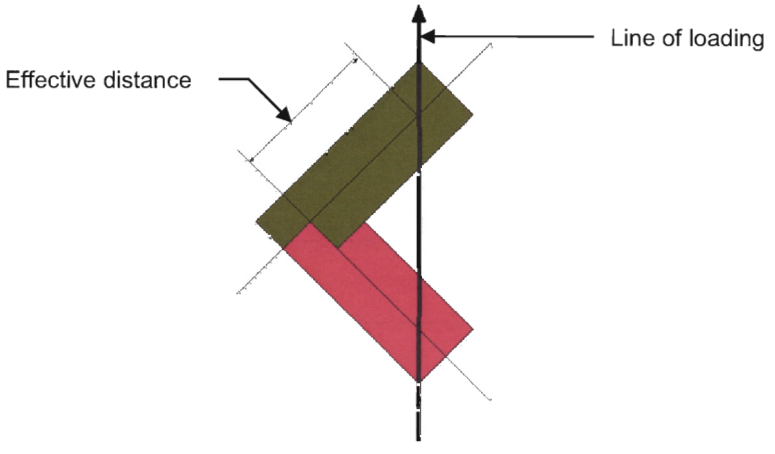

Figure 7.8 Effective length to be used in the 90-degree corner joint model.

A diameter of 5mm was used to represent the section area of the LINK 1 element with an equivalent cross-sectional area of 19.63 mm^2. A Poisson's ratio of 0.30 is used because material is fabricated from steel.

The average value from the 82-degree angle Radiata pine, as shown in Figure 7.9, was obtained using SPSS statistical software. Figure 7.9 also contains the FEM results of the model from Figure 7.1. A deviation of - 5% of the load and +8% of the deflection between the FEM and the average value can be seen. A good correlation was attained between the FEM and the experimental works.

The material input properties for the LINK 1 elements were based on the FEM results, as shown in Table 7.4. The material property input requires values for stress (σ) and strain (ε) values. From mechanics, values from load (P), length (L), deformation (δ) and the cross-section area, we can compute for the values for σ and ε.

$$\sigma = P/A \qquad \text{(eq. 8.1)}$$

$$\varepsilon = \delta/L \qquad \text{(eq. 8.2)}$$

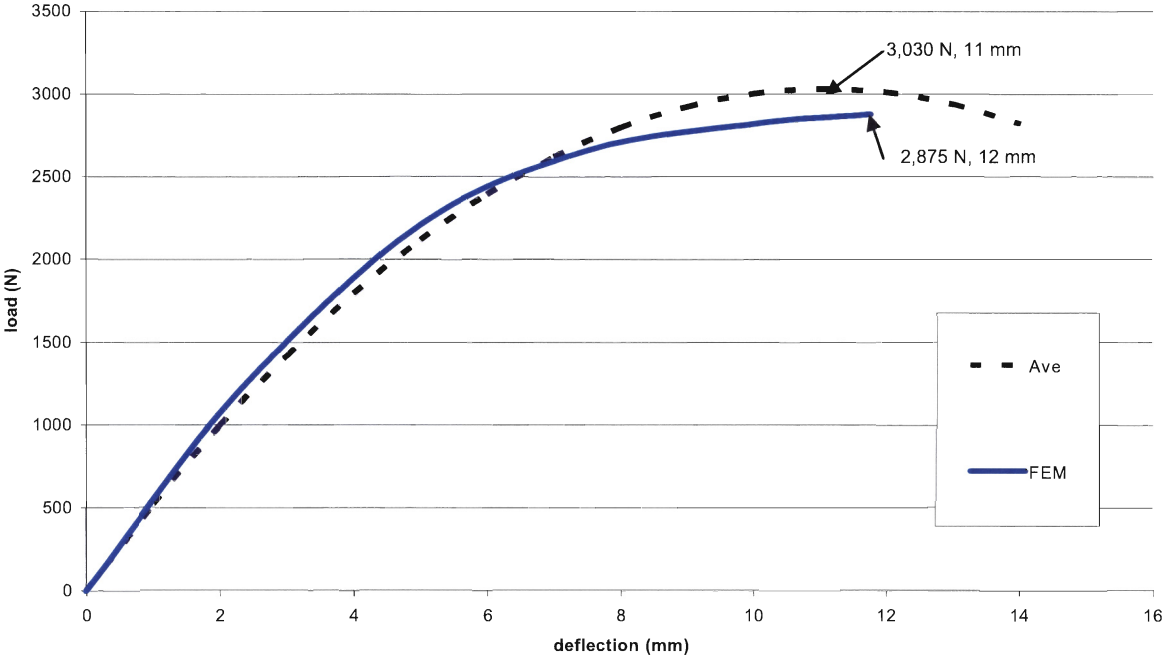

Figure 7.9 Load-deflection curves for FEM and average results from the 82-degree corner made with Radiata pine frame.

Isolating the FEM load deflection curve, we are able to obtain the input values for a non-linear material as shown in Table 7.4.

Table 7.4 Equivalent input values for the non-linear LINK 1 element

Stress (δ)	Strain (ε)
28.52	0.0057
50.68	0.0100
78.81	0.0162
103.79	0.0238
128.55	0.0357
140.86	0.0452
142.64	0.0524

The other metal let-in braces are presented in tabular form: Table 7.5 for Apitong-framed metal corner brackets and Table 7.6 for Radiata Pine-framed metal corner brackets.

Table 7.5 Apitong-framed corner with metal brackets.

Degree of frame		Compression		Tension	
		Stress (δ)	Strain (ε)	Stress (δ)	Strain (ε)
82	1			15.28	5.6e-3
	2			25.47	0.0119
	3			30.56	0.0186
	4			35.66	0.0282
	5			30.56	0.0378
	6			20.38	0.0439
90	1	76.41	5.2e-3	20.37	3.5e-3
	2	114.62	9.6e-3	30.56	6.8e-3
	3	76.41	0.0148	40.75	0.0127
	4	63.67	0.0226	47.88	0.0246
	5			40.75	0.0321
	6			23.94	0.0402
98	1			15.28	5.6e-3
	2			25.47	0.0119
	3			32.56	0.0196
	4			41.26	0.0242
	5			30.56	0.0318
	6			20.38	0.0392

Table 7.6 Radiata pine-framed corner with metal brackets (the 82-degree corner angle was presented in Table 7.4).

Degree of frame	Compression			Tension	
	Stress (δ)		Strain (ε)	Stress (δ)	Strain (ε)
90	1	127.36	4.4e-3	50.94	7.1e-3
	2	188.11	9.8e-3	101.88	0.0184
	3	127.36	0.0118	124.81	0.0382
	4	101.88	0.0168	101.88	0.0523
	5			76.41	0.0566
98	1			50.94	5.3e-3
	2			101.88	0.0114
	3			127.36	0.0156
	4			142.64	0.0239
	5			148.19	0.0339
	6			127.36	0.0405
	7			101.88	0.0437

From Tables 7.1 to 7.6, the required modulus of elasticity (MOE) is computed by dividing the first Stress by the first Strain. Tables 7.4 to 7.6 also show the breakdown of the input properties as assigned as a multi-linear kinematic hardening property in the ANYS program.

7.3.3 Sheathing

Each wall frame has two side-by-side pieces of wwcb or plywood. Each wwcb has standard dimensions of 0.6m x 2.4m with 8mm thickness. The wall consisted of two segments has four side-by-side pieces of wwcb, each with different dimensions (mm) and variable sloping heights (w x h1 x h2 x t): (a) 545 x 2100 x 2175 x 8, (b) 532.5 x 2175 x 2250 x 8, (c) 557.5 x 2250 x 2325 x 8 and (d) 545 x 2325 x 2400 x 8. All units are in millimetres (mm) as shown in Figure 7.10.

All sheathings are generally dominated by elastic in-plane shear (ANSYS, 1998). They were modelled using plane stress elements (PLANE42), as shown in Figure 7.11 and 7.12. Four nodes typically define the plane stress elements. Each node has two degrees of freedom; translations in the nodal x and y directions. Because of the way the sheathing-to-frame connection was modelled, a distance in the z-dimension is provided, even though it is not relevant for plane analysis. A distance of 100mm in the z-plane from the timber frame (BEAM 3) was chosen, although the distance should be 16.5mm, which counts from the centroid of the framing members to the centroid of the sheathing material. This difference in the distance has no bearing on the behaviour of the model, because of the manner in which the fasteners are

located and modelled. Furthermore, it is easier to visualise the geometry of the models when assigned to greater distances.

The nodes of the sheathing elements are located at the same x and y node locations specified by nail spacing. The sheathing material properties for MOE are 3 MPa for wwcb and 10 MPa for plywood. The Poisson's ratio used for both of the sheathing is 0.29.

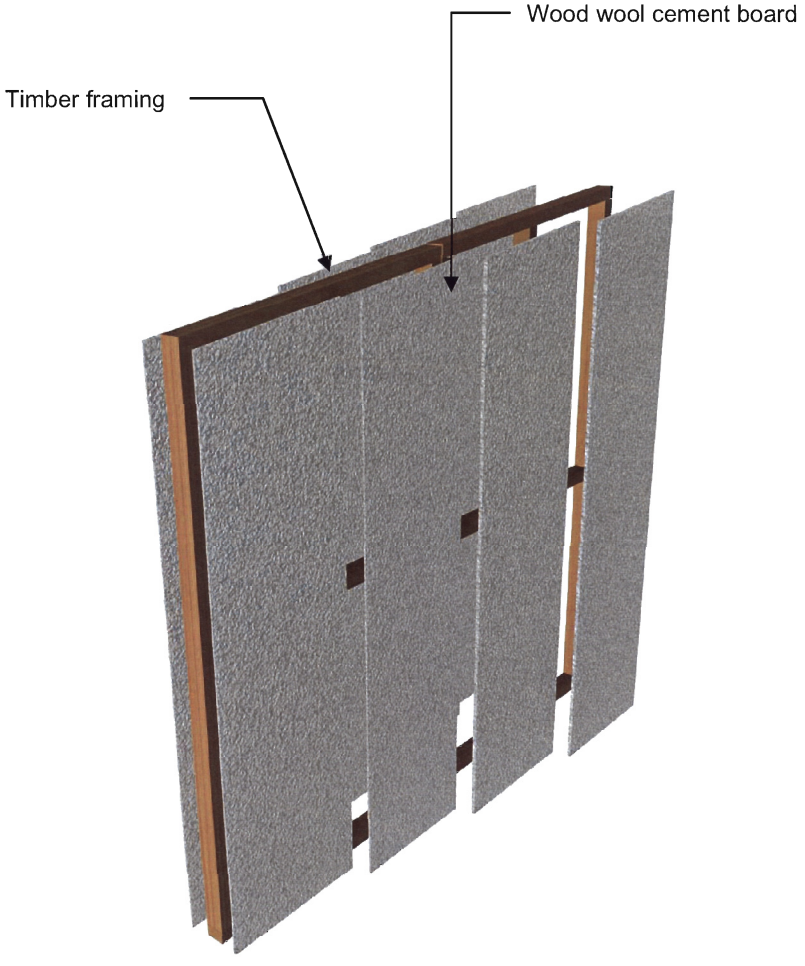

Figure 7.10 Blow-up sketch of wwcb from the sheathing.

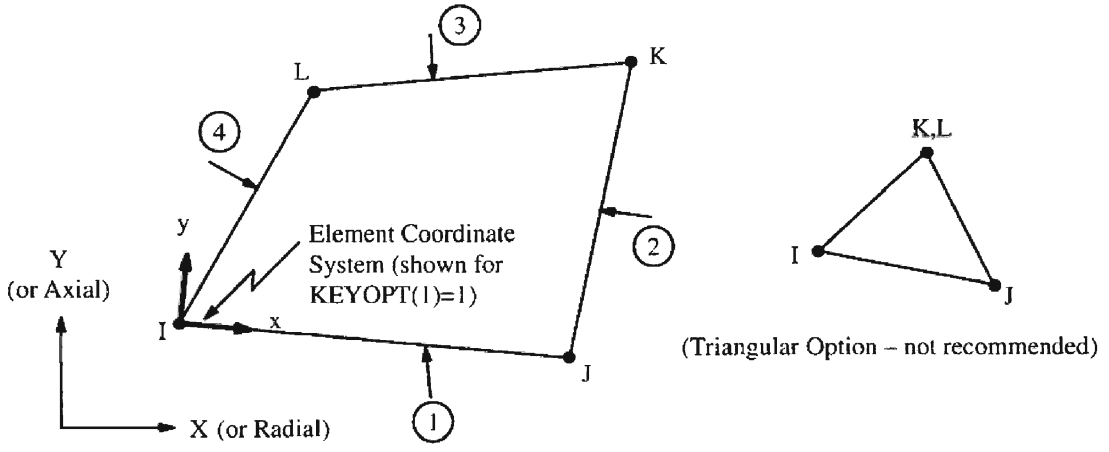

Figure 7.11 PLANE 42; 2D Structural Solid (ANSYS 1998).

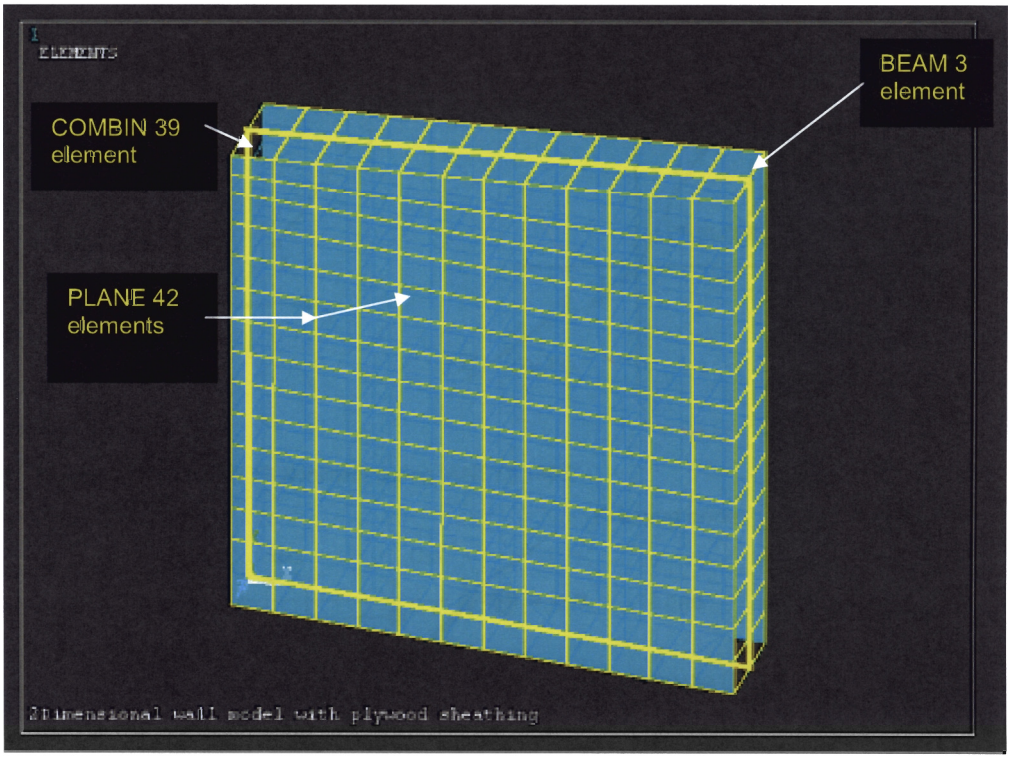

Figure 7.12 PLANE 42 element to model the wall sheathing.

7.3.4 Fasteners

One of the most important components of the timber frame wall system is the sheathing-to-frame connection. This connects the sheathing (PLANE 42) and frame (BEAM 3) elements to act as one system. To model the elastic stiffness at each fastener location in both the x- and y-direction, two spring elements (COMBIN 39) were needed. At each fastener location, two COMBIN 39 elements represent one nail. A typical geometry of the COMBIN 39 is shown in Figure 7.13.

The two springs connect the framing node to the corresponding coincident node of the sheathing element. The element can only deform in a direction assigned to the program. The unidirectional springs were assigned as COMBIN 39 (Ux); this means that this element will only deform in the x direction, correspondingly a COMBIN 39 (Uy) deforms in the y-direction, as shown in Figure 7.14. The element has a length of 200 mm along the z-axis; the element nodes are connected with the framing nodes and the sheathing nodes. This distance in the z-axis does not affect the FEM results because of the way the two springs are modelled.

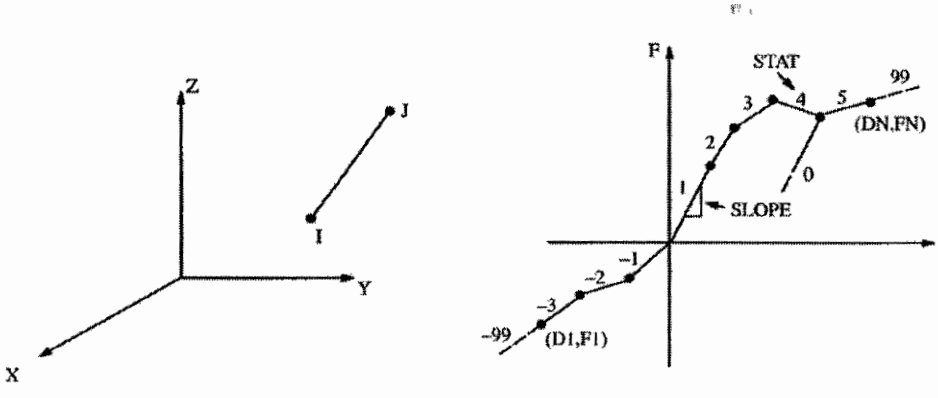

Figure 7.13 COMBIN 39 Nonlinear spring (ANSYS 1998).

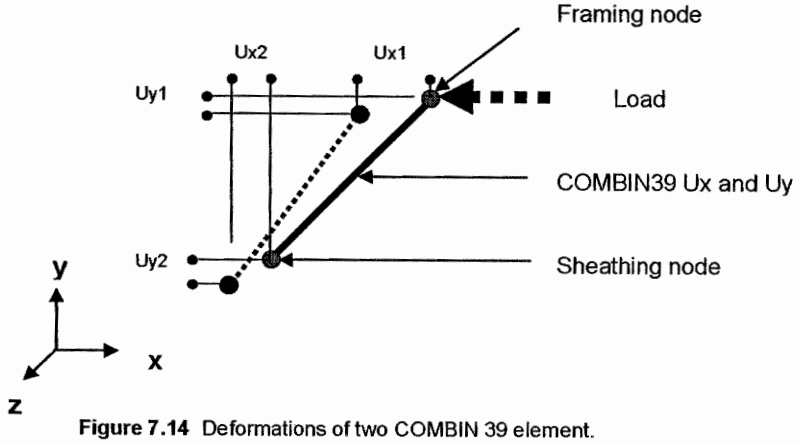

Figure 7.14 Deformations of two COMBIN 39 element.

The non-linear load deflection behaviour of the fastener was determined based on the results of the sheathing-to-framing connection tests. The load-deflection curve of the experimental test for the lateral testing of nails for F11 plywood sheathing is shown in Figure 7.15. There were 10 sets of data for each of the materials, the wood wool cement board sheathing and the plywood sheathing. The tabulated average value for the test is shown in Table 7.7.

The non-linear load-deflection curve behaviours of the connections were modelled in ANSYS using the COMBIN 39 capability by inputting the multi-linear curve shown in Figure 8.15. The curve was to fit the average load-deflection data from the test as superimposed on the average value from the experimental results. The input properties are the deflection and load.

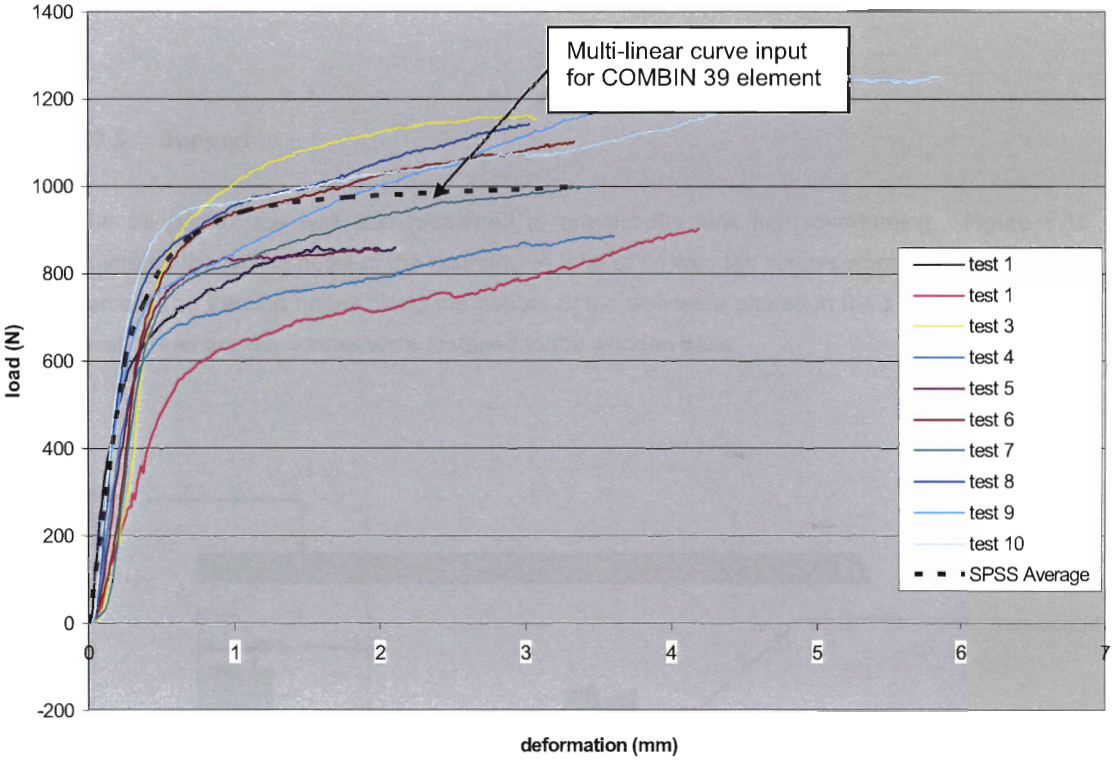

Figure7.15 Load-deflection curve for lateral nail resistance test for plywood sheathing.

Table 7.7 Load and deflection input data for real constants for a COMBIN 39 for lateral nail resistance test for a wwcb and plywood sheathing.

Sheathing	Input #	Deflection (mm)	Load (N)
Plywood	1	0.35	795
	2	1.38	989
	3	3.35	1000
Wwcb	1	0.47	700
	2	1.14	902
	3	2.45	955

7.3.5 Support

The sill part of the wall was restrained to prevent the wall from overturning. Figure 8.16 illustrates the typical detail of the restraint. A total of 14 wooden screws were used in each wall frame. The framing nodes along the bottom of the wall were pinned in the x and y direction at locations where the screws were fastened to the wooden base.

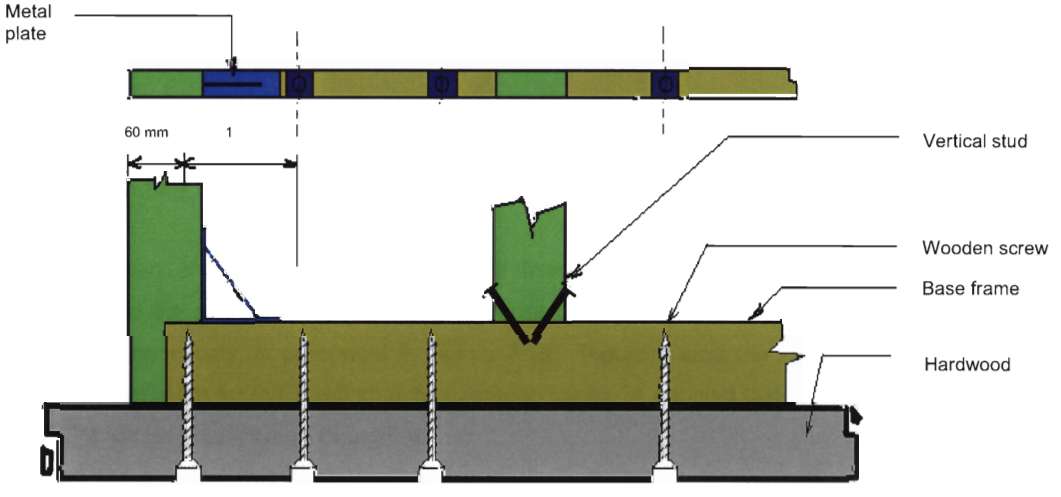

Figure 7.16 Set-up of supports (refer to Figure 4.20 for the cross section detail).

7.3.6 Loading

As shown in Figure 7.17, a horizontal load applied on the top corner of the wall in the model represents the load from the hydraulic ram. To obtain the non-linear response, the load was input incrementally. The first load was 2,500 N, which was still in the elastic region of the load-deflection curve. At each load increment, the analysis was allowed to iterate until convergence to an equilibrium state. The analysis was terminated when convergence was not achieved; non-convergence was an indication that the ultimate load-carrying capacity of the structure was being approached.

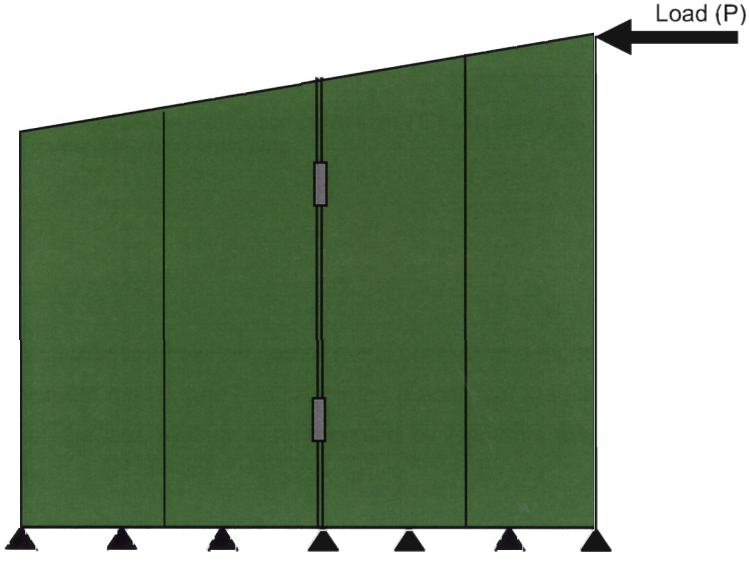

Figure 7.17 Location of the load on the wall specimen.

7.4 Preliminary FE model result

A typical load and deflection curve obtained from the wall finite element model nonlinear analysis and the average load-deflection curve for the experimental work represented as FEM and Ave respectively, is presented in Figure 7.18. Figure shows the FEM with the average experimental value for the wwcb sheathed Apitong frame. A detailed discussion of the results of the FEM will be presented in Chapter 8.

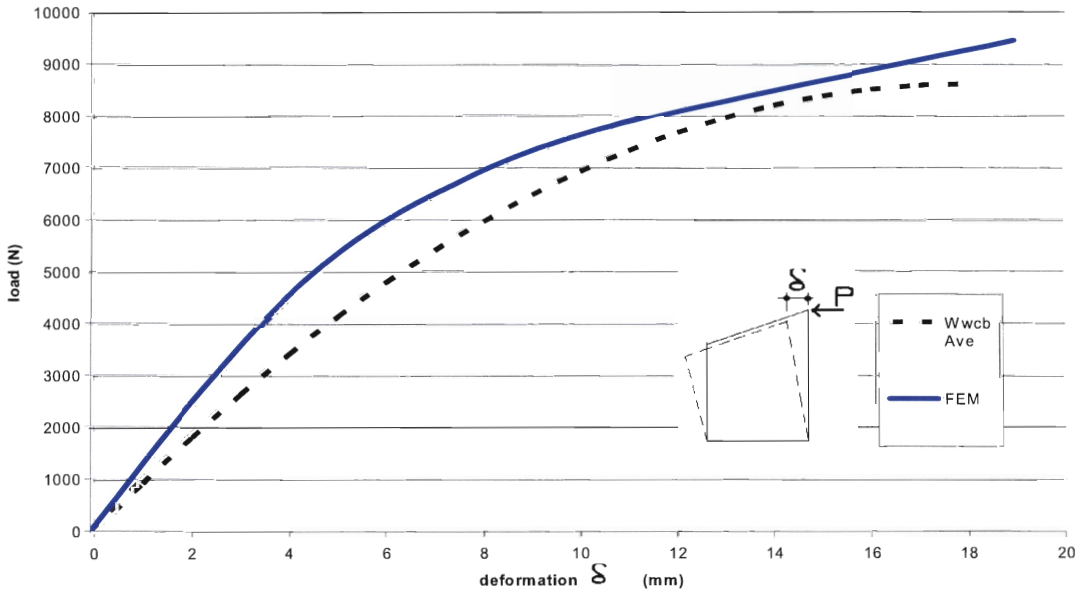

Figure 7.18 Typical load-deflection curve from FE model and average from wall tests of Apitong frame with wwcb sheathing.

7.5 Summary

This chapter has discussed how the corner metal bracket was modelled and its integration into the wall finite element model, and has presented a nonlinear load-deflection curve FEM result. Each member of the wall system is represented by elements available in the ANSYS finite element software.

There were two main components of the model used in the wall modelling: 1) corner metal brackets and 2) sheathing-to-frame connection. The timber-framed end-connection was commonly modelled as a pin-ended-connection, because of the integration of the metal let-in braces. A nonlinear LINK 1 element was used to represent this bracket. It was necessary to model the corner bracket in the wall system. Two COMBIN 39 elements were used to represent one nail. Each COMBIN 39 element is assigned to deform in the x- or y- direction.

The next chapter will present the results of the Finite Element Model and compare them to the experimental results.

8 Discussions for Experimental and FEM results

8.1 Introduction

Chapters 5 and 7 of this thesis have presented results from the experimental works of the wood-framed wall with two types of sheathing, namely, a wood wool cement board and plywood, and the F-shelter respectively. The wood-framed wall was subjected to a unidirectional loading until failure. The F-shelter was subjected to a non-destructive static test up to 5 kN and a destructive test using simulated ground motion or earthquake time history records. The simulated ground records used in this experiment was the 1995 Kobe earthquake and the Zone IV earthquake. Results were presented on an individual basis, as presented in Chapters 5 and 6 for clarity.

Chapter 7 also presented the design procedure of the finite element model for the wood framed wall. A three dimensional model of the wall for a two dimensional non-linear analysis was generated. The results of this finite element model are presented in this chapter.

Furthermore, a graphical representation of the load-deflection curves for both experimental and finite element model results are presented, for a clearer explanation of the results.

8.2 Results from the Finite Element Model (FEM)

As mentioned in the introduction of this chapter, a finite element model was generated; a two-dimensional FEM of the wall capable of predicting the non-linear behaviour. The following subsections will present the result of the model.

8.2.1 Corner bracket stiffness

Table 8.1 shows a summary of the average values of the corner bracket experimental work and the finite element model results subjected to a tensile load. A good correlation on the peak loads between the FEM and the experiment for the three angles was attained. However, a constant value of 12% deflection variance between the FEM and the experiment was attained because of the inconsistency deflection failure from the experiments.

Table 8.1 FEM vs. Experimental work for Apitong-framed corner bracket in tension

Angle	Peak loads (N)		Variance (%)	δ_{max} (mm)		Variance (%)
	Expt	FEM		Expt	FEM	
82-degree	662	700	+6	9	8	-12
90-degree	915	939	+3	9	8	-12
98-degree	865	810	-7	7	8	+12

8.2.2 Non-linear behaviour of the wall

Wood wool cement board sheathed wood frames are the primary elements of the lateral loading resisting system of the F-shelter. While seemingly ordinary, the shear wall is a complex physical structure that includes various types of structural members and connections. This study has undertaken an experimental work and development of a detailed finite element model of the wall, using ANSYS finite element program. A static, non-linear behaviour of the wall was calibrated correspondingly with the results of the experiments.

8.2.2.1 Wall frames

In the experimental test, two wood frames were tested, namely, the Apitong wood frame and the Radiata pine. Both wall frames were subjected to a unidirectional loading, as mentioned in Chapter 4, and the results of this were presented in Chapter 5. Representations of the specimens were also presented in Chapter 5, Table 5.7 as A and R. A typical load–deflection curve for the Apitong and Radiata Pine timber frame is shown in Figure 8.1. The Apitong wood frame has a 10% higher lateral load capacity compared to the Radiata pine wood frame. As stated in Chapter 5, this is a result of the rusted nails connecting the corner metal brackets to the timber frame. The rusted nails made the corner joints more rigid compared to the newly fastened nails on the Radiata pine frame, although it should have been the Radiata having a higher stiffness value since it has a higher value of modulus of elasticity. This part of the discussion will present finite element results from the wall frame models. The FEM of the wall frame was shown in Figure 7.3, as represented by BEAM 3 elements from ANSYS.

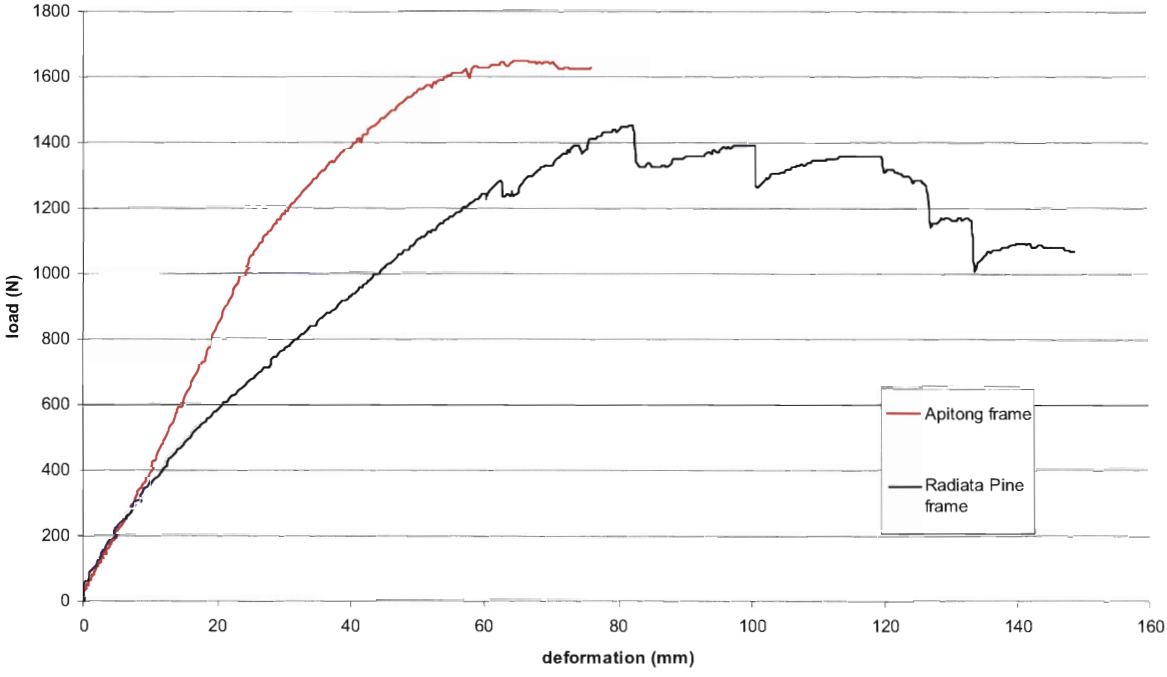

Figure 8.1 Load-deflection curve for the two wood-framed walls.

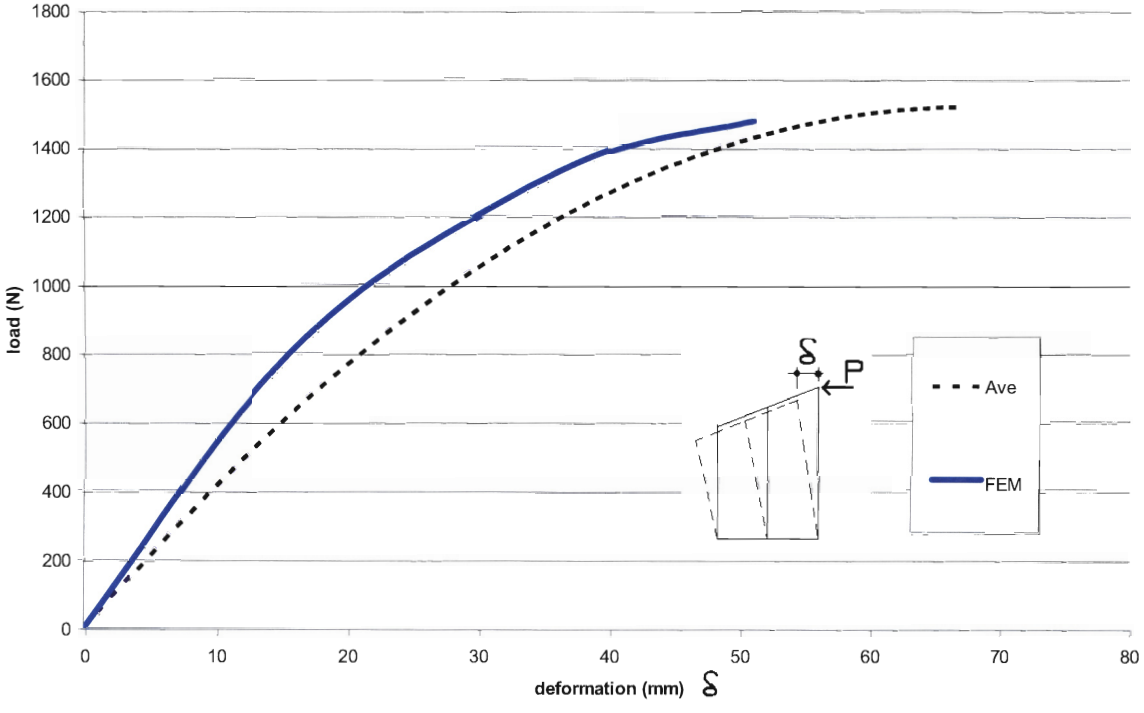

Figure 8.2 FEM and average load-deflection curves for the Apitong-framed wall.

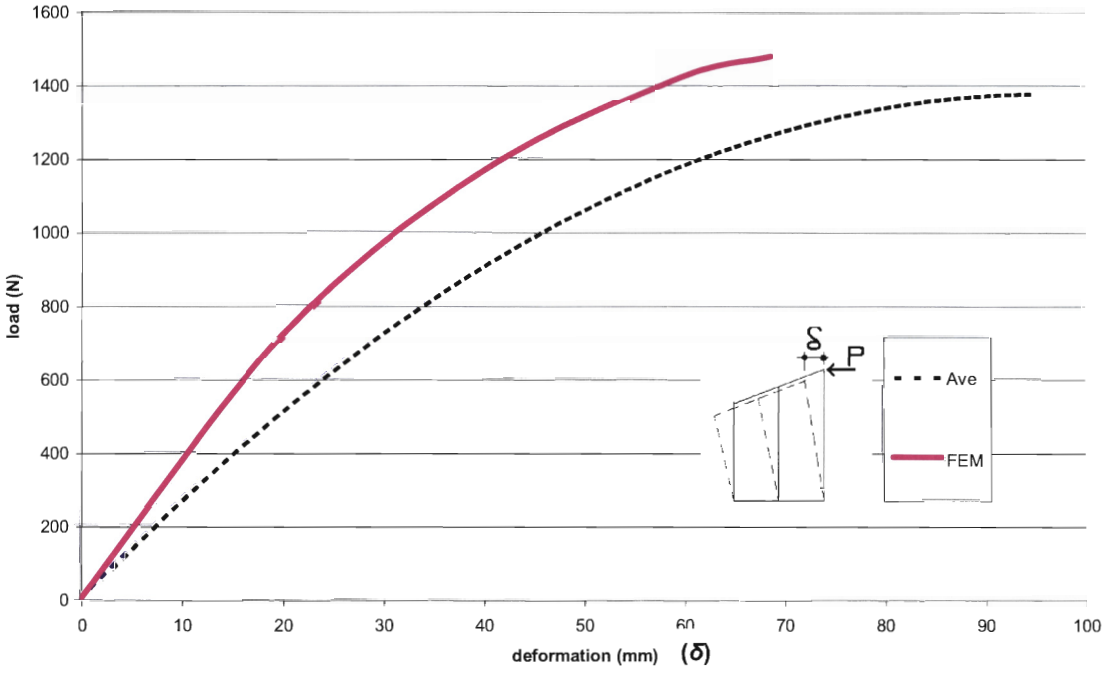

Figure 8.3 FEM and average load-deflection curves for the Radiata pine-framed wall.

The abrupt descent of the load-deflection curve line is brought about by the failure of nail fasteners on the metal let-in braces used to connect the joints of the wall frame. It is unfortunate that this mode in the Apitong wall frame experiment did not show because of the author's failure to record the decreasing load after the specimen had attained the maximum load capacity. Only the maximum load and maximum deformation were recorded.

From initial inspection or visual inspection of graphical Figures 8.2 and 8.3, it is seen that a good correlation between the experimental values with the FEM exists. Table 8.2 shows the exact values of the results from the graphs.

Table 8.2 Tabulated results of experimental versus FEM

Specimen	Maximum deformation (δ*max*, mm)			Maximum load (P*max*, N)		
	Ave. Experiment	FEM	Ratio[a]	Ave. Experiment	FEM	Ratio[a]
Apitong	67	51	1.3	1,524	1,480	1.0
Radiata Pine	96	69	1.4	1,378	1,475	0.9

[a] Ratio = Ave / FEM

A -3% deviation between the average experimental value compared to that of the FEM for maximum load for the Apitong frame and a +7% deviation is observed between the FEM and the average experimental value for the maximum load capacity of the Radiata Pine timber frame. The load-deflection curves from the experiment showed a difference of 142 N from the highest value to the lowest value for the Apitong frame and a difference of 104 N for the Radiata pine frame. All these are within the ±15% limit of the results based on the ASTM (2001) standard.

Figure 8.4 shows for the displacement in x-direction at maximum load. Minimal displacement could be seen at the far right end value at the bottom part of the model, equivalent to 5.6mm movement. The sill or the base part of the model did not show any movement, due to assigning a pinned connection in the x- and y- directions. The maximum displacement (DMX) is 50.77 mm.

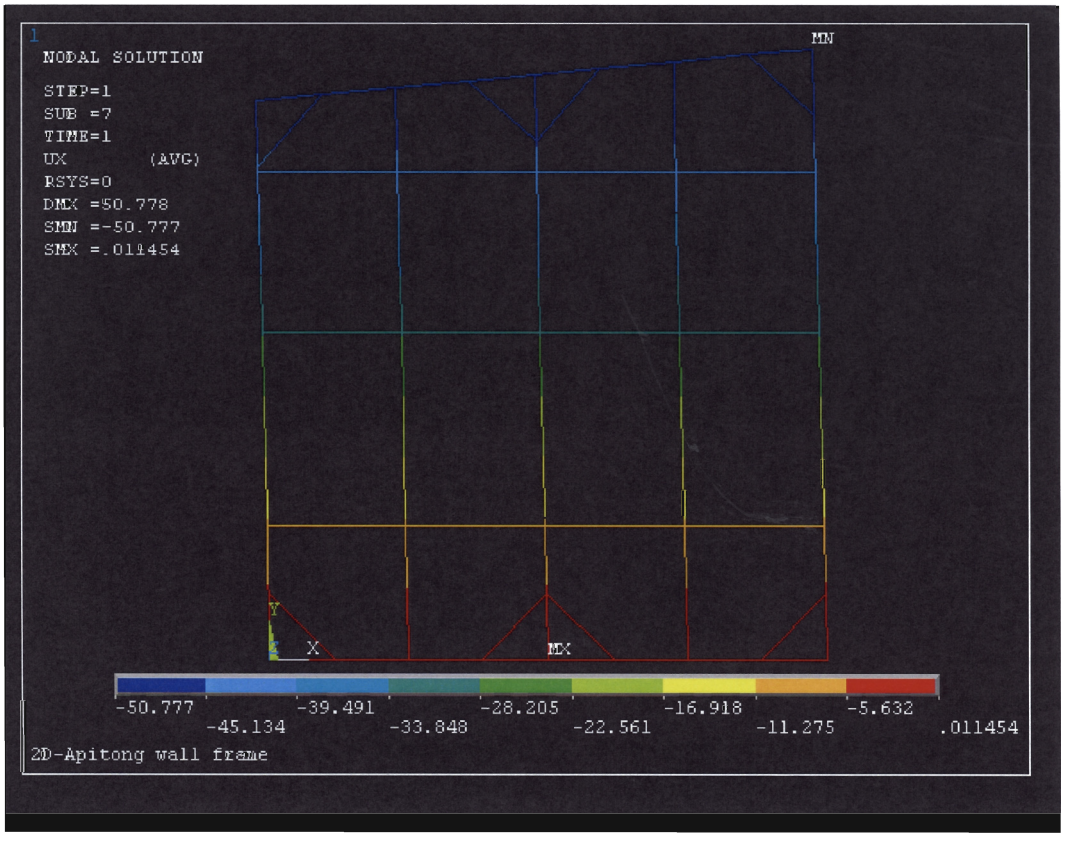

Figure 8.4 Nodal solution for x-direction displacement of Apitong wall frame at P*max.*

Figure 8.5 shows the deformed and undeformed figure of the model after loading analysis for the Radiata pine wall frame at maximum load (P*max*). Also shown are the pin-ended members that allow rotation along the z-axis. Both Figure 8.4 and 8.5 show displacements in the x-direction, however, Figure 8.4 shows displacement in color coded fashion for easy visual inspection.

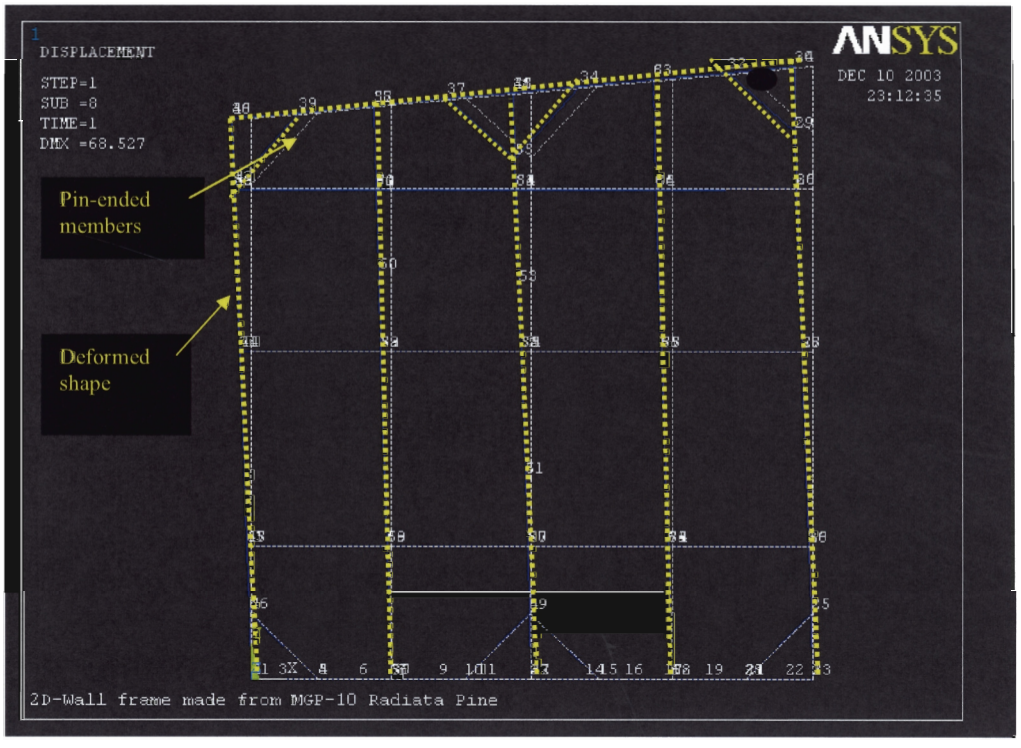

Figure 8.5 Deformed and undeformed shape of the Radiata Pine wall frame model at P*max*.

Differences of -31% and -39% in the maximum deformation is observe for the average to FEM value for Apitong and Radiata pine timber frame. This shows that the FEM made was rigid and distances are exact, allowing no spaces for extra movement. On the other hand, actual specimens have some spaces between joints and connections, allowing certain displacements when loaded. This is brought about by uncontrolled condition of fabrication, thus allowing errors in dimension and geometry.

8.2.2.2 Wall with sheathings

The same numbers of specimens were tested on wall with sheathings as in the wall frames. There were three specimens for the Apitong frame wall, with an 8mm medium-density wwcb and two specimens for the Radiata pine framed wall with a 7mm F11 structural plywood. Both walls were sheathed on both sides. The wall with wwcb is represented by the letter "W" and the wall with plywood sheathing is represented by the letter "P". The choice of plywood sheathing in comparison with the wwcb was that it was foreseen that it would be a good alternative sheathing material to that of the wwcb.

The points of comparison of the two wall sheathings were presented in Chapter 5 through the use of the Equivalent Elastic Energy Parameters (EEEP), as recommended by the ASTM. The EEEP is best described in Figure 4.24, as illustrated by Salenokovich (2000). The elastic stiffness of the wall was obtained, as well as the yield loads and yield displacements and ductility of the composite structure.

8.2.2.2.1 Wood wool cement board sheathing

A medium-density material with 8mm thickness pre-cut to different sizes was used as a sheathing for the Apitong timber frame. This wall is represented by "W". In the experiment, three specimens were used and labelled as W1, W2 and W3. However, W3 was discarded due to inconsistency of material thickness and density, thus providing the W3 with a 50% higher ultimate load, compared to the lowest value of 8,463 N. The non-inclusion of the W3 is also recommended by ASTM E564-2000, which states that a value that is 15% greater than the lowest value re removed. A PLANE 42 element was used to represent the finite element model for the sheathing and input properties as follows: modulus of elasticity (MOE) equivalent to 2.96 MPa and Poisson's Ratio of 0.29.

The following Figures, 8.6 to 8.10 represent nodal stresses at the x-direction of the model. Each figure's load and displacement value are presented in Table 8.3.

Table 8.3 Load and displacement values from the FEM analysis

Figure number	Load (N)	Displacement (mm)
8.6	2,750	2
8.7	5,000	5
8.8	6,475	7
8.9	7,800	11
8.10	9,450	19

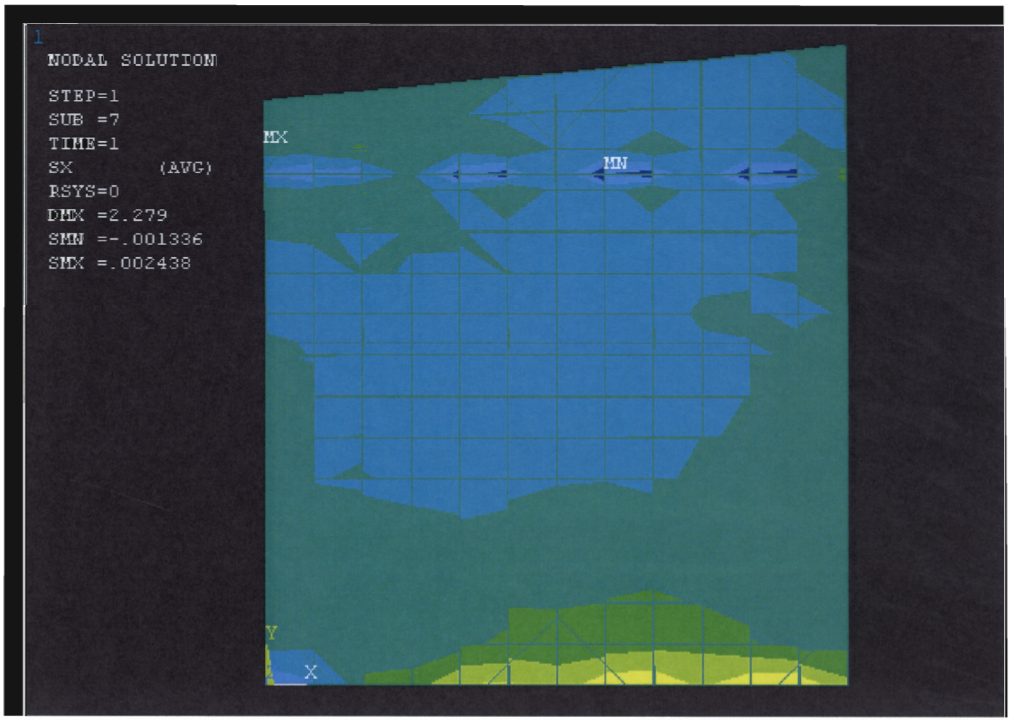

Figure 8.6 Nodal solution image at 2.28mm displacement for stress (x-direction in the sheathing panels).

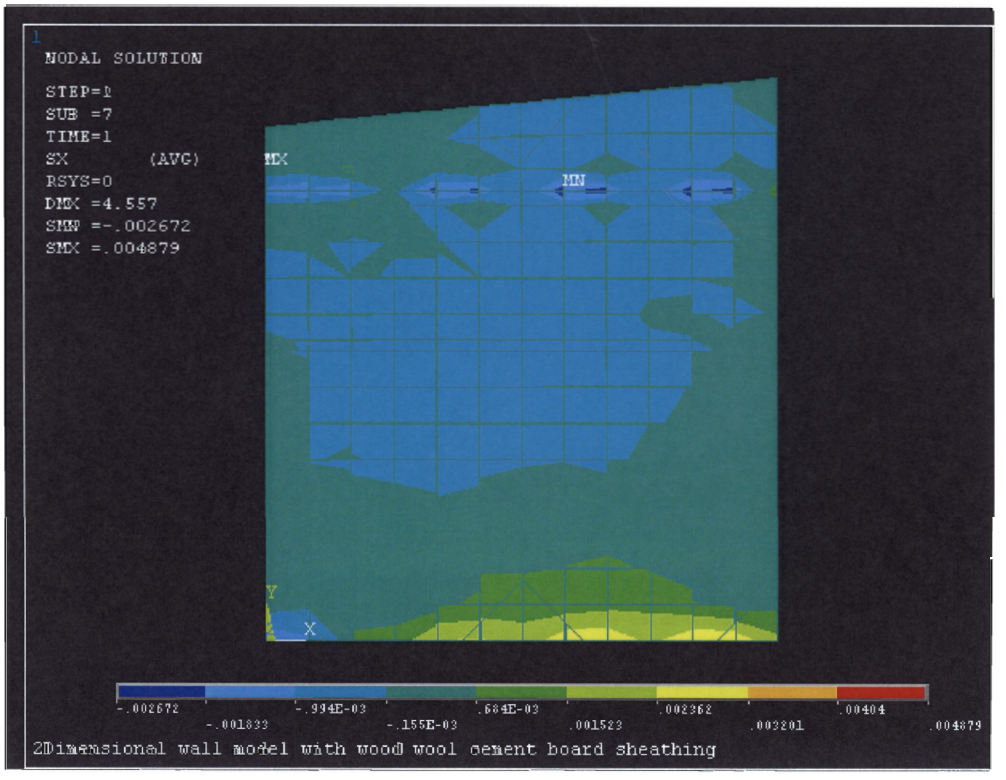

Figure 8.7 Nodal solution image at 4.56mm displacement (x-direction in the sheathing panels).

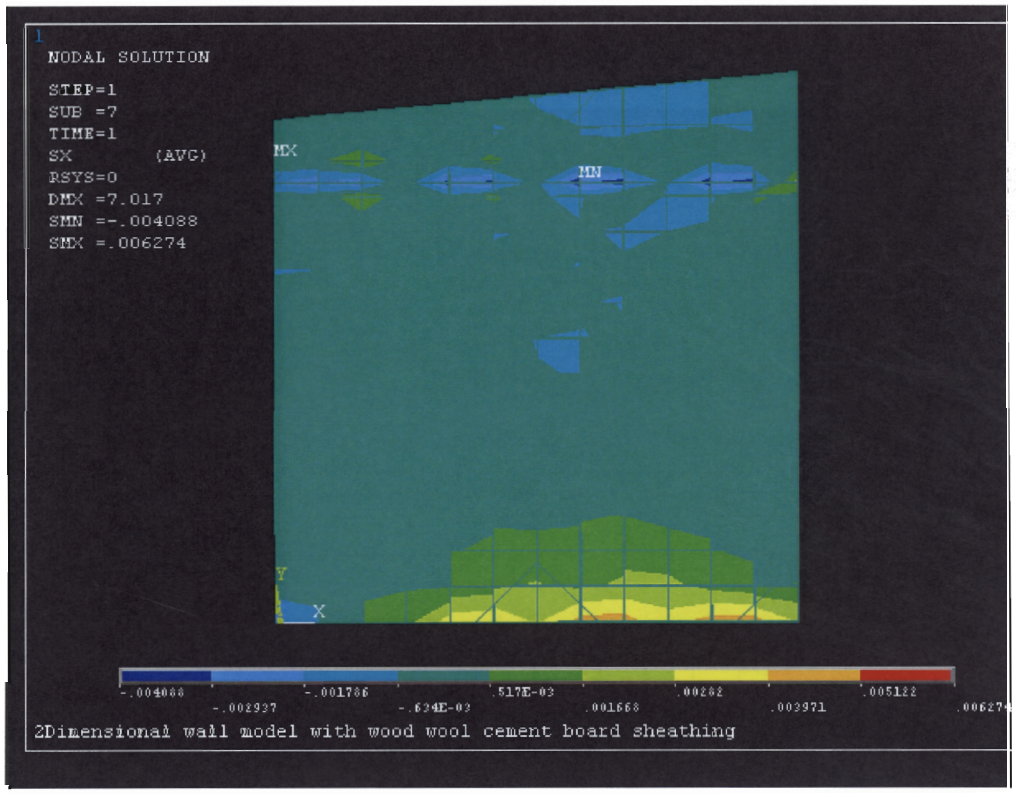

Figure 8.8 Nodal solution image at 7.02mm displacement.

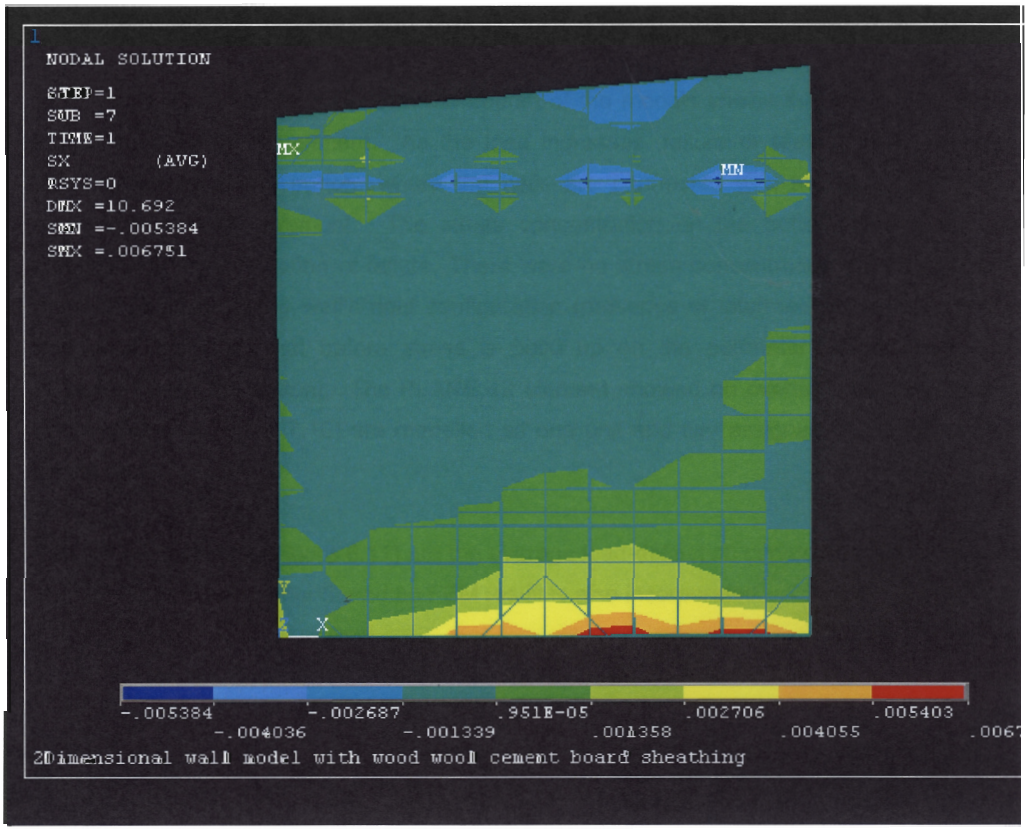

Figure 8.9 Nodal solution image at 10.6mm displacement.

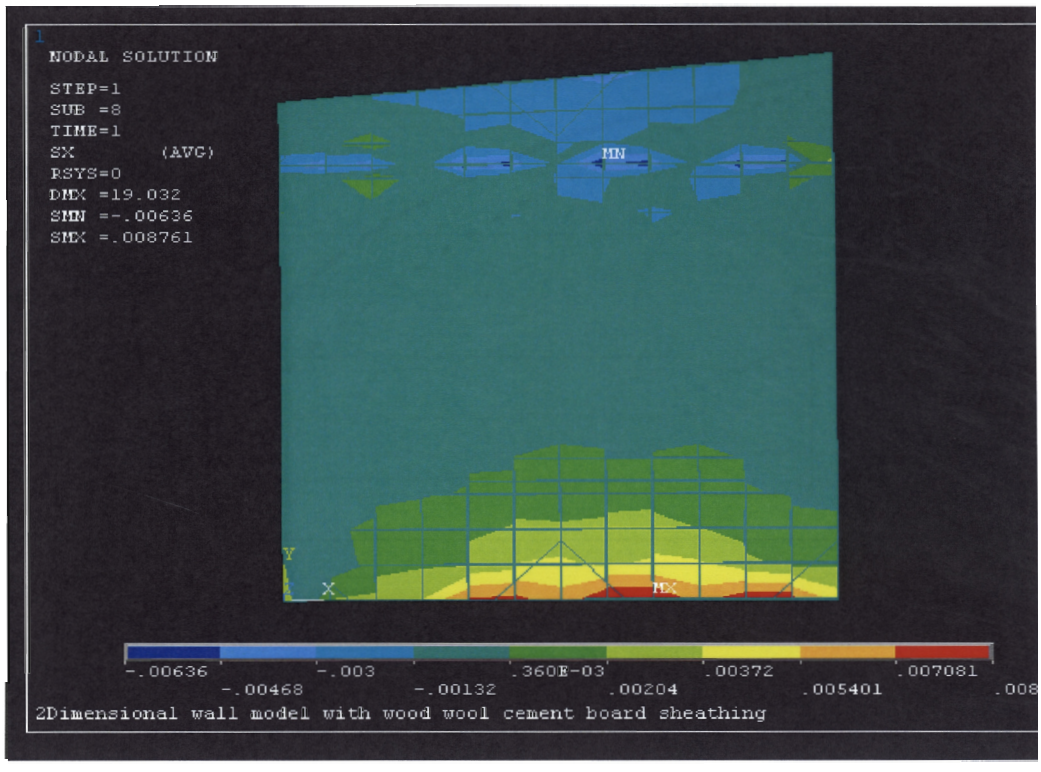

Figure 8.10 Nodal solution image at 19mm displacement.

Build-up of stress concentrations at the bottom of the models shows the same observation as that relating to the experiment. As the load increases, failure or tearing of the wood wool cement boards at the bottom where the nails are connected with the sheathing gradually showing signs of movement. The stress concentration on the bottom part of the model corresponds to the location of failure. There were no stress concentration on the perimeter of the wall because of the wall's rigid configuration (presence of intermediate vertical studs and horizontal bracings) that before stress is build up on the perimeter, failure have already emanated from the bottom. The PLANE 42 element showed no overlaps, because individual panels (refer to Figure 7.10) are modelled as one unit and two assigned sheathing-to-framing connector.

The following graphs (Figure 8.11) are the average load-deflection curves from the experimental tests presented in Chapter 5, and an FEM result is also incorporated.

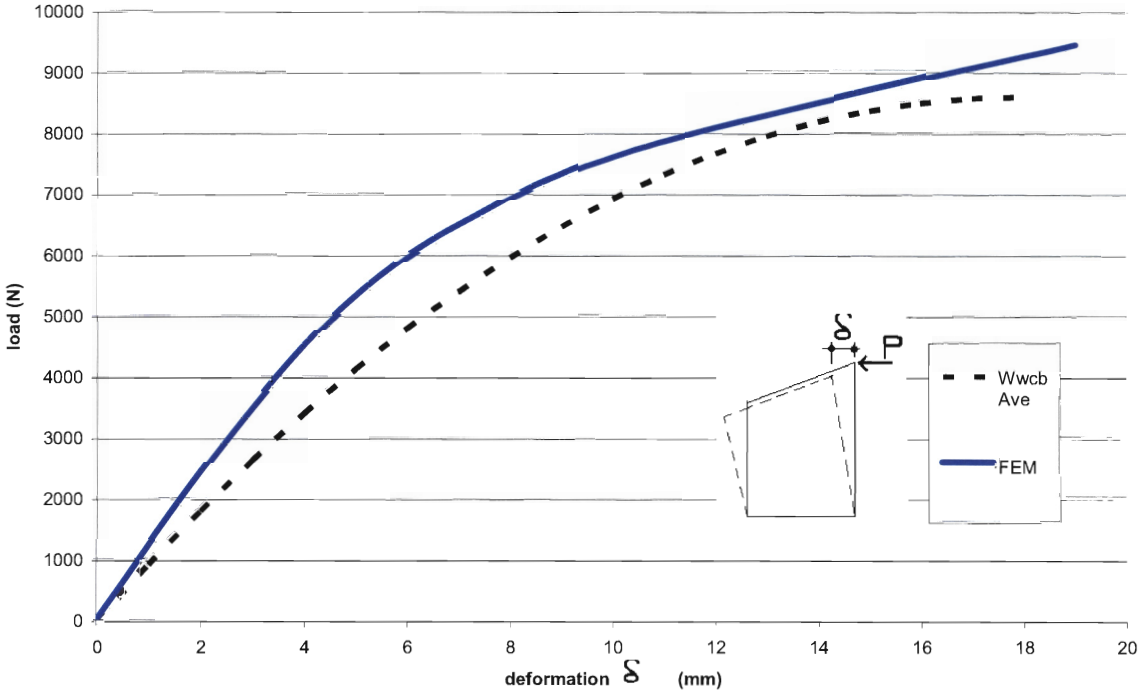

Figure 8.11 Load-deflection curves for wwcb-sheathed wall Apitong frame.

8.2.2.2.2 F11 structural plywood sheathing

Two specimens were tested in this study. The specimens were labelled as P1 and P2. As explained in Chapter 5, P2 was removed from the set of data because the specimen was pre-stressed or loaded before it was tested. Minimising the gap between the specimen and the wooden base had preloaded P2. Thus, P1 was used to compare with the FEM result. The experiment applied an incremental unidirectional loading. Deformation was measured at six points of the specimen; however, this section will only present the deformation on the location of the loading area. This is for the purpose of comparing its experimental result together with the result from the finite element modelling.

The procedure in generating the FEM of the wall was presented in Chapter 7 and also presented in Figure 8.12 as FEM. It used the same element types as used in generating a model with the wwcb-sheathed wall. This model has a separate data for other element types such as the LINK 1 and COMBIN 39. These data were obtained from the preliminary experiments mentioned in Chapter 4.

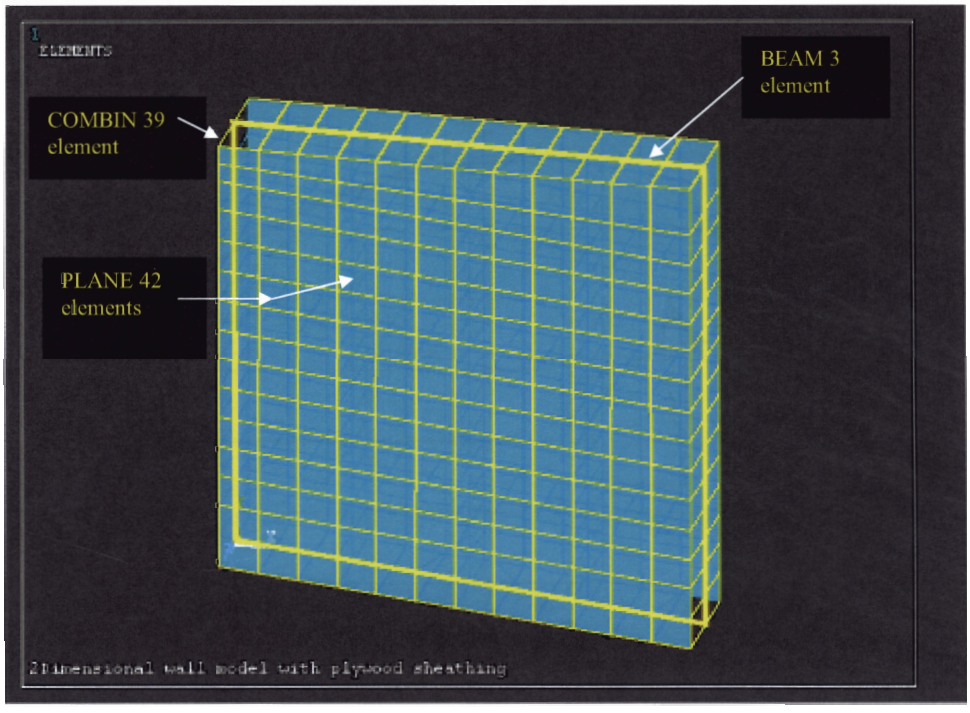

Figure 8.12 Plywood-sheathed wall model

The nodal solutions images and element stresses for the wall model are provided in Appendix N (attached compact disc).

Figure 8.13 shows a load-deflection curve for the experimental data for P1, compared with the FEM result for plywood sheathing. Although we have provided an FEM result, it is not conclusive to say that there is a good correlation between the FEM and the experimental work. The removal of P2 is caused by a 10 mm gap on the far end of the wall. Closing the gap by tightening the bolt caused an initial strain on the specimen. The discussion used the data for P1.

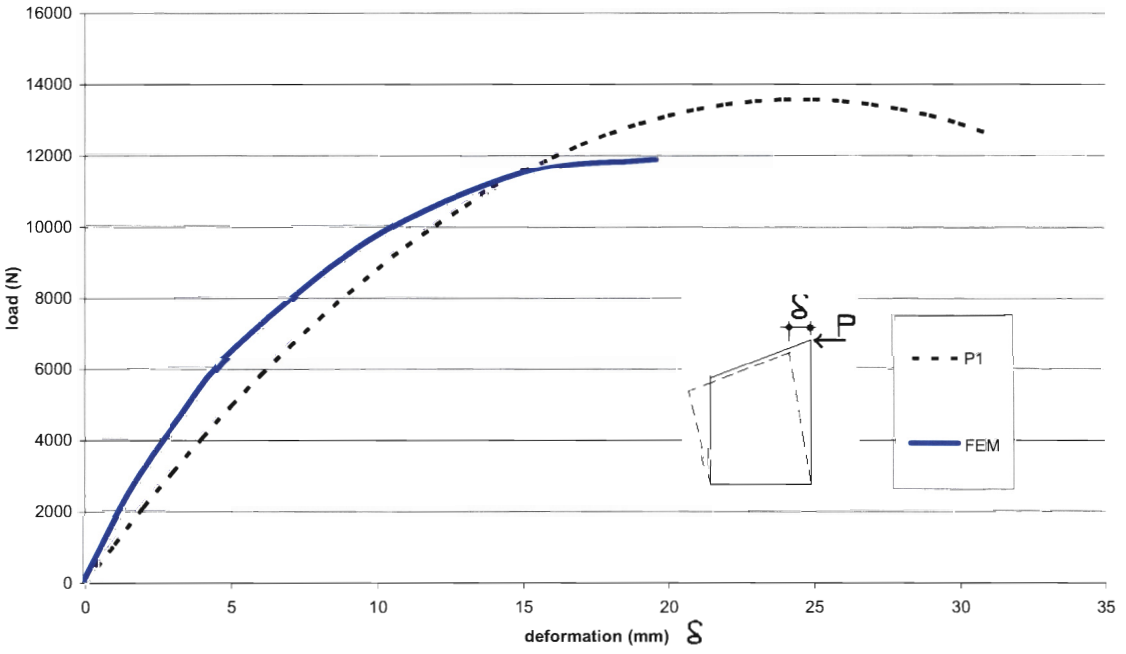

Figure 8.13 Load-deflection curve for the plywood-sheathed Radiata pine timber frame.

Table 8.4 presents tabulated results from the experimental value and the FEM results. The computed SPSS averaged values for the experiments are compared with the FEM results.

Table 8.4 FEM versus the experimental averaged value

Specimen	**Maximum deformation (mm, *δ*)**			**Maximum load (N, *P*)**		
	Ave	**FEM**	**Ratio**[a]	**Ave**	**FEM**	**Ratio**[a]
Wwcb	18	19	0.95	8,607	9,450	0.91
Plywood	25	20	1.25	13,566	11,900	1.14
Variation (%)	+5 / -25			+ 9 / - 14		

[a] Ratio = Ave / FEM

Individual discussions for the results are elaborated on the succeeding sections. The point of comparison for the discussion is the average values and the FEM results.

8.3 Discussions

Section 8.2 has presented results for the experimental work and compared it with finite element analysis results. Explanations of the results were also included. This section will further elucidate the values obtained from both the finite element modelling results and the experimental work.

8.3.2 Non-linear behaviour of the timber-framed wall

Shear walls are commonly used to provide lateral stiffness and strength in wood buildings. Therefore, an accurate prediction of the static behaviour of timber shear walls is necessary in order to evaluate the safety of existing timber buildings and improper design practice.

Research has been conducted in the past to develop models for prediction of the lateral load capacity of shear walls, from relatively simple linear elastic models for predicting static linear wall behaviour (Toumi and McCutcheon, 1978) to non-linear regimes by including the effect of the non-linear load-deflection behaviour of fasteners (McCutcheon, 1985). This study has tried to exploit the use of a special element to model the non-linear behaviour of the frame-to-sheathing connector.

The experimental work on timber-framed walls used an incremental unidirectional type of loading and preliminary tests such as joint testing and lateral nail resistance test (see Chapter 4 for details). These experimental works were used to calibrate the two dimensional FE model to predict the wall's non-linear behaviour. The ability of the model to predict the lateral stiffness and ultimate load capacity was demonstrated.

8.3.2.2 Comparison with the static tests

Figures 8.2 and 8.3 present a comparison between the average experimental and FEM load-deflection curve results for the two timber frames used, namely, Apitong and Radiata pine. It could be seen that the wall's stiffness and ultimate capacity were well predicted by the FEM.

8.3.2.2.2 Timber-framed wall only with corner metal braces

Due to the assumption that nailed timber end connections exhibit minimal or zero resistance to moment (as verified with an FEM having coupled end nodes), a corner metal bracket was incorporated to strengthen the lateral stiffness of the frame. Both timber frames exhibited a lower maximum displacement value than the FEM. The reason for this is because the corner joints fabricated were not perfectly fitted. Most of the connections had unavoidable gaps. Such gaps would tend to close-in first when loaded, registering initial displacements. Transporting the

specimens could also have loosened joints and fasteners. This scenario pictures the actual condition in the field during the fabrication and fitting of the frames. As a result, the Apitong frame had a -31% FEM, while the Radiata pine had a -39% FEM result compared to the deformation in the experimental works.

There was less variation in the maximum load capacity of each of the timber frames. The Apitong frame had a -3% FEM result while Radiata Pine frame has a +7% FEM result compared to those obtained in the experimental work. The tighter fitting of the nail fasteners connecting the frame and the corner metal brackets contributes to the higher experimental value for the Apitong frame. Deterioration of the Apitong-frame joints was caused by corrosion of the nails, possibly during the transport of the specimens from the Philippines to Australia.

8.3.2.2.3 Timber framed wall with sheathings

The sheathing materials used in this study were wood wool cement boards (with randomly oriented strands) and F11 structural plywood. The FEMs generated in the wall frames were used in this model. The most important component of the model is the sheathing-to-frame connector that is used to predict the nonlinear behaviour of a timber-framed wall.

There is a good correlation between the FEM results and the SPSS predicted average values for the Apitong frame sheathed with wood wool cement boards. The maximum deformation FEM result is +5% higher than that from the experimental work, while the maximum load capacity for FEM result is +9% higher. The lower values in the experimental work could be attributed to the loosening of the nail holes in the sheathing during transport from the Philippines to Australia. Constant vibration of the wwcb might have reduced its strength due to the development of hairline cracks in the sheathing. The worse condition would be the variation of MOE within the material itself. Also noting that the wwcb is manufactured manually, resulting in a product that differed from the laboratory scale.

It is difficult to draw conclusions based on the result of the FEM and the experimental work for the plywood sheathed wall. Only the result from one specimen was used because specimen P2 was initially stressed due to the 10 mm gap between the wall on the far end and wooden base. As a result, the value for P1 were much lower by 49% than P2. Hence, P1 was used in the comparison of the FEM with experimental result. Table 8.4 shows the FEM and the average value from the experimental work. For the maximum deformation, FEM was 25% lower and for the maximum load capacity, 14% lower FEM values compared to the experimental value. The low results from the FEM might be attributed to the low capacity from the lateral nail resistance test. The comparison is not conclusive, since there is only one data set to which the FEM is compared.

8.3.2.2.4 Analysis

In Chapter 3 of this study, the author mentioned that the wwcb sheathed wall was designed using an equivalent static load for wind load as per the National Structural Code of the Philippines (NSCP 1992). The resulting lateral load being carried by the wall is 3,500 N. However, with the new NSCP (2001), the maximum wind speed was changed from 200 kph to 250 kph. The resulting equivalent wind load for the new code is 5,000 N. Thus, it was imperative to check whether the designed wall was still capable of carrying the 5,000 N load through verification with the experimental works. Figure 8.14 shows the graphical illustration of the FEM, EEEP curve and the loads corresponding to the editions of NSCP.

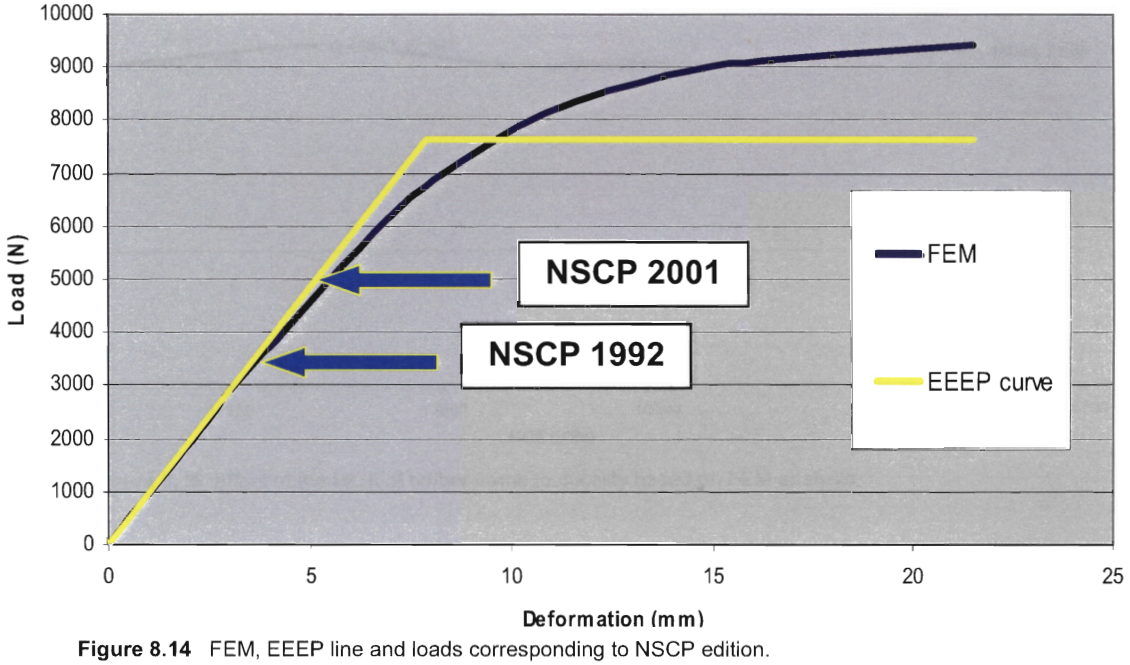

Figure 8.14 FEM, EEEP line and loads corresponding to NSCP edition.

The NSCP 1998 and 2001 equivalent loads are still in the elastic region of the EEEP line. The NSCP 1992 is only 45% and NSCP 2001 is only 65% of the equivalent yield load of the wall system in the EEEP line. Thus, the wall's maximum load capacity was under-utilised, even in extreme wind conditions.

8.3.2.2.4.1 Effect of timber frame MOE to ductility and load capacity

Without the corner brackets the deformation or displacement value for the plywood-sheathed wall was the same, i.e., 22mm displacement. This failure is attributed to the shallow penetration of fasteners of the wall. Increasing the MOE has no effect on the ductility of the wall; however it increased the load capacity (Figures 8.15).

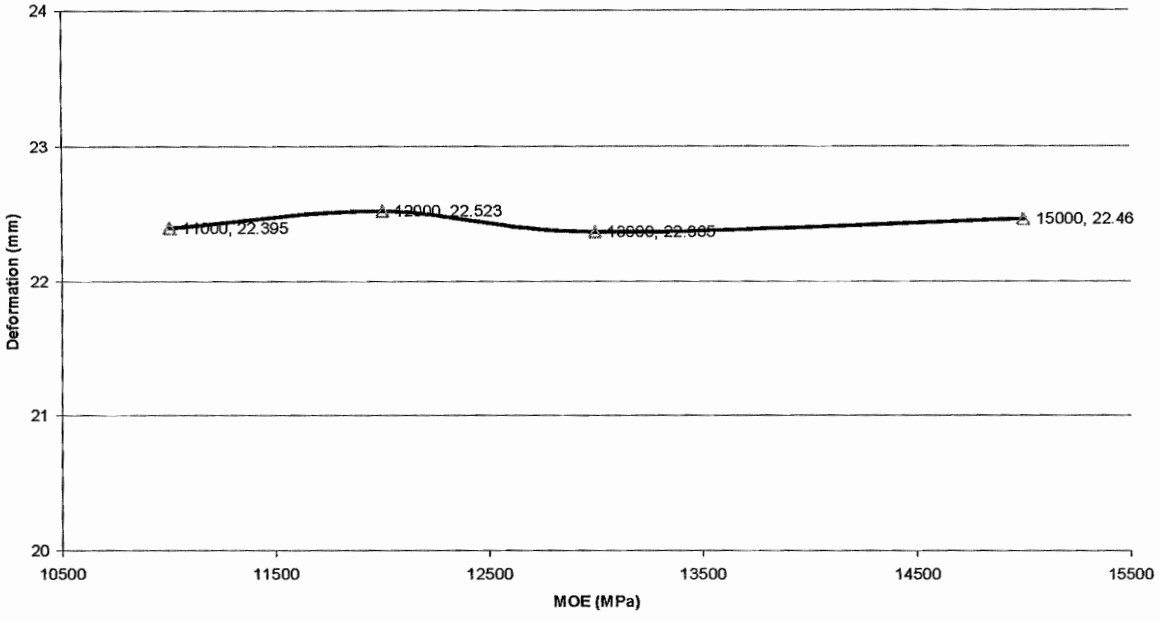

Figure 8.15 Effect of the MOE of timber frame to ductility based on FEM analysis.

The effect of removing the corner metal brackets for the plywood-sheathed wall was examined. This would also reduce the work in assembling the frame. Figure 8.16 shows that without the corner metal brackets, Radiata pine should have an MOE of at least 15 GPa.

The total maximum load without corner metal brackets for the plywood-sheathed wall is 10,840 N. This is 9% lower than the FEM value for the wall with corner metal brackets. The 1,060 N difference of the FEM results can be attributed to the corner metal brackets. This is 28% lower than that of the FEM capacity of the frame with corner metal brackets. The capacity of the frame with metal brackets is 1,475 N.

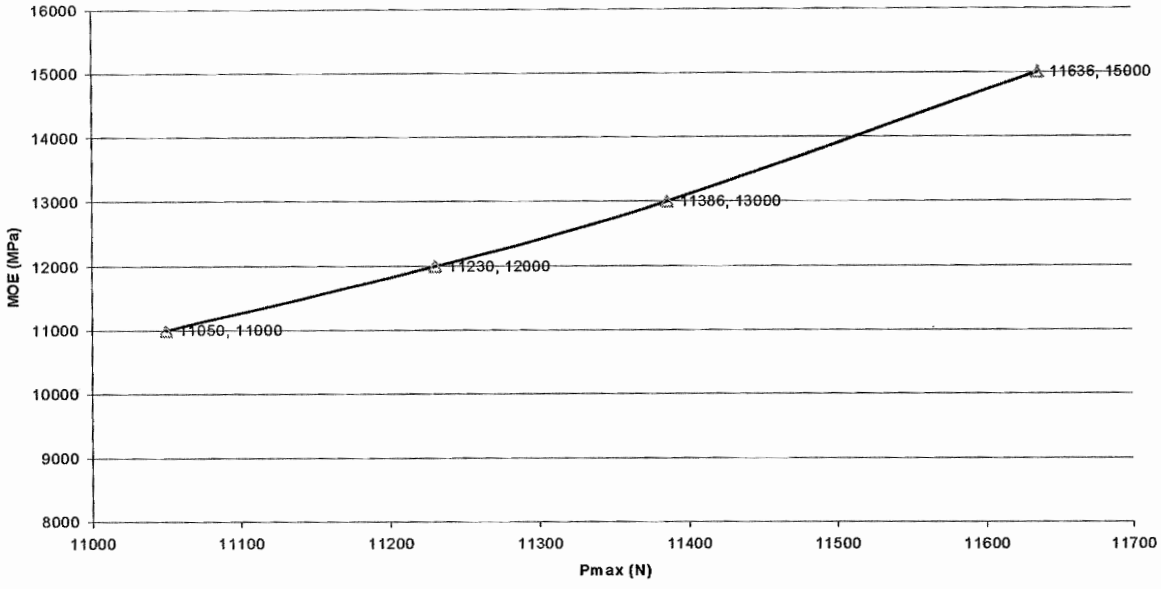

Figure 8.16 MOE vs. Pmax based on FEM analysis without corner metal brackets.

8.4 Summary

This chapter has presented graphical illustrations of load-deflection curves. Results of the experimental works were compared to the finite element model (FEM) results.

The FEM non-linear analysis of the timber-framed wall was used to predict the structure's response to loads and compared to the experimental work. A good correlation was obtained for the wwcb sheathed wall's FEM and experimental results. However, correlation between the FEM and the experimental work on the plywood sheathed wall is not conclusive.

The removal of corner metal brackets in the plywood sheathed wall caused a reduction in the maximum load by 9%, compared to the wall with corner brackets. The MOE of the timber frame for this particular set-up did not affect the ductility of the wall with respect to these wwcb and plywood sheaths with a 25mm length of nail.

9 Conclusions

9.1 Introduction

This study involved both experimental and modelling works. The experimental results were used to calibrate the finite element models generated from ANSYS program and determine the F-shelter's behaviour when subjected to static and dynamic loads such as the Kobe and Zone IV earthquake simulations.

Four types of structural tests on various components were conducted as follows:

1. Corner-joint testing
   1.1 Compression test for 82, 90 and 98-degree angle joints
   1.2 Tension test for 82, 90 and 98-degree angle joints
2. Lateral nail resistance test
   2.1 Apitong timber frame with wwcb sheathing
   2.2 Radiata Pine timber frame with plywood sheathing
3. Wall testing
   3.1 Wall with wwcb
   3.2 Wall with plywood sheathing
4. Full size F-shelter testing
   4.1 Non-destructive static test
   4.2 Destructive test set up on the shaker table

In addition, screw/nail withdrawal tests were also conducted to verify data secondary sources.

The following conclusions are made:

9.2 Corner metal brackets

Compression and tensile load test was conducted on the timber joint with corner metal bracing.

9.2.1 Experimental

In Apitong and Radiata pine wall frames with metal bracket and nail fasteners, the general mode of failure in compression tests was buckling of the diagonal steel rod and separation of the timber joint connection; and for tension test, withdrawal of the outer fastener.

9.2.2 FEM

1,475N increase in wall capacity was predicted by incorporating the corner metal brackets in the Radiata pine framed shear wall. Whereas, the lateral resistance of the shear wall was significantly increased with the use of corner metal brackets, this could further be increased by using longer screws and improving the end grain connection of the timber frame.

9.3 Full size testing

9.3.1 Monotonic test on walls

Based on the EEEP parameters, the ductility ratio and failure displacement are very close. Values for the plywood sheathing are 2% higher for the ductility ratio; and for wwcb higher by 2% for the displacement at failure. The full strength potential of the sheathings were not utilised because the 25mm length of the nails was insufficient. This resulted in a small difference in the ductility ratio and displacement failure.

The mode of failure in plywood sheathed walls is nail pull-out indicating that the full strength of the plywood was not utilized. Failure in the wwcb sheathed walls showed material failure, i.e., tearing and nail pull through.

Plywood sheathing has a 58% higher ultimate load capacity compared to the wwcb. It follows that the yield load is also higher by 18%. It is noteworthy that the yield displacement for wood wool cement board and plywood are not significantly different.

9.3.2 Static test of the F-shelter

Two types of test were conducted on the F-shelter: 1) static tests and 2) dynamic tests through earthquake simulation tests on the shaker table. This section will only provide conclusions for the unreinforced F-shelter, as this is the actual construction method of the F-shelter.

The presence of openings in walls such as windows and doors caused the development of torsion when axial load was applied. Imperfections in joint fitting such as gaps results in premature displacements in the direction of the lateral load during testing.

9.3.3 Dynamic test of the F-shelter

The prototype F-shelter can withstand earthquakes such as the Kobe and the Zone IV, up to 70% and 80% of full scale displacement excitation, respectively.

9.4 Alternative timber frame, sheathing material and fastener

When plywood sheathing material, Radiata pine timber framing and Ø3mm galvanized nail fastener are used as substitute, the full capacity of the plywood is not utilized due to the insufficient length of the nail used. The ductility of the wall made of substitute approximates that in the prototype F-shelter.

9.5 Finite element model of the wwcb and plywood sheathed wall

Using FEM, the project has developed a two prediction models on the non-linear behaviour of the wall under static load. A three dimensional model simulating the timber-framed shear wall's non-linear behaviour in a 2D analysis was developed. This required prior testing and FE modeling of the corner joint with metal bracket in compression and tensile and lateral resistance test of the sheathing-to-frame connector (AS 1649, 2001).

Compared to the experimental values, the Apitong timber frame FEM values were 3% lower, the Radiata pine timber frame 7% higher, the Apitong frame with wwcb sheathing 10% higher, and the Radiata pine with plywood sheathing 14% lower.

10 Recommendations and areas for future research

10.1 Recommendations

The purpose of the project is to create an FEM capable of predicting the structure's behaviour under prescribed load with the view of improving the serviceability and strength of the structure against external loads. Although it was shown that the structure withstood the simulated earthquake loads, the following recommendations provided will further improve the performance of the structure.

1. Further full-scale testing under dynamic loads, particularly wind-load simulation. The increase of wind velocity as revised in the National Structural Code of the Philippines shows that its effect on structures has significant changes. Thus, a wind tunnel testing facility that simulates local wind conditions will further provide more reliable data on the structure's response to wind load.

2. Further full-scale testing using local earthquake time history records. The earthquake time history records used in this study were the Kobe and Zone IV earthquake that are both from foreign countries. The magnitude and frequency occurrence of locally generated earthquakes are different from those simulated earthquakes. The Philippine Institute of Volcanology and Seismology of the Department of Science and Technology has recently installed accelerometers in strategic locations of the country to monitor and record earthquakes. This seismic records will be very useful in determining the structure's response to dynamic load.

3. Full-scale testing of wall frames using improved connections and locally produced sheathing materials. Improvements to the connection have been discerned to reinforce the frame. Locally produced sheathing materials such as plywood, marine plywood, bamboo mat and coco coir binderless board as alternative structural sheathing. Thus, indigenous materials are used as alternatives and not compromising the structural reliability of the F-shelter.

4. A three-dimensional finite element model of the whole structure, capable of predicting its behaviour under static and dynamic loads. This study focused on the non-linear analysis of the timber-framed wall. A better understanding of the structure and flexibility of the design would be addressed if a three-dimensional FEM is constructed.

10.2 Areas for future research

Although results of this study have shed some light on the behaviour of the F-shelter when subjected to static and dynamic loading and also monotonic test on walls, there remain areas where research needs to be performed, to validate the accuracy of experiment results. These include:

1. Additional experimental tests need to be performed on walls with plywood sheathings. Results from the experiments showed that result of only one specimen was valid, whereas, the other was discarded due to geometrical inconsistency of the specimen P2. More tests will validate the results of this experiment.

2. The test on specimen W3 needs to be repeated because of the inconsistency of the results. As per the recommendation by ASTM (2000), results exceeding 15% of the other results should be carefully examined and likewise be removed from the data. A repeat of the test using the same specimen and configuration will further validate the results from this experiment.

3. The experiments performed showed that the method applied is a global response parameter for strength and stiffness (load-deflection relationship). It is recommended that other stress-measuring devices such as strain gauges on strategic locations on the specimen be included when performing the test. This is to verify and quantify stresses from the predictive capability of the finite element model generated form ANSYS 7.2. These additional data or stresses on the experimental work will further validate the results of the finite element model.

4. Modify measuring gauges to measure lateral movement or out-of-plane deformations. In this project, the specimens were sandwiched or laterally supported and is not the actual representation of service condition, i.e., the wall is restrained at the base and on top. The experiment performed took the global response of the wall with additional bottom restraints (wooden screws) and lateral supports. This is in anticipation of creating a finite element model for the wall, capable of predicting the measured stresses.

5. Generation of a finite element model of the F-shelter that could predict the structures' behaviour when applied with external loads. The full-size or the whole-house testing could be used to calibrate this proposed FEM of the F-shelter, although, additional tests are required to account for the connections. Bolt holes were redrilled and gaps were present in the structure. It is recommended that a controlled construction environment be established to create a suitable structure for testing.

6. The F-shelter needs to be tested on its weaker side. In this project, the structure was tested on its strong axis. It is not feasible to test the structure on a different side, because the fixed layout of the shaker table would not accommodate the F-shelter positioned for testing in the weak direction.

References

ANSYS 1998. Introduction to ANSYS-release 5.7. Instructor's Guide.

Australian Standard. 2001. Timber – Methods of Test for Mechanical Fasteners and Connectors – Section 2.1: Withdrawal Test – for Category A Fasteners only. AS 1649 – 2001. Sydney.

Australian Standard. 2001. Timber – Methods of Test for Mechanical Fasteners and Connectors –Section 2.2: Lateral Resistance Test for Joints – for Categories A, B, C and D Fasteners. AS 1649 – 2001. Sydney, NSW.

Australian Standard/New Zealand Standard. 1994. Plywood – Structural. AS/NZS 2269. Homebush, NSW/Wellington NZ. p.18

American Society for Testing and Materials. 1986. Testing Mechanical Fasteners in Wood. D 1761-86b. ASTM – West Conshohocken, PA.

American Society for Testing and Materials. Standard Test Methods of Conducting Strength Tests of Panels for Building Construction. E72-98. ASTM – West Conshohocken, PA.

American Society for Testing and Materials. 1987. Static Load Test for Shear Resistance of Framed Walls for Buildings. E - 564. ASTM – West Conshohocken, PA.

Balana, C.D. 1999. RP no. 1 in natural disasters in 98 years. Daily Inquirer. 01 August issue.p3.

Baker, A.J. and D.W. Pepper. 1991. Finite Elements 123. McGraw Hill, Inc., New York, NY.

Bruer, J.R. 1998. What every engineer should know about Finite Element Analysis. Marcel Dekker, Inc. New York and Basel.

Chehab, M. 1982. Seismic analysis of a two-storey wood framed house using the response spectrum technique. MS thesis, Dept. of Civil engineering, Oregon State University, Corvallis, Oregon.

Cook, R.D. 1994. Finite element modeling for stress analysis. John Wiley and Sons, Inc. Canada.

Dinehart, D.W., and H.W. Shenton. 1998. Model for Dynamic Analysis of wood frame Shear walls. Journal of Structural Engineering. 126(9): 899-908.

Dolan, J.D. 1989. The dynamic response of timber shear walls. Ph.D. dissertation. University of British Columbia, Vancouver, Canada.

Dolan, J.D. and A.C. Johnson. 1997. Monotonic test of long shear walls with openings. Virginia Polytechnic Institute and State University, Timber Engineering Report. No. TE 1996-001. Blacksburg, Virginia.

Filiatrault, A. and B. Folz. 2002. Performance-base Seismic Design of Wood Frame Buildings. Journal of Structural Engineering. 128(1): 39-47.

Fisette, Paul R. 1997. Bracing foam-sheathed walls. Building Materials and Wood Technology. University of Massachusetts, Amherst, Ma.

Foliente, Greg C. 1996. Issues in seismic performance and evaluation of timber structural systems in Proceedings of the 1996 International Timber Engineering Conference, Vol. 1, New Orleans, LA, pp. 1.29-1.36.

Folz, B. and A. Filiatrault. 2001. Cyclic Analysis of Wood Shear Walls. Journal of Structural Engineering, ASCE, 127(4). April 2001:433-441.

Goodman, J.R., R.J. Schmidt, M.E. Criswell, and A.H. Stewart. 1996. Laterally loaded Manufactured Homes. Draft report.

Gupta, A.K. and G.P. Kuo. 1987. Modeling of a wood-framed house. Journal of Structural Engineering, ASCE 13(2): 260-278.

He, M., F. Lam, and R.O Foschi. 2001. Modeling three dimensional timber light framed buildings. Journal of Structural Engineering. ASCE, 127(8) August 2001: 901-913.

Heine, C. 1997. The effect of overturning restraint of the performance of fully sheathed and perforated timber shear walls. MS thesis, Virginia Polytechnic Institute and State University, Blacksburg, Virginia.

Hite, M.C. and H.W. Shenton. 2002. Modeling the nonlinear behavior of wood frame shear walls. 15th ASCE Engineering Mechanics Conference. Columbia University, New York, NY. June 2-5, 2002.

International Organization for Standardization (ISO). 1998. Timber Structures – Joints made with Mechanical Fasteners, Quasi-Static Reversed-Cyclic Test Method. WG7 Draft. ISO TC 165 Secretariat, Standards Council of Canada.

Jablin, Mark C. 1995. Finite Element Modeling of Manufactured Homes Using Interface Elements. MS thesis, University of Wyoming, Laramie Wyoming.

Judd, J.P. and F.S. Fonseca. 2002. Finite Element analysis of wood shear walls and diaphragms using ABAQUS. ABAQUS User's Conference.

Johnson, A.C. 1997. Monotonic and Cyclic Performance of long shear walls with openings. MS thesis, Virginia Polytechnic Institute and State University, Blacksburg. Virginia.

Kasal, B. and R.J. Leihcti. 1992a. Nonlinear finite element model for light-framed stud walls. Journal of Structural Engineering. 118 (11).

Kasal, B. and R.J. Leichti. 1992b. Incorporating load sharing in shear wall design of Light-frame structures. Journal of Structural Engineering. 118(12): 3350-3361.

Kasal, B., R.J. Leichti, R.Y. Itani. 1994. Non-linear finite element model of complete light-frame wood structures. Journal of Structural Engineering. 120 (1): 100-118.

Kausel, Eduardo. 1996. New seismic testing method I: Fundamental Concepts. Journal of Engineering Mechanics. 124 (5): 565-575.

Macleod, I.A. and S.C. Hartvig. 1997. Issues and strategies for evaluation of structural Design options. Journal of the International Association for bridge of structural Engineering. 9 (3): 201-205.

McCutcheon, W.J. 1985. Racking deformations on wood shear walls. Journal of Structural Engineering. 111 (2): 257-269.

National Climate Monitoring Center (NCMC). 2001. Tropical cyclone statistics in the Philippine Area of Responsibility 1948-2000. PAGASA-DOST.

National Structural Code of the Philippines (NSCP). 1992. Building Towers and Other Vertical Structures Fourth Edition. Association of Structural Engineers of the Philippines.

National Structural Code of the Philippines (NSCP). 2001. Buildings, Towers and Other Vertical Structures Fifth Edition. Association of Structural Engineers of the Philippines.

Nelson, E.L., D.L. Wheat and D.W. Fowler. 1985. Structural behavior of wood shear wall assemblies. Journal of Structural Engineering, 111 (3): 654-666.

Paavere, P and G. Foliente. 2000. Finite Element modeling of an L-shaped House (Phase II). Unpublished report for CSIRO project.

Paultre, P. and J. Proulx. 1997. Dynamic testing of large scale structures. Journal of the International Association for Bridge and Structural Engineering. IABSE, 7 (1).

Philippine Atmospheric Geophysical Astronomical Service Administration. 2000 Tropical Cyclone Statistics in the PAR 1948-2000. 2000. PAGASA, DOST.

Philippine Institute of Volcanology and Seismology. 2000. Distribution of Active Faults in the Philippines. PHIVOLCS , DOST.

Philips, T. L. 1990. Wood shaving characteristics of 3-dimensional wood diaphragms. MS thesis, Washington State University, Pullman, WA.

Rellin, M. Jr., A. Jesuitas, L. Sulapat, and I. Valeroso. 2001. Extreme wind hazard mapping in the Philippines. NDRB Technical Report No. 111.

Salenikovich, A.J. 2000. The racking performance of light frame shear walls. PhD dissertation, Virginia Polytechnic Institute and State University, Blacksburg, VA.

Schnobrich, W.C. 1990. The Finite Element Method. Structural Engineering Handbook Third Edition. Mcgraw Hill Publishing Company. pp 1-46 – 1-78.

Stewart, A.H., J.R. Goodman and E.M. Slasbury. 1989. Lateral Force distribution in manufactured housing form full-scale testing. Structural Design, Analysis and Testing Proceedings, ASCE Structures Congress.

Sugiyama, H. and T. Matsumoto. 1994. Empirical equations for the estimation of racking strength of a plywood sheathed shear wall with openings. Mokuzai Gakkaishi 39 (8): 924-929.

Simpson Strong-Tie Co., Inc. 1999. Catalog C-99. Wood Construction Connectors. Simpson Strong-Tie Co., Inc., Pleasanton, CA.

Soriano, F.P., T.R.E. Rondero, and C.R. Cariño. 2000. Design and development of shop fabricated emergency shelters. Paper presented during the STARRDEC Regional R & D symposium held at Baac, Marinduque on 24 August 2000.

Stewart, W.G. 1987. The seismic design of plywood sheathed shear walls. PhD thesis. University of Canterbury, Canterbury, New Zealand.

Sugiyama, H. and T. Matsumuto, 1994. A simplified method of calculating the shear strength of a plywood-sheathed shear wall with openings III. Mokuzai Gakkaishi, 40 (3): 1-7.

Tarabia, A.M. and R.Y. Itani. 1994. Seismic analysis of light-frame wood structures in Proceedings from Second International workshop on full scale behavior of low-rise buildings. James Cook Cyclone Structural testing Station. North Queensland, Australia. 7-8 July 1994.

Tuomi, R.L. and D.S. Gromala. 1977. Racking Strength of Walls: Let-in corner bracing sheet materials, and effect of loading rate. Research paper FPL 301 U.S. Department of Agriculture, Forest Products Laboratory, Madison, pp. 21.

Toumi, R.L. and W.S. McCutcheon. 1978. Racking strength of light frame nailed walls. Journal of the Structural Division. 104 ST7: pp 1131-1140.

Wolfe, Ronald N. 1983. Contribution of Gypsum wallboard to racking resistance of light-frame walls. Forest Products Laboratory Research Paper. FPL 439.

http://www.reliefweb.int/w/rwb.nsf/s/7BC6DA4839DB07A949256BF8002A4897 Philippines, DSWD Disaster Updates - Floods due to monsoon rains 11 July 2002.

http://nwn.ege.com/publications/kobe/introduct.htm. Hugo Ken Nanbu or the Kobe Earthquake.

http://www.fnri.dost.gov.ph/htm/dost3c.htm Department of Science and Technology Medium Term Plan (1999-2004).

http://adb.org/Documents?Policies/Urban_Sector/urban0201.asp?p=policies Urban Sector Strategy: II. The Urban Sector.

http://www.em-dat.net/disasters/Visualisation/profiles/natural-table-emdat.php?country=Philippines&Submit=Display+Profile Philippines, Country Profile for Natural Disasters.

http://www.icc-es.org/reports/pdf_files/UBC/3701.pdf Metal bracing, Foundation anchors and Joist hangers. 01 September 1990.

Appendix

(Appendix A-N located here in the attached compact disk)